Some stagnation-point flows over a lubricated surface

by

Khalid Mahmood

Department of Mathematics and Statistics
Faculty of Basic and Applied Sciences
International Islamic University,
Islamabad, Pakistan
2016

Some stagnation-point flows over a lubricated surface

by

Khalid Mahmood

Supervised by

Prof. Dr. Muhammad Sajid

Co-Supervised by

Dr. Nasir Ali

Department of Mathematics and Statistics
Faculty of Basic and Applied Sciences
International Islamic University, Islamabad,
Pakistan
2016

Some stagnation-point flows over a lubricated surface

by

Khalid Mahmood

A thesis submitted
in the partial fulfillment for the degree of
Doctor of Philosophy
in
Mathematics

Supervised by

Prof. Dr. Muhammad Sajid

Co-Supervised by

Dr. Nasir Ali

Department of Mathematics and Statistics
Faculty of Basic and Applied Sciences
International Islamic University, Islamabad,
Pakistan
2016

Author's Declaration

I, **Khalid Mahmood** Reg. No. **25-FBAS/PHDMA/F12** hereby state that my Ph.D. thesis titled: **Some stagnation point flows on a lubricated surface** is my own work and has not been submitted previously by my for taking any degree from this university, **International Islamic University, Sector H-10, Islamabad, Pakistan** or anywhere else in the country/world.

At any time if my statement is found to be incorrect even after my Graduate the university has the right to withdraw my Ph.D. degree.

Name of Student: **(Khalid Mahmood)**
Reg. No. **25-FBAS/PHDMA/F12**
Dated: **02-03-2017**

Plagiarism Undertaking

I solemnly declare that research work presented in the thesis titled: **Some stagnation point flows on a lubricated surface** is solely my research work with no significant contribution from any other person. Small contribution/help wherever taken has been duly acknowledged and that complete thesis has been written by me.

I understand the zero tolerance policy of the HEC and University, **International Islamic University, Sector H-10, Islamabad, Pakistan** towards plagiarism. Therefore, I as an Author of the above titled thesis declare that no portion of my thesis has been plagiarized and any material used as reference is properly referred/cited.

I undertake that if I am found guilty of any formal plagiarism in the above titled thesis even after award of Ph.D. degree, the university reserves the rights to withdraw/revoke my Ph.D. degree and that HEC and the University has the right to publish my name on the HEC/University Website on which names of students are placed who submitted plagiarized thesis.

Student/Author Signature: 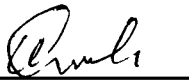

Name: **(Khalid Mahmood)**

Certificate of Approval

This is to certify that the research work presented in this thesis, entitled: **Some stagnation point flows on a lubricated surface** was conducted by **Mr. Khalid Mahmood,** Reg. No. **25-FBAS/PHDMA/F12** under the supervision of **Prof. Dr. Muhammad Sajid, TI** no part of this thesis has been submitted anywhere else for any other degree. This thesis is submitted to the **Department of Mathematics & Statistics, FBAS, IIU, Islamabad** in partial fulfillment of the requirements for the degree of **Doctor of Philosophy in Mathematics, Department of Mathematics & Statistics, Faculty of Basic & Applied Science, International Islamic University, Sector H-10, Islamabad, Pakistan.**

Student Name: Khalid Mahmood Signatures: _____

Examination Committee:

a) External Examiner 1:
Name/Designation/Office Address) Signatures: _____
Prof. Dr. Tasawar Hayat
Professor of Mathematics, QAU, Islamabad.

b) External Examiner 2:
Name/Designation/Office Address) Signatures: _____
Prof. Dr. Saleem Asghar
Professor of Mathematics, COMSATS, IIT, Islamabad.

c) Internal Examiner:
Name/Designation/Office Address) Signatures: _____
Dr. Ahmer Mehmood
Associate Professor of Mathematics, IIU, Islamabad.

Supervisor Name: Signatures: _____
Prof. Dr. Muhammad Sajid, TI

Co-Supervisor Name: Signatures: _____
Dr. Nasir Ali

Name of Dean/HOD Signatures: _____
Prof. Dr. Muhammad Arshad Zia

Acknowledgement

First of all, I pay my special thanks to the creator of mankind, the everlasting Allah, who gave us this life, taught us everything we did not know, granted us health, knowledge and intelligence to extract the hidden realities in the universe through scientific and critical approach. I just want to add this verse, start learning with the name of Almighty Allah and you will find the right way you even never expected. I thank the Lord Almighty with whose kindness I have achieved this very important goal in my life. I offer salutations upon the Holy Prophet, Hazrat Muhammad (PBUH) who has lightened the life of all mankind with His guidance. He is a source of knowledge and blessings for the entire creations. His teachings make us to ponder and to explore this world with directions of Islam.

I express my profound gratitude to my respectable supervisor Prof. Dr. Muhammad Sajid and honorable co-supervisor Dr. Nasir Ali, who helped me throughout my PhD thesis. Their valuable comments and suggestions put me on the straight path when I was led astray. I also pay my regards to my teachers Prof. Dr. M. Arshad Zia, Dr. Tariq Javed and Dr. Ahmed Zeeshan who always directed me to right dimensions and made it possible for me to achieve an attractive goal.

I would like to thank all my friends especially, Dr. M. Naveed, Dr. Sami Ullah, Dr. Khurram Javed, Dr. Akbar Zaman, Dr. Irfan Mustafa, Dr. Abuzar Ghaffari, Dr. Abid Majeed, Mr. Asif Javed, Mr. Zeeshan Asghar, Mr. Aamır Abbasi, Mr. Raheel Ahmed, Mr. M. Usman, Mr. M. Bilal, Mr. Ziafat Mehmood, Mr. Saleem Iqbal, Mr. Arshad Siddiqui, Mr. Abdul Haleem and Mr. Noveel Sadiq who helped me during my studies in all respect. I am also thankful to my principal Dr. Ehsan Mahmood who always spare me from college whenever I needed. Special thanks to my colleagues Mr. M. Zubair, Mr. Maqsood Ahmed, Mr. M. Ishtiaq and other college fellows who always encouraged me during studies.

I extend my gratitude to my family, specially my wife and brothers for encouragement and support, for their support in hard times. I am indebted to my parents for their prayers and love. I am nothing without you my mom and dad. You are always in my heart. Your sustained hope led me to where I am today.

I am very thankful to Higher Education Commission, Pakistan for providing me laptop.

Khalid Mahmood

Dedicated to_____

This thesis is dedicated to my supervisor, ***Prof. Dr. Muhammad Sajid****, who accepted me as PhD student. It is matter of pride and privilege for me to be his student. He is the chief architect of all my achievements. I owe gratitude to him for his enthusiastic and vigilant supervision. His sober, graceful and elegant personality along with his dedication to work will provide me a creative force at all the difficult times to come in the future.*

Abstract

The main objective of the present thesis is to study the orthogonal / non-orthogonal stagnation-point flows on a stationary / rotating lubricated surface. The lubricated thin layer is modeled as a power-law fluid. The fluid impinging on the lubricated surface is described by constitutive relationships of viscous, second grade and couple stress fluids. Additional features like heat transfer analysis, slip effects due to lubrication and impact of magnetic field are also studied. Interfacial condition between bulk fluid and the lubricant are derived by imposing the continuity of shear stress and velocity of both fluids. The transformed boundary value problems consist of highly non-linear and coupled differential equations subject to non-linear and coupled boundary conditions. An implicit finite difference scheme known as Keller-box method is employed to solve such a complicated system of equations numerically. The quantities of interest like fluid velocity, temperature, pressure, skin friction and local Nusselt number are analyzed for several values of involved parameters. The effects of involved parameters on the location of the stagnation point are also displayed. Finally, a comparison of the obtained solutions with the existing results for the no-slip case is also presented.

Contents

Preface

One of the classical flow problems in fluid dynamics that has received considerable attention of the researchers working in the field is the two-dimensional stagnation-point flow. A stagnation-point flow is observed in the situations whenever the fluid impinges on a solid object. The fluid velocity reduces to zero and the fluid pressure, heat and mass transfer rates are highest at the stagnation-point. Stagnation-point flow has been encountered in numerous applications in engineering and technological processes. It can be located in the stagnation region of flow passing a body of any shape. The literature survey reveals that the stagnation-point flow can be discussed either when the flow impinges on the wall orthogonally called orthogonal stagnation-point flow or when the flow impinges on the wall obliquely called oblique stagnation-point flow. The study of impinging jet problems has been of considerable interest during past few decades because of great technical importance in many industrial applications, such as drying of papers and films, tempering of glass and metal during processing, cooling of gas turbine surfaces and electronic components, surface painting, pest-citing and de-icing.

Stagnation point flows past a lubricated surface is another area that has got attention of researchers in the recent past due to their significant importance in the engineering and technological fields. An extensive amount of literature is available for the stagnation-point flows over rough surfaces. However, the stagnation-point flows and heat transfer past a lubricated surface is an area which has not been investigated in depth despite of its enormous practical applications in industry and engineering, such as cooling of nuclear reactors and cooling of electronic devices by fans, in the design of radial diffusers and thrust bearings, drag reduction and many hydrodynamic processes.

The study of heat transfer in boundary layer flows is important in many engineering applications such as the design of thrust bearings and radial diffusers, transpiration cooling, drag reduction, thermal recovery of oil, etc. The heat transfer rate is very important in the process of manufacturing of sheets. The mass and heat transfer mechanism occurs in many processes such as polymer engineering, electro chemistry, cooling and drying of paper and textiles etc

In certain stagnation flow problems, the Navier-Stokes equations reduce to nonlinear ordinary differential equations through similarity transformations. But these equations fail to explain the phenomenon like shear thinning, shear thickening, normal stresses, shear relaxation and retardation In such situations, the constitutive equations of non-Newtonian fluids are preferred which are highly nonlinear partial differential equations having order higher than Navier-stokes equations The situation becomes more complex when one considers a lubricated surface due to the which the corresponding boundary conditions are also nonlinear. The exact or analytical solutions in such cases are not possible in general and one needs to look for numerical solutions. In the present thesis such highly nonlinear coupled equations subject to nonlinear coupled boundary conditions are solved numerically by implementing an implicit finite difference scheme namely the Keller-box method. The chapter wise layout of the thesis is as follows:

Chapter one contains literature review and background relating to stagnation-point flows. The governing mass and momentum conservation equations for rectangular and cylindrical coordinates are included. In the later part of the chapter, the Keller-box method is described through the solution of a simple boundary value problem. It is also pertinent to mention here that the constitutive equation of a power-law fluid is used to model the thin lubrication layer of variable thickness in all subsequent chapters. This equation along with the constitutive equations of other non-Newtonian models is also included in chapter one.

Chapter two investigates non-orthogonal stagnation-point flow of a viscous fluid over a lubricated surface. To derive the interfacial condition, the continuity of velocity and shear stress has been imposed. The flow equations are reduced to a set of ordinary differential equations by means of similarity transformations. The numerical solutions are obtained through Keller-box method. Flow characteristics along with location of stagnation-point are discussed for the effects of emerging parameters through graphs and tabular data. A comparison of the obtained solutions with the existing results for the no-slip case is also presented. The results of this chapter are accepted for publication in **Journal of Applied Mechanics and Technical Physics**.

Chapter three is presented to discuss non-orthogonal stagnation-point flow of a second grade fluid past a lubricated surface The statement of the problem is based upon the

continuity of velocity and shear stress at the interface of both fluids along with laws of conservation of mass and linear momentum. The boundary value problems are solved numerically by Keller-box method for the certain range of slip parameter, Weissenberg number and a free parameter. A comparison between the numerical results of this chapter with the already reported data is made. The contents of this chapter are published in **Zeitschrift fur Naturforschung A (ZNA), 2016, 71(3), 273–280.**

Chapter four is concerned with oblique stagnation-point flow of a couple stress fluid over a lubricated surface. Governing partial differential equations of couple stress fluid are converted into ordinary differential equations using similarity transformations. Analysis has been performed by imposing continuity of velocity and shear stress of both the fluids at the interface. Influence of slip and couple stress parameters on the horizontal and shear velocity components, wall shear stress and stagnation-point is displayed graphically and in the tabular form. The present solution is found in good agreement with the existing results. Findings of this chapter have been submitted to **Bulgharian Chemical Communication.**

Chapter five describes slip flow of a second grade fluid past a lubricated rotating disc. The interfacial conditions between fluid and lubricant are imposed on the surface of disc by assuming a thin lubrication layer. The effects of slip parameter and Weissenberg number on the three components of fluid velocity and pressure are analyzed graphically while effects on both components of skin friction are demonstrated through tables. The computed results show that spin-up by a second grade bulk fluid near the rotating disc is reduced by increasing slip at the interface. The obtained results are published in **International Journal of Physical Sciences, 11, 96-103 (2016).**

Chapter six is devoted to study heat transfer analysis in the time-dependent slip flow over a lubricated rotating disc. Appropriate transformations are utilized to convert the governing partial differential equations into nonlinear coupled ordinary differential equations. Interfacial conditions have been derived with the help of continuity of shear stress and velocity of the lubricant and the core fluid. Impact of physical parameters in the presence of lubrication on fluid velocity, temperature and pressure is displayed graphically. The skin friction coefficients and local Nusselt number are examined through tables. The results in the special case are found in good agreement with the existing results in the literature. The

results of this chapter are published in **Engineering Science and Technology, an International Journal, 19 (2016) 1949–1957.**

Chapter seven is devoted to analyze the heat transfer in the time-dependent axisymmetric stagnation-point flow over a lubricated surface. It is assumed that surface temperature of the disc is time-dependent. Continuity of velocity and shear stress at the interface layer between the fluid and the lubricant is imposed to obtain the numerical solution of the governing partial differential equations. The computations are presented in the form of graphs and tables in order to examine the influence of pertinent parameters on the flow and heat transfer characteristics. An increase in lubrication results in the reduction of surface shear stress and consequently viscous boundary layer becomes thin. However, the thermal boundary layer thickness increases by increasing lubrication. It is further observed that wall shear stress and heat transfer rate at the wall grow due to unsteadiness. The results for the steady case are deduced from the present solutions and are found in good agreement with the existing results in the literature. Findings of this chapter are published in **Thermal Science, DOI: 10.2298/TSCI160203257M.**

Chapter eight examines MHD mixed convection stagnation-point flow of a viscous fluid over a lubricated vertical surface. The obtained set of flow and energy equations are converted into ordinary differential equations by means of similarity variables. To derive the interfacial conditions, continuity of shear stress and velocity of the lubricant and core fluid is imposed. Impact of emerging parameters in the presence of lubrication on fluid velocity and temperature is displayed graphically The contents have been accepted in **Industrial Lubrication and Tribology**.

Chapter nine is presented to describe the effects of lubrication in MHD mixed convection stagnation-point flow of a second grade fluid adjacent to a vertical plate. A power-law fluid is utilized for the purpose of lubrication. Interfacial conditions are obtained by implementing continuity of shear stress and velocity of both fluids. Boundary value problems are obtained by using suitable similarity variables. Influence of different parameters on the velocity and temperature profiles are represented through graphs and tables. These findings are published in **Revista Mexicana de Fisica, 63 (2017) 134–144.**

Chapter 1

Introduction

This chapter is included to introduce readers with the relevant literature and governing equations. The equations that govern the flow and heat transfer namely continuity, momentum and energy equations are presented both in rectangular and cylindrical coordinates. The constitutive relationships of the viscous, second grade, couple stress and power-law fluids and governing equations of magnetohydrodynamics are also included. The Keller-box numerical method is explained through an example at the end of this chapter.

1.1 Literature review

The concept of boundary layer theory introduced by Prandtl [1] has gained significant importance in fluid mechanics. Schlichting [2] studied different aspects of the boundary layer flow and transportation phenomena in fluid mechanics and a good comparison between the theoretical and experimental results was achieved by him. Extensive research work is available in the literature on the boundary layer flows for viscous and non-Newtonian fluids.

One of the classical flow problems in fluid dynamics is the stagnation-point flow and it has received considerable attention of the researchers working in the field because of its importance in many engineering disciplines. A stagnation-point occurs whenever a fluid hits the surface at certain angle. Stagnation-point flows are involved in cooling of nuclear reactors, extrusion of polymer sheets, cooling of computer and other electronic devices by fans, manufacturing of artificial fibers and many hydro-dynamical processes. The literature survey reveals that one can discuss the stagnation-point flow either when the flow impinges on the wall orthogonally or when the flow impinges on the wall obliquely. The pioneering work on the stagnation-point flow was carried out by Hiemenz [3]. He provided an exact solution for the Newtonian case. Stagnation-point flow towards a stretching plate was examined by Chiam [4]. Wang [5] studied stagnation flow impinging on a shrinking sheet.

The pioneering work on the axisymmetric stagnation-point flow was carried out by Homann [6] and Frossling [7]. The three-dimensional orthogonal stagnation-point flow was studied by Howarth [8] and Davey [9].

In the above mentioned studies the velocity and flow pattern are independent of time. However, in many engineering and technological problems, the flow starts impulsively from rest and the unsteady aspects become more interesting. The unsteady stagnation-point flow over a flat plate was initially discussed by Yang [10]. Williams [11] and Cheng et al. [12] investigated the unsteady axisymmetric three dimensional stagnation flow on a stationary disc. Nazar et al. [13] studied the time-dependent two-dimensional stagnation-point flow over a flat stretching sheet moving with velocity proportional to the distance from stagnation-point. The unsteady stagnation-point flow with a span-wise oscillating wall was addressed by Fang and Lee [14]. Cheng and Dai [15] investigated the unsteady two-dimensional stagnation-point flow of a viscous fluid over a stretching sheet using homotopy analysis method. Unsteady stagnation-point flow impinging over a flat plate was discussed by Zhong and Fang [16] for the planner and axisymmetric cases. The unsteady flow past a stretching sheet in the vicinity of stagnation point was investigated by Pop and Na [17] They proved that the unsteady flow approaches the steady state situation for large values of time.

The study for oblique stagnation-point flow has been discussed by many investigators such as Stuart [18], Tamada [19] and Dorrepaal [20, 21] etc. They considered the oblique flow as the combination of orthogonal stagnation-point flow with a shear flow parallel to the wall. Later the problem was reviewed by Drazin and Riley [22] and Tooke and Blyth [23] to include a free parameter associated with the superimposed shear flow component. This model has been applied to MHD flow by Borrelli et al. [24] and on moving surface by Lok et al. [25] Lok et al. [26] discussed non-orthogonal stagnation-point flow towards a stretching sheet. Tilley and Weidman [27] discussed non-orthogonal stagnation-point for two-fluids Labropulu et al. [28] discussed heat transfer analysis for the oblique flow impinging on a stretched sheet. Axisymmetric non-orthogonal stagnation-point flow over a circular cylinder has been considered by Weidman and Putkaradze [29]. Recently, Ghaffari et al. [30, 31] and Javed et al. [32] discussed different aspects for the oblique stagnation point flows

A solution of the Navier-Stokes and energy equations illustrating skin friction and temperature distribution in the stagnation-point flow over an infinite plate was presented by Stuart [33]. Gorla [34] investigated heat transfer in an axisymmetric stagnation flow on a cylinder. Axisymmetric stagnation-point flow with heat transfer of a viscous fluid on a moving cylinder with unsteady axial velocity and uniform transpiration was analyzed by Saleh and Rahimi [35]. In another paper Abbasi and Rahimi [36] studied three-dimensional stagnation-point flow and heat transfer on a flat plate with transpiration. Recently, Abbasi and Rahimi [37] carried out an investigation of heat transfer in two-dimensional stagnation-point flow impinging on a flat plate. Massoudi and Razeman [38] studied heat transfer analysis of a viscoelastic fluid at a stagnation-point Elbashbeshy and Bazid [39] analyzed heat transfer in an unsteady boundary layer flow over a stretching sheet and found that thermal and momentum boundary layer thickness depends upon unsteadiness parameter.

In the above studies mostly the constitutive equation of a viscous fluid is considered. However, it is now an established fact that Navier-Stokes equations are inadequate for the fluids that exist in industry and technology. Such fluids are called non-Newtonian fluids. Examples include food, rubber, gel, petrol, paper coating, plasma, grease, polymer solutions, polymer melts blood, paints, oils etc Flow of non-Newtonian fluids has attracted attention of many scientists and researchers because of their fundamental and practical importance in the industry, applied sciences, engineering as well as in the daily life. Shear stress of such fluids is nonlinearly related with shear rate and it makes difficult to analyze their flow. Several non-Newtonian models have been developed to discuss the phenomena like normal stress effect, shear thinning, shear thickening, stress relaxation and retardation etc. The governing equations representing the flows of these fluids are highly nonlinear and are difficult to solve even by a numerical approach.

Among several non-Newtonian fluids, the second grade fluid is one that has received much attention recently as it exhibits viscous and elastic-like characteristics when undergoing deformation. Honey, plastic films and artificial fibers are some examples of fluids whose rheological behavior can be discussed through the constitutive equation of second grade fluids. The equations of motion of second grade fluid are highly nonlinear and one order higher than the Navier-Stokes equations. For this reason, additional boundary conditions

are required to discuss the flow problems associated with the second grade fluid model. Rajagopal [40] and Beard and Walters [41] developed the boundary layer equations of second grade fluids and Rajagopal and Kaloni [42] discussed the issue of paucity of boundary conditions for these fluids. Rajagopal et al. [43] and Rajagopal and Gupta [44] solved the flow problem related to second grade fluid by using a supplement boundary condition at the free stream. The analysis for the stagnation-point flows of second grade fluids was carried out by Srivatsava [45], Rajeswari and Rathna [46], Beard and Walters [47], Garg and Rajagopal [48] and Ariel [49]. Beard and Walters [47] used a regular perturbation technique to tackle the paucity of boundary conditions. Garg and Rajagopal [48] and Ariel [49] overcame this difficulty by augmenting the boundary conditions at infinity. Ayub et al. [50] investigated viscoelastic second grade fluid flow near a stagnation-point due to a stretching sheet. Labropulu et al. [51] have extended the classical Hiemenz's flow of a viscoelastic second grade fluid to oblique stagnation-point flow. Oblique stagnation-point flow of an incompressible viscoelastic second grade fluid towards a stretching surface is investigated by Mahapatra et al. [52]. The unsteady stagnation-point flow of a second grade fluid has been discussed by Labropulu et al. [53]. Effects of Weissenberg number on the flow and heat transfer in the stagnation-point were analyzed by Li et al [54].

Couple stress fluid model is another important non-Newtonian model first proposed by Stokes [55], to describe the polar effects. The couple stress fluid can be described by a new type of tensor called couple stress tensor in addition to the Cauchy stress tensor. In such fluids, polar effects play a significant role which are present due to the couple stresses and body couples. Because of significant importance in the industrial and engineering applications, many researchers have analyzed the flows of couple stress fluids. Some examples of fluids that can be described by couple stress model are animal blood, liquid crystals, polymer thickened oil and polymeric suspensions. Devakar et al. [56] discussed the Stokes problems for couple stress fluid. In another investigation, Devakar et al. [57] investigated the flow of couple stress fluid flowing between parallel plates. Heat transfer analysis for the flow of a couple stress fluid near a stagnation-point has been carried out by Hayat et al [58]. Muthuraj et al. [59] studied viscous dissipation effects on hydromagnetic flow of a couple stress fluid in a vertical channel. Heat transfer analysis has been carried

out by Srinivasacharya et al. [60] for couple stress flow due to expanding and contracting walls in a porous channel. Flow of couple stress fluid due to free convection through a porous channel was carried out by Hiremath and Patil [61]. Umavathi et al. [62] discussed heat transfer for the channel flow of a couple stress fluid sandwiched between two viscous fluids. They showed that couple stress parameter is responsible for enhancing the fluid velocity. Ramesh and Devakar [63] studied porous-saturated effects of heat and mass transfer on the peristaltic transport of electrically conducting couple stress fluid through porous medium in a vertical asymmetric channel.

The problems on magnetohydrodynamic (MHD) stagnation-point flows have been discussed by Chamkha [64], Chamkha and Issa [65], Kumari [66] and Prasad et al. [67]. In recent years many researchers are taking interest in the area where such flow situation occurs. The study of MHD flow of an electrically conducting fluid is of significant importance in modern metallurgical and metal working processes. Magnetic field affects the velocity gradient and heat transfer rate at the surface due to increase in the Lorentz force. Attia [68] reported the effects of increasing magnetic field on velocity and boundary layer thickness in a stagnation-point flow. The influence of an applied magnetic field on Maxwell fluid for the flow of both steady and unsteady cases in a region of stagnation-point was studied by Kumari and Nath [69]. They found that velocity gradient at the surface and heat transfer are modified under the influence of Hartmann number. Singh et al. [70, 71] investigated effects of magnetic and radiation parameters on stretching sheet for steady and unsteady flows. Ziya et al. [72, 73] discussed MHD free convection flow of a viscous fluid through inclined porous plate in the presence of high temperature. MHD stagnation-point flow of a power-law fluid towards a stretching surface was discussed by Mahapatra et al. [74]. Problem of mixed convection flow near the stagnation-point against a heated vertical semi-infinite permeable surface for viscous fluid in the presence of an applied magnetic field has been investigated by Abdelkhalek [75]. Aydin and Kaya [76] presented mixed convection flow of a viscous dissipating fluid over a vertical flat plate. Problem of mixed convection in stagnation-point flows adjacent to vertical surfaces was investigated by Ramachandran et al. [77]. Devi et al. [78] discussed unsteady mixed convection flow in stagnation region adjacent to a vertical surface. A study on combined forced and free convection in stagnation flows of micropolar fluid over a vertical non-isothermal surface

was presented by Hassanien and Gorla [79]. Lok et al. [80] studied unsteady mixed convection flow of a micropolar fluid near the stagnation-point on a vertical surface. MHD mixed convection boundary layer flow towards a stagnation-point on a vertical surface with induced magnetic field was presented by Nazar et al. [81]. Ishak et al. [82] considered a steady MHD flow towards a stagnation-point on a vertical surface immersed in a micropolar fluid. In a later attempt, Ishak et al. [83] investigated the problem of MHD mixed convection flow near the stagnation-point on a vertical permeable surface. Hayat et al. [84] presented mixed convection effects in the stagnation-point flow adjacent to a vertical surface in a viscoelastic fluid. Hayat et al. [85] also discussed the Homotopy based analytical solution of steady MHD two-dimensional mixed convection boundary layer flow of a viscous incompressible fluid near the stagnation-point on a vertical stretching surface embedded in a fluid-saturated porous medium with thermal radiation effects. MHD mixed convection in a vertical annulus filled with Al_2O_3-water nano-fluid considering nanoparticles migration was analyzed by Malvandi et al. [86]. Recently Afrand et al. [87] discussed effects of magnetic field on free convection flow in inclined cylindrical annulus containing molten Potassium. Safaei et al. [88] carried out numerical study of laminar mixed convection heat transfer of power-law non-Newtonian fluid in square enclosures by finite volume method. Recently Naveed et al. [89] studied hydromagnetic flow past a time-dependent curved stretching surface. Khalid et al. [90] produced theoretical results to investigate time-dependent MHD flow of a Casson fluid. They considered a free convective flow along an oscillating surface placed vertically in a porous medium. Effects of an applied magnetic field in an unsteady radioactive flow of a nanofluid with dust particles past a stretching surface was examined by Kumar et al. [91]. Heat and mass transfer for a MHD Casson fluid past an exponentially permeable stretching sheet is investigated by Raju et al. [92].

The flow of fluid in the vicinity of a rotating disc has many applications in fluid mechanics, engineering and industry. A few examples of such flows include spin coating, water treatment plants, washing machines, spinning disc reactors, turbines, viscometers, sports discs, fans rotors, electrochemical engineering, computer storage devices, centrifugal pumps etc. Shear stress generated by the flowing fluid is utilized to control the boundary layer thickness, to produce photographic films and papers, to clean the surface of objects,

to cool the hot skin of machines and crafts and to regulate the thickness in the wire coating mechanism. Furthermore, the flow over a rotating surface also finds direct applications to waste water treatment, turbo-machinery, viscometry, centrifugal pumps, computer discs, sports discs and rotating blades. The stagnation-point flow of Newtonian fluid over a rotating disc was initially discussed by Von Karman [93]. He transformed the set of partial differential equations into ordinary differential equations by introducing an elegant similarity transformation and solved the resulting equations by momentum integral method. Due to importance of rotating flows in the fields of engineering and technology much extensions and modifications with more accurate solutions of Von Karman's flow have been presented in the literature. In 1934, Cochran [94] obtained asymptotic solution of the Von Karman's flow problem Benton [95] improved the Cochran's results and extended the problem by taking into account the unsteady case. Sparrow and Gregg [96] studied the steady state heat transfer from a rotating disc by taking different values of Prandtl numbers. Some more investigations on the rotating disc were made by Kakutani [97], Sparrow and Chess [98], Pande [99], Watson and Wang [100], Kumar et al. [101] and Miklavcic and Wang [102]. Asghar et al. [103] carried out Lie group analysis of flow and heat transfer of a viscous fluid on a rotating disk stretched in radial direction. Recently, Turkyilmazoglu [104-108] investigated different aspects of fluid flow and heat transfer due to rotating disc. Impact of normal blowing on the fluid flow caused by a rotating disc was studied by Kuiken [109]. Watanabe and Oyama [110] discussed heat transfer analysis of electrically conducting fluid near a rotating disc. Wang [111] considered the flow towards a stagnation-point near an off-centered rotating disc. He found that disposition of disc makes the flow phenomenon more complex. The problem of Wang [111] was reconsidered by Nourbakhsh et al. [112]. They reshaped the results using an analytical technique. The unsteady MHD flow with heat transfer of a fluid film spread over a rotating infinite disc was treated by Kumari and Nath [113]. They obtained two solutions by taking thin and thick films of fluid. Munawar et al. [114] analyzed unsteady flow near a stagnation-point due to a rotating disc. Thacker et al. [115] re-examined the work of Sparrow and Chess [98] by applying suction and injection at the disc surface. Hannah [116] discussed the axisymmetric stagnation-point flow of a viscous fluid towards a rotating disc for the first time. Tifford and Chu [117] found the exact solution of the problem considered by Hannah

[116]. Asghar et al. [118] investigated MHD flow due to non-coaxial rotation of an accelerated disc. Attia [119] studied the flow due to a rotating disc under the influence of an external uniform magnetic field.

In all above investigations the conventional no-slip has been imposed at fluid-solid interface. However, there are many situations where the no-slip boundary condition is not realistic and can be replaced by the linear slip boundary condition proposed by Navier [120] and Maxwell [121] independently. Typical examples are emulsions, foams, suspensions and polymer solutions. Beavers and Joseph [122] discussed the slip boundary condition in detail. Yeckel et al. [123] discussed stagnation-point flow on a rigid plate against a thin lubrication layer for the first time. Blyth and Pozrikidis [124] studied stagnation-point flow of a viscous fluid past a liquid film on a plane wall. A literature survey indicates that a number of flow problems of viscous fluids have been analyzed using the Navier slip boundary condition [125-128]. Flow of a viscous fluid over a stretching sheet with partial slip was examined numerically by Wang [129]. The problem considered by Wang [129] is solved for an exact solution by Anderson [130]. Ariel [131] discussed the slip effects on an axisymmetric flow over a stretching sheet and obtained a numerical solution of the problem. Fazlina et al. [132] discussed slip effects on mixed convective stagnation-point flow and heat transfer over a vertical surface. Sajid et al. [133] analyzed the unsteady flow of a viscous fluid with partial slip through a porous medium. The partial slip condition is replaced by a general slip boundary condition in a recent article by Sajid et al. [134] Ariel et al. [135] analyzed the slip effects on the stretching flow of a Walter-B fluid and obtained an exact solution of the problem The heat transfer analysis for the slip flow of a second grade fluid is discussed by Hayat et al. [136] using the homotopy analysis method Sahoo [137] examined the partial slip on axisymmetric flow of an electrically conducting viscoelastic fluid. More recently, Sahoo [138] provided the numerical solution for the axisymmetric slip flow of a second grade fluid over a radially stretching sheet. Frusteri and Osalusi [139] investigated the effects of slip at permeable disc. Impact of slip for the flow through two stretchable disks is studied by Munawar et al. [140] using HAM. Labropulu and Li [141] discussed stagnation-point flow of a second grade fluid with slip. Latiff et al [142] explored time-dependent forced bio-convection slip flow of a micropolar

nanofluid over a shrinking/stretching surface. Influence of multiple-slip in buoyancy-driven bio-convection nanofluid flow is analyzed by Uddin et al. [143].

The study of flow phenomenon over a lubricated surface has important applications in machinery components such as fluid bearings and mechanical seals. Coating is another major application including the preparation of thin films, printing, painting and adhesives. In biological fluids, the applications of such flows include flow of red blood cells in narrow capillaries and of liquid flow in the lungs and eyes. A review of literature suggests that various attempts are available for the flow over a lubricated surface. In 1980, Joseph [144] discussed boundary conditions for thin lubrication layers. Andersson and Valnes [145] derived generalized slip-flow boundary conditions for non-Newtonian lubrication layers. The slip flow over a lubricated surface is considered by Solbakken and Anderson [146]. The slip boundary conditions for the viscous flow past a power-law lubricant was derived by Andersson and Rousselet [147] for the first time. They obtained the similarity solution numerically for power-law lubricant by taking the value of power-law index $n = 1/3$. The axisymmetric stagnation-point flow of a viscous fluid past a power-law lubricant has been discussed by Santra et al. [148]. Recently Sajid et al. [149] extended the work of Santra et al. for a generalalized slip boundary condition proposed by Thompson and Troian [150] on the basis of molecular dynamics simulation. In another paper Sajid et al. [151] investigated stagnation-point flow of Walter-B fluid over a lubricated surface. The axisymmetric stagnation-point flow of second and third grade fluids over a lubricated surface has been examined respectively by Ahmed et al. [152] and Sajid et al. [153]

A literature survey indicates that the literature is scarce on orthogonal stagnation-point flow over a vertical lubricated surface, non-orthogonal stagnation-point flows over a lubricated surface and flow over a lubricated rotating disc. Our aim in the present thesis is to discuss the various aspects regarding stagnation-point flows and heat transfer of Newtonian / non-Newtonian fluids over a plate/disc lubricated with power-law fluid. A new slip condition at the interface of the bulk fluid and power- law fluid has been derived and results for no-slip and full-slip cases have been deduced from the obtained numerical solutions. The main objective is to investigate the influence of emerging parameters on the flow and heat

transfer characteristics in the presence of lubrication. The numerical solutions are developed by using Keller-box method [154-161].

1.2 Continuity equation in rectangular and cylindrical coordinates

The equation representing the mass conservation is given by

$$\frac{\partial \rho}{\partial t} + \nabla.(\rho \boldsymbol{V}) = 0, \tag{1.2}$$

in which ρ is density, t is time and $\boldsymbol{V} = [u, v, w]$, where u, v and w are the components of velocity in three orthogonal directions respectively. The continuity equation respectively in rectangular and cylindrical coordinates is given as

$$\frac{\partial \rho}{\partial t} + \frac{\partial}{\partial x}(\rho u) + \frac{\partial}{\partial y}(\rho v) + \frac{\partial}{\partial z}(\rho w) = 0, \tag{1.3}$$

$$\frac{\partial \rho}{\partial t} + \frac{1}{r}\frac{\partial}{\partial}(r\rho u) + \frac{1}{r}\frac{\partial}{\partial \phi}(\rho v) + \frac{\partial}{\partial z}(\rho w) = 0. \tag{1.4}$$

Equation (1.2) for steady incompressible flow becomes

$$\nabla.\boldsymbol{V} = 0. \tag{1.5}$$

In terms of Cartesian and cylindrical coordinates, Eq. (1.5) gives

$$\frac{\partial u}{\partial x} + \frac{\partial v}{\partial y} + \frac{\partial w}{\partial z} = 0, \tag{1.6}$$

$$\frac{\partial u}{\partial r} + \frac{u}{r} + \frac{1}{r}\frac{\partial v}{\partial \phi} + \frac{\partial w}{\partial z} = 0. \tag{1.7}$$

1.3 Equation of motion in rectangular and cylindrical coordinates

Equation of motion in vector form is given by

$$\rho\left(\frac{\partial \boldsymbol{V}}{\partial t}\right) + \rho(\boldsymbol{V}.\nabla \boldsymbol{V}) = -\nabla P + \nabla.\boldsymbol{\tau} + \rho \boldsymbol{b}, \tag{1.8}$$

where $\boldsymbol{\tau}$ is the extra stress tensor, P is the pressure and $\boldsymbol{b}$ is the body force per unit volume. Neglecting body force, Eq. (1.8) in component form for Cartesian coordinates yields

$$\rho\left(\frac{\partial u}{\partial t}+u\frac{\partial u}{\partial x}+v\frac{\partial u}{\partial y}+w\frac{\partial u}{\partial z}\right)=-\frac{\partial P}{\partial x}+\left(\frac{\partial \tau_{xx}}{\partial x}+\frac{\partial \tau_{yx}}{\partial y}+\frac{\partial \tau_{zx}}{\partial z}\right), \tag{1.9}$$

$$\rho\left(\frac{\partial v}{\partial t}+u\frac{\partial v}{\partial x}+v\frac{\partial v}{\partial y}+w\frac{\partial v}{\partial z}\right)=-\frac{\partial P}{\partial y}+\left(\frac{\partial \tau_{xy}}{\partial x}+\frac{\partial \tau_{yy}}{\partial y}+\frac{\partial \tau_{zy}}{\partial z}\right), \tag{1.10}$$

$$\rho\left(\frac{\partial w}{\partial t}+u\frac{\partial w}{\partial x}+v\frac{\partial w}{\partial y}+w\frac{\partial w}{\partial z}\right)=-\frac{\partial P}{\partial z}+\left(\frac{\partial \tau_{xz}}{\partial x}+\frac{\partial \tau_{yz}}{\partial y}+\frac{\partial \tau_{zz}}{\partial z}\right). \tag{1.11}$$

Similarly, Eq. (1.8) in cylindrical coordinates gives

$$\rho\left(\frac{\partial u}{\partial t}+u\frac{\partial u}{\partial r}+\frac{v}{r}\frac{\partial u}{\partial \phi}-\frac{v^2}{r}+w\frac{\partial u}{\partial z}\right)=-\frac{\partial P}{\partial r}+\left(\frac{1}{r}\frac{\partial(r\tau_{rr})}{\partial r}+\frac{1}{r}\frac{\partial \tau_{\phi r}}{\partial \phi}-\frac{\tau_{\phi\phi}}{r}+\frac{\partial \tau_{zr}}{\partial z}\right), \tag{1.12}$$

$$\rho\left(\frac{\partial v}{\partial t}+u\frac{\partial v}{\partial r}+\frac{v}{r}\frac{\partial v}{\partial \phi}+\frac{uv}{r}+w\frac{\partial v}{\partial z}\right)=-\frac{1}{r}\frac{\partial P}{\partial \phi}+\left(\frac{1}{r^2}\frac{\partial(r^2\tau_{r\phi})}{\partial r}+\frac{1}{r}\frac{\partial \tau_{\phi\phi}}{\partial \phi}+\frac{\partial \tau_{z\phi}}{\partial z}+\frac{\tau_{\phi r}-\tau_{r\phi}}{r}\right), \tag{1.13}$$

$$\rho\left(\frac{\partial w}{\partial t}+u\frac{\partial w}{\partial r}+\frac{v}{r}\frac{\partial w}{\partial \phi}+w\frac{\partial w}{\partial z}\right)=-\frac{\partial P}{\partial z}+\left(\frac{1}{r}\frac{\partial(r\tau_{rz})}{\partial r}+\frac{1}{r}\frac{\partial \tau_{\phi z}}{\partial \phi}+\frac{\partial \tau_{zz}}{\partial z}\right). \tag{1.14}$$

1.4 Energy equation in rectangular and cylindrical coordinates

Equation that governs the heat transfer in a fluid flow is given by

$$\rho c_p\left(\frac{\partial T}{\partial t}+(\boldsymbol{V}\cdot\nabla)T\right)=k^*\nabla^2T+\boldsymbol{\tau}:\nabla\boldsymbol{V}, \tag{1.15}$$

in which c_p is the specific heat, T is the temperature, k^* is the thermal conductivity and the last term is due to the viscous dissipation. In terms of Cartesian and cylindrical coordinates we can write

$$\rho c_p\left(\frac{\partial T}{\partial t}+u\frac{\partial T}{\partial x}+v\frac{\partial T}{\partial y}+w\frac{\partial T}{\partial z}\right)=k^*\left(\frac{\partial^2T}{\partial x^2}+\frac{\partial^2T}{\partial y^2}+\frac{\partial^2T}{\partial z^2}\right)+\left[\tau_{xx}\frac{\partial u}{\partial x}+\tau_{xy}\frac{\partial v}{\partial x}+\tau_{xz}\frac{\partial w}{\partial x}+\tau_{yx}\frac{\partial u}{\partial y}+\tau_{yy}\frac{\partial v}{\partial y}+\tau_{yz}\frac{\partial w}{\partial y}+\tau_{zx}\frac{\partial u}{\partial z}+\tau_{zy}\frac{\partial v}{\partial z}+\tau_{zz}\frac{\partial w}{\partial z}\right], \tag{1.16}$$

$$\rho c_p\left(\frac{\partial T}{\partial t}+u\frac{\partial T}{\partial r}+\frac{v}{r}\frac{\partial T}{\partial \phi}+w\frac{\partial T}{\partial z}\right)=k^*\left(\frac{\partial^2 T}{\partial r^2}+\frac{1}{r}\frac{\partial T}{\partial r}+\frac{1}{r^2}\frac{\partial^2 T}{\partial \phi^2}+\frac{\partial^2 T}{\partial z^2}\right)+\left[\tau_{rr}\frac{\partial u}{\partial r}+\tau_{r\phi}\frac{\partial v}{\partial r}+\right.$$

$$\left.\tau_{rz}\frac{\partial w}{\partial r}+\tau_{\phi r}\left(\frac{1}{r}\frac{\partial u}{\partial \phi}-\frac{v}{r}\right)+\tau_{\phi\phi}\left(\frac{1}{r}\frac{\partial v}{\partial \phi}+\frac{u}{r}\right)+\tau_{\phi z}\frac{1}{r}\frac{\partial w}{\partial \phi}+\tau_{zr}\frac{\partial u}{\partial z}+\tau_{z\phi}\frac{\partial v}{\partial z}+\tau_{zz}\frac{\partial w}{\partial z}\right]. \quad (1.17)$$

1.5 Maxwell's equations for magnetohydrodynamics

The subject which deals with the mutual interaction of the magnetic field and fluid flow is called magnetohydrodynamics (MHD). Maxwell's equations are the set of four equations which relates the magnetic and electric fields to their sources, current density and charge density. These equations are described as

$$\nabla . \boldsymbol{E} = \frac{\rho_e}{\varepsilon_o}, \quad \text{(Gauss's law in differential form)}, \quad (1.18)$$

$$\nabla \times \boldsymbol{B} = \mu_o \boldsymbol{J} + \mu_o \varepsilon_o \frac{\partial \boldsymbol{E}}{\partial t}, \quad \text{(Ampere- Maxwell equation)}, \quad (1.19)$$

$$\nabla \times \boldsymbol{E} = -\frac{\partial \boldsymbol{B}}{\partial t}, \quad \text{(Faraday's law)}, \quad (1.20)$$

$$\nabla \times \boldsymbol{B} = 0, \quad \text{(Solenoidal constraint on } \boldsymbol{B}\text{)}, \quad (1.21)$$

$$\boldsymbol{F} = \boldsymbol{J} \times \boldsymbol{B}, \quad \text{(Lorentz force)}, \quad (1.22)$$

$$\boldsymbol{J} = \sigma(\boldsymbol{E} + \boldsymbol{V} \times \boldsymbol{B}), \quad \text{(Ohm's law)}, \quad (1.23)$$

in which μ_o is the magnetic permeability, $\boldsymbol{B}$ the magnetic field, $\boldsymbol{E}$ the electric field, $\boldsymbol{J}$ the current density, ρ_e the charge density, ε_o the permittivity of the free space and σ the electrical conductivity. Conservation of charge density gives

$$\nabla . \boldsymbol{J} + \frac{\partial \rho_e}{\partial t} = 0. \quad (1.24)$$

In MHD, the charge density ρ_e has no significant role. Usually, ρ_e is significant only in Gauss's law and we simply drop Gauss' law and ignore ρ_e. Also in MHD the displacement currents are negligible as compared with the current density $\boldsymbol{J}$ and so the Ampere-Maxwell equation reduces to the differential form of the Ampere's law given by

$$\nabla \times \boldsymbol{B} = \mu_o \boldsymbol{J}. \quad (1.25)$$

We summarize the electrodynamics equations used in MHD as

Ampere's law and charge conservation

$$\nabla \times \boldsymbol{B} = \mu_o \boldsymbol{J}, \qquad \nabla . \boldsymbol{J} = 0. \tag{1.26}$$

Faraday's law and the solenoidal constraint on $\boldsymbol{B}$

$$\nabla \times \boldsymbol{E} = -\frac{\partial \boldsymbol{B}}{\partial t}, \quad \nabla . \boldsymbol{B} = 0. \tag{1.27}$$

Ohm's law and the Lorentz force

$$\boldsymbol{J} = \sigma(\boldsymbol{E} + \boldsymbol{V} \times \boldsymbol{B}), \quad \boldsymbol{F} = \boldsymbol{J} \times \boldsymbol{B}. \tag{1.28}$$

1.6 Newtonian and non-Newtonian fluids

1.6.1 Newtonian fluids

Fluids which obey the Newton's law of viscosity are called Newtonian fluids. Newton's law of viscosity is given by

$$\tau_{ij} = \mu A_{(1)ij}, \tag{1.29}$$

in which τ_{ij} is shear stress and $A_{(1)ij}$ is the first Rivlin-Ericksen tensor. The coefficient of viscosity for Newtonian fluids is constant at all shear rates.

1.6.2 Non-Newtonian fluids

Fluids which deviates from Newton's law of viscosity are known as non-Newtonian fluids. Viscosity of non-Newtonian fluids is not constant and is a function of shear rate. Generally non-Newtonian fluids are complex mixtures e.g. slurries, pastes, gels, polymer solutions etc. Due to complex nature of these fluids, it is impossible to represent them with a single constitutive relationship. These fluids exhibit different properties like shear thinning, shear thickening normal stress effects, stress relaxation, stress retardation, micro-rotation, couple stresses, body couples etc. The detail analysis of non-Newtonian fluids can be seen in the books by Bird et al [162], Harris [163] and Chhabra and Richardson [164]. In this thesis we have considered the constitutive relationships of second grade, couple stress and power-law fluids and details are given in following subsections.

1.6.2.1 Second grade fluid

The components of the Cauchy stress tensor for an incompressible second grade fluid are [165]

$$\tau_{ij} = \mu A_{(1)ij} + \alpha_1 A_{(2)ij} + \alpha_2 A_{(1)ik} A_{(1)kj}. \tag{1.30}$$

Here α_1 and α_2 are the material moduli known as cross-viscosity and viscoelasticity coefficients respectively. Fosdick and Rajagopal [166] argued that for a second grade model to be thermodynamically compatible, following constraints should hold

$$\mu \geq 0, \quad \alpha_1 \geq 0, \quad \alpha_1 + \alpha_2 = 0. \tag{1.31}$$

The components of first and second Rivlin-Ericksen tensors $\boldsymbol{A}_{(1)}$ and $\boldsymbol{A}_{(2)}$ are given by

$$A_{(1)ij} = V_{i,j} + V_{j,i} \quad \text{and} \quad A_{(2)ij} = a_{i,j} + a_{j,i} + 2V_{m,i}V_{m,j}, \tag{1.32}$$

where a_i's are the components of acceleration given by

$$a_i = \frac{\partial V_i}{\partial t} + V_j V_{i,j}. \tag{1.33}$$

1.6.2.2 Couple stress fluid

Couple stress fluid is another important non-Newtonian fluid that describes the polar effects. The couple stress fluid can be described by a new type of tensor called couple stress tensor in addition to the Cauchy stress tensor. In such fluids, polar effects play a significant role which are present due to the couple stresses (moment per unit area) and body couples (moment per unit volume) Because of significant importance of couple stress fluids in the industrial and engineering applications, many researchers have analyzed these flows. Some examples are animal blood, liquid crystals, polymer thickened oil and polymeric suspensions. The constitutive equation for a couple stress fluid is

$$\tau_{ij} = \tau_{ij}^S + \tau_{ij}^A, \tag{1.34}$$

where $\boldsymbol{\tau}^S$ and $\boldsymbol{\tau}^A$ are symmetric and antisymmetric parts of stress tensor $\boldsymbol{\tau}$ respectively and are defined as

$$\tau_{ij}^S = \mu A_{(1)ij}, \quad \tau_{ij}^A = -2\eta W_{ij,kk} - \frac{\rho}{2} e_{ijk} l_k, \tag{1.35}$$

in which W_{ij} is the vorticity tensor, e_{ijk} the alternating tensor and l_k the body couples. The tensor W_{ij} is defined as

$$W_{ij} = \frac{1}{2}(V_{j,i} - V_{i,j}) \tag{1.36}$$

Substituting the values of τ_{ij}^S and τ_{ij}^A in Eq. (1.34) we get

$$\tau_{ij} = \mu A_{(1)ij} - 2\eta W_{ij,kk} - \frac{\rho}{2} e_{ijk} l_k. \tag{1.37}$$

In the absence of body couples, Eq. (1.37) implies

$$\tau_{ij} = \mu A_{(1)ij} - 2\eta W_{ij,kk}. \tag{1.38}$$

1.6.2.3 Power-law fluid

The power law fluid is a generalized Newtonian fluid which has been used extensively in the industry especially as a lubricant. The rheological equation of power-law fluid is given by

$$\tau_{ij} = k(\dot{\gamma})^{n-1} A_{(1)ij}. \tag{1.39}$$

where, k is apparent viscosity and n is the flow behaviour index. Fluid behaves as viscous, shear thinning and shear thickening, respectively for $n = 1, n < 1$ and $n > 1$. $\dot{\gamma}$ given in Eq. (1.39) is the second invariant of the first Rivlin-Ericksen tensor and is defined as

$$\dot{\gamma} = \sqrt{\frac{1}{2} A_{(1)ij} A_{(1)ij}}. \tag{1.40}$$

1.7. Boundary conditions for a thin lubrication layer

1.7.1. Slip-Flow Boundary Condition

Navier [120] proposed the idea of slip boundary condition on the assumption that fluid can slide over a solid surface. He assumed that velocity and shear stress at the wall are linearly proportional. Mathematically:

$$u_s = \beta \tau_s, \tag{1.41}$$

where, β is the slip length or slip coefficient. The no-slip boundary condition can be obtained by taking $\beta = 0$. The Navier hypothesis holds at macroscale for which β must be small.

1.7.2. Interfacial boundary conditions due to lubrication

Joseph [144] derived an interfacial slip-flow condition over a lubricated surface. He showed that, at the interface, velocity gradient is proportional to the square of the velocity. Inside the thin lubrication layer, he applied the lubrication theory and neglected the influence of pressure gradient which results in the following interfacial condition

$$\frac{\partial u}{\partial y} = \frac{\mu_L u^2}{2\mu Q}, \tag{1.42}$$

where μ_L and μ are respectively the viscosities of lubricant and the bulk fluid. Moreover, Q represents the constant volumetric flow rate of the lubricant. Joseph [144] suggested that to accommodate the effect of lubrication layer on the bulk fluid, the no-slip boundary condition can be replaced by the interfacial boundary condition (1.42) if the lubrication film is sufficiently thin.

1.7.3. Interfacial conditions for a non-Newtonian lubrication layer

Andersson and Valnes [145] derived an interfacial boundary condition by taking the lubricant as a power-law fluid. The detailed derivation is as under

The shear stress for the power-law fluid after applying the lubrication theory is given by

$$\tau_{xy} = k\left(\frac{\partial U}{\partial y}\right)^n. \tag{1.43}$$

Here, U is the horizontal component of velocity of the lubricant. For $n = 1$, Eq. (1.43) represents a viscous fluid with k as the dynamic coefficient of viscosity. The power-law lubricant is confined to a very thin layer of variable thickness $\delta(x)$ on the solid surface as shown in the Fig. 1.1.

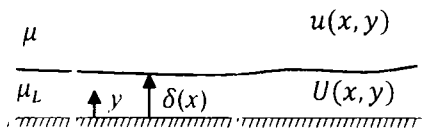

Fig. 1.1: The geometry of the thin lubrication layer [144].

Following Joseph [144], assume that the lubrication layer is sufficiently thin so that lubrication theory can be applied. As a result of this assumption the non-linear convective terms in the momentum equation are negligible and the governing equation reduces to

$$0 = -\frac{dp}{dx} + K\frac{\partial}{\partial y}\left(\frac{\partial U}{\partial y}\right)^n, \tag{1.44}$$

subjected to the no-slip condition $U(x,0) = 0$. At the interface $y = \delta(x)$, the velocity and shear stress of both fluids must be continuous. Joseph [144] proved that the pressure gradient dp/dx does not depend upon the thickness $\delta(x)$ of the lubrication layer and thus $\delta(x)$ can be taken arbitrarily small so that the pressure gradient can be neglected. Substituting $dp/dx = 0$ in Eq. (1.44) and integrating the resulting equation twice, we get the linear solution $U = \tilde{U}(x)y/\delta(x)$ Here, $\tilde{U}$ denotes the velocity of both fluids at the interface. This solution is the same as obtained by the Joseph [144] for the viscous lubricant and is recognized as the conventional drag flow approximation. The principle for neglecting the term dp/dx in Eq (1.44) is that it is considerably smaller than $K\left(\tilde{U}/\delta\right)^n/\delta$. Using the solution of Eq. (1.44), the continuity of the shear stress at the interface $y = \delta(x)$ can be expressed as

$$K\left(\frac{\tilde{U}}{\delta}\right)^n = \mu\frac{\partial u}{\partial y} \tag{1.45}$$

In order to eliminate the thickness $\delta(x)$ of the lubrication layer, we define the volumetric flow rate as [144]

$$Q = \int_0^{\delta(x)} U(x,y)dy = \frac{\tilde{U}(x)\delta(x)}{2}. \tag{1.46}$$

Substituting the value of $\delta(x)$ in Eq. (1.45), we get

$$K\left(\frac{u^2(x,\delta)}{2Q}\right)^n = \mu\frac{\partial u(x,\delta)}{\partial y}, \tag{1.47}$$

where the velocity $\tilde{U}$ at the interface $y = \delta(x)$ has been replaced by the velocity u of the bulk fluid. As the thickness of the lubrication layer is very small, therefore the interfacial condition (1.47) can be imposed at $y = 0$ rather than at $y = \delta(x)$. i.e.

$$K\left(\frac{u^2(x,0)}{2Q}\right)^n = \mu\frac{\partial u(x,0)}{\partial y}. \tag{1.48}$$

This is a new interfacial boundary condition for non-Newtonian lubricants, from which Joseph's proposed boundary condition (1.42) can be recovered for $n = 1$.

1.8 Keller-box method

The flow problems considered in different geometries are represented by nonlinear partial differential equations. In many cases these can be transformed to boundary value problems through suitable assumptions The exact and analytical solutions are not easy to obtain. In such situations one would expect to compute a numerical solution of the problem to analyze the flow situation. In this thesis our mathematical models result in nonlinear boundary value problems with nonlinear boundary conditions. We have implemented an implicit finite difference method to obtain numerical solutions of the modeled nonlinear boundary value problems. Keller-box Method is a two-point implicit finite-difference scheme, which have been used extensively to investigate the boundary layer flows in different geometries by the researchers working in this area. The detail procedure of this scheme can be found in the book of Keller and Cebeci [156] Here higher order differential equations are reduced to system of first-order differential equations by introducing new functions. The obtained first-order system is approximated on an arbitrary rectangular net with forward-difference derivatives and averages at the midpoints of the net rectangle. As a result, the system of first order differential equation is reduced to system of linear/nonlinear algebraic equations. The resulting system of algebraic equations which is if nonlinear then linearized by Newton's method and solved by the block-elimination method.

The details of implementation are established by the following example of coupled boundary value problem in a semi-infinite domain. Consider the boundary value problems

$$f''' - 2f'^2 + ff'' + g = 0, \tag{1.49}$$

$$g'' - fg' + f'g = 0, \tag{1.50}$$

$$f(0) = 0,\ f'(0) = 0,\ g(0) = 1,\ f'(\infty) = 0,\ g(\infty) = 0. \tag{1.51}$$

To reduce Eqs. (1.49) and (1.50) into a system of first order equations, we introduce new variables in the following way

$$f' = u, \quad u' = v, \quad g' = w. \tag{1.52}$$

Therefore, the above system of equations implies

$$v' - 2u^2 + fv + g = 0,$$

$$w - fw + ug = 0. \tag{1.53}$$

The transformed boundary conditions are

$$f(0) = 0,\ u(0) = 0,\ g(0) = 1,\ u(\infty) = 0,\ g(\infty) = 0. \tag{1.54}$$

Assuming the following grid points

$$\eta_0 = 0,\ \eta_j = \eta_{j-1} + h_j,\ \ j = 1, 2, 3, \ldots, J;\ \eta_J = \eta_\infty,$$

and using the centered-difference gradients and averages at the mid points of the net, Eqs. (1.52) and (1.53) are approximated by the relations

$$\frac{f_j - f_{j-1}}{h_j} = u_{j-\frac{1}{2}},\qquad \frac{u_j - u_{j-1}}{h_j} = v_{j-\frac{1}{2}},\qquad \frac{g_j - g_{j-1}}{h_j} = w_{j-\frac{1}{2}}, \tag{1.55}$$

$$\frac{v_j - v_{j-1}}{h_j} - 2\left(u_{j-\frac{1}{2}}\right)^2 + \left(f_{j-\frac{1}{2}}\right)\left(v_{j-\frac{1}{2}}\right) + \left(g_{j-\frac{1}{2}}\right) = 0, \tag{1.56}$$

$$\frac{w_j - w_{j-1}}{h_j} - \left(f_{j-\frac{1}{2}}\right)\left(w_{j-\frac{1}{2}}\right) + \left(u_{j-\frac{1}{2}}\right)\left(g_{j-\frac{1}{2}}\right) = 0, \tag{1.57}$$

where $f_{j-\frac{1}{2}} = \frac{f_j + f_{j-1}}{2}$ etc. Equations (1.56) and (1.57) are nonlinear algebraic equations and therefore have to be linearized before the factorization scheme can be used. We write the Newton iterates in the following way:

For the $(j+1)\,th$ iterates, we write

$$f_{j+1} = f_j + \delta f_j,\ \text{etc.}, \tag{1.58}$$

for all dependent variables. By substituting these expressions into Eqs. (1.55)-(1.57) and dropping the quadratic and higher-order terms in δf_j etc., a linear tridiagonal system of equations will be obtained as follows:

$$\delta f_j - \delta f_{j-1} - h_j\left(\frac{u_j + u_{j-1}}{2}\right) = (r_1)_{j-\frac{1}{2}}, \tag{1.59}$$

$$\delta u_j - \delta u_{j-1} - h_j\left(\frac{v_j + v_{j-1}}{2}\right) = (r_4)_{j-\frac{1}{2}}, \tag{1.60}$$

$$\delta g_j - \delta g_{j-1} - h_j\left(\frac{w_j + w_{j-1}}{2}\right) = (r_5)_{j-\frac{1}{2}}, \tag{1.61}$$

$$(\psi_1)\,\delta f_j + (\psi_2)\,\delta f_{j-1} + (\psi_3)\,\delta u_j + (\psi_4)\,\delta u_{j-1}$$

$$+ (\psi_5)\,\delta v_j + (\psi_6)\,\delta v_{j-1} + (\psi_7)\,\delta g_j + (\psi_8)\,\delta g_{j-1} = (r_4)_{j-\frac{1}{2}}, \tag{1.62}$$

$$(\mu_1)\,\delta f_j + (\mu_2)\,\delta f_{j-1} + (\mu_3)\,\delta u_j + (\mu_4)\,\delta u_{j-1}$$

$$+ (\mu_5)\,\delta g_j + (\mu_6)\,\delta g_{j-1} + (\mu_7)\,\delta w_j + (\mu_8)\,\delta w_{j-1} = (r_5)_{j-\frac{1}{2}}, \tag{1.63}$$

subject to boundary conditions

$$\delta f_0 = 0,\ \delta u_0 = 0,\ \delta v_0 = 0,\ \delta g_0 = 0,\ \delta w_0 = 0, \tag{1.64}$$

where

$$(\psi_1)_j = (\psi_2)_j = \frac{h_j}{4}(v_j + v_{j-1}),$$

$$(\psi_3)_j = (\psi_4)_j = -h_j(u_j + u_{j-1}),$$

$$(\psi_5)_j = 1 + \frac{h_j}{4}(f_j + f_{j-1}),$$

$$(\psi_6)_j = -1 + \frac{h_j}{4}(f_j + f_{j-1}),$$

$$(\psi_7)_j = (\psi_8)_j = \frac{h_j}{2},$$

$$(\mu_1)_j = (\mu_2)_j = -\frac{h_j}{4}(w_j + w_{j-1}),$$

$$(\mu_3)_j = (\mu_4)_j = \frac{h_j}{4}(g_j + g_{j-1}),$$

$$(\mu_5)_j = (\mu_6)_j = \frac{h_j}{4}(u_j + u_{j-1}),$$

$$(\mu_7)_j = 1 - \frac{h_j}{4}(f_j + f_{j-1}),$$

$$(\mu_8)_j = -1 - \frac{h_j}{4}(f_j + f_{j-1}),$$

$$(r_2)_{j-\frac{1}{2}} = -(v_j - v_{j-1}) + 2h_j\left(u_{j-\frac{1}{2}}\right)^2 - h_j\left(f_{j-\frac{1}{2}}\right)\left(v_{j-\frac{1}{2}}\right) - h_j\left(g_{j-\frac{1}{2}}\right),$$

$$(r_3)_{j-\frac{1}{2}} = -(w_j - w_{j-1}) + h_j\left(f_{j-\frac{1}{2}}\right)\left(w_{j-\frac{1}{2}}\right) - h_j\left(u_{j-\frac{1}{2}}\right)\left(g_{j-\frac{1}{2}}\right).$$

In matrix-vector form, we can write

$$\boldsymbol{A\delta} = \boldsymbol{r}, \tag{1.65}$$

in which

$$\boldsymbol{A} = \begin{bmatrix} [A_1] & [C_1] & & & & & \\ [B_2] & [A_2] & [C_2] & & & & \\ & \ddots & \ddots & \ddots & & & \\ & & \ddots & \ddots & \ddots & & \\ & & & \ddots & \ddots & & \\ & & & & [B_{J-1}] & [A_{J-1}] & [C_{J-1}] \\ & & & & & [B_J] & [A_J] \end{bmatrix},$$

$$\boldsymbol{\delta} = \begin{bmatrix} [\delta_1] \\ [\delta_2] \\ \ddots \\ [\delta_{J-1}] \\ [\delta_J] \end{bmatrix}, \quad \boldsymbol{r} = \begin{bmatrix} [r_1] \\ [r_2] \\ \ddots \\ [r_{J-1}] \\ [r_J] \end{bmatrix}, \tag{1.66}$$

where in Eq. (1.66) the elements are defined by

$$[A_1] = \begin{bmatrix} 1 & 0 & 0 & 0 & 0 \\ 0 & 1 & 0 & 0 & 0 \\ 0 & 0 & 0 & 1 & 0 \\ 0 & -1 & -c_j & 0 & 0 \\ 0 & 0 & 0 & -1 & -c \end{bmatrix}, \quad c_j = \frac{1}{2}h_j,$$

$$[A_j] = \begin{bmatrix} 1 & c_j & 0 & 0 & 0 \\ (\psi)_j & (\psi_3)_j & (\psi_5)_j & (\psi_7)_j & 0 \\ (\mu)_j & (\mu_3)_j & 0 & (\mu_5)_j & (\mu_7)_j \\ 0 & 0 & -1 & -c_j & 0 \\ 0 & 0 & 0 & -1 & -c_j \end{bmatrix}, \quad 2 < j < J-1,$$

$$[A_J] = \begin{bmatrix} 1 & c_J & 0 & 0 & 0 \\ (\psi)_J & (\psi_3)_J & (\psi_5)_J & (\psi_7)_J & 0 \\ (\mu)_J & (\mu_3)_J & 0 & (\mu_5)_J & (\mu_7)_J \\ 0 & 1 & 0 & 0 & 0 \\ 0 & 0 & 0 & 1 & 0 \end{bmatrix},$$

$$[B_j] = \begin{bmatrix} 1 & c_j & 0 & 0 & 0 \\ (\psi)_j & (\psi_4)_j & (\psi_6)_j & (\psi_8)_j & 0 \\ (\mu)_j & (\mu_4)_j & 0 & (\mu_6)_j & (\mu_8)_j \\ 0 & 0 & 0 & 0 & 0 \\ 0 & 0 & 0 & 0 & 0 \end{bmatrix}, \quad 2 < j < J,$$

$$[C_j] = \begin{bmatrix} 0 & 0 & 0 & 0 & 0 \\ 0 & 0 & 0 & 0 & 0 \\ 0 & 0 & 0 & 0 & 0 \\ 0 & 0 & -1 & -c_j & 0 \\ 0 & 0 & 0 & -1 & -c_j \end{bmatrix}, \quad 1 < j < J-1,$$

$$[\delta_j] = \begin{bmatrix} \delta f_j \\ \delta u \\ \delta v_j \\ \delta g \\ \delta y_1 \end{bmatrix}, \quad 1 < j < J,$$

TH-16741

$$\left[r_j\right] = \begin{bmatrix} (r_1)_{-(1/2)} \\ (r_2)_{-(1/2)} \\ (r_3)_{-(1/2)} \\ (r_4)_{-(1/2)} \\ (r_5)_{-(1/2)} \end{bmatrix}, \quad 1 < j < J,$$

Now, we let

$$\boldsymbol{A} = \boldsymbol{L}\boldsymbol{u}, \tag{1.67}$$

where

$$\boldsymbol{L} = \begin{bmatrix} [a_1] & & & & \\ [B_2] & [a_2] & & & \\ & \ddots & \ddots & & \\ & & \ddots & \ddots & \\ & & & [B_J] & [a_J] \end{bmatrix},$$

$$\boldsymbol{u} = \begin{bmatrix} [I] & [\Gamma_1] & & & \\ & [I] & [\Gamma_1] & & \\ & & \ddots & \ddots & \\ & & & [I] & [\Gamma_{J-1}] \\ & & & & [I] \end{bmatrix},$$

where $[I]$ is the unit matrix while $[a_j]$ and $[\Gamma_j]$ are 5×5 matrices whose elements are determined by the following equations:

$$\begin{aligned} &[a_1] = [A_1], \\ &[A_1][\Gamma_1] = [C_1], \\ &[a_j] = [A_j] - [B_j][\Gamma_{j-1}], \quad j = 2,3,\ldots,J, \\ &[a_j][\Gamma_j] = [C_j], \quad j = 2,3,\ldots,J-1. \end{aligned}$$

Eq. (1.67) can be substituted into Eq. (1.65) to get

$$\boldsymbol{L}\boldsymbol{U}\boldsymbol{\delta} = \boldsymbol{r}. \tag{1.68}$$

Defining

$$\boldsymbol{U}\boldsymbol{\delta} = \boldsymbol{W}. \tag{1.69}$$

Equation (1.68) becomes

$$\boldsymbol{L}\boldsymbol{W} = \boldsymbol{r}, \tag{1.70}$$

where

$$\boldsymbol{W} = \begin{bmatrix} [W_1] \\ [W_2] \\ [W_3] \\ [W_4] \\ [W_5] \end{bmatrix},$$

and the $[W_j]$ are 5×1 column matrices. The elements of $\boldsymbol{W}$ can be solved from Eq. (1.70)

$$\begin{aligned} [a_1][W_1] &= [r_1], \\ [a_j][W_j] &= [r_j] - [B_j][W_{j-1}]. \end{aligned} \tag{1.71}$$

Once the elements of $\boldsymbol{W}$ are found, Eq. (1.69) then gives the solution $\boldsymbol{\delta}$, the elements of which are obtained by the following relations:

$$\begin{aligned} [\delta_j] &= [W_j], \\ [\delta_j] &= [W_j] - [\Gamma_j][\delta_{j+1}]. \end{aligned}$$

Once the elements of $\boldsymbol{\delta}$ are found, Eq. (1.65) can be used to find the $(j+1)th$ iteration.

The procedure described is implemented in Mathematica for the boundary value problems consisting of nonlinear ordinary differential equations together with nonlinear boundary conditions considered in the subsequent chapters.

Chapter 2

Oblique flow towards a stagnation-point over a lubricated surface

This chapter deals with the oblique flow of an incompressible viscous fluid near a stagnation point on a lubricated plate. A generalized Newtonian fluid known as the power-law fluid is used as the lubricant. To obtain the non-similar solution of the partial differential equations, continuity of shear stress and velocity of both fluids has been imposed at the interface The Keller-box numerical method is chosen to develop the solutions of the present flow situation. The effects of physical parameters on the fluid velocity, wall shear stress, boundary layer displacement and streamlines are discussed through graphs and tables

2.1 Mathematical formulation

Consider steady, two-dimensional oblique stagnation-point flow of a viscous fluid past a semi-infinite lubricated plate. A power-law fluid is used as lubricant. The lubricated plate is placed in the xz-plane as shown in Fig. 2.1.

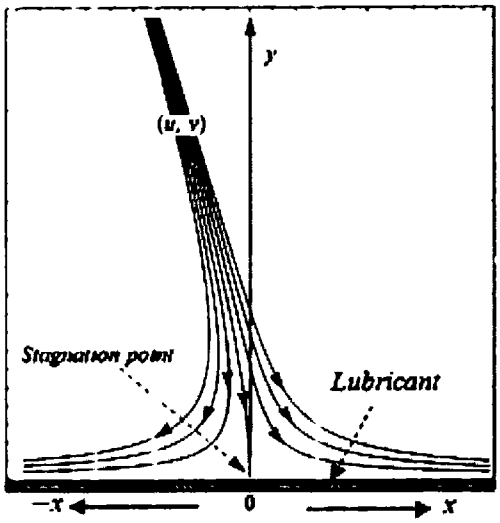

Figure 2.1: Schematic diagram for the considered flow situation.

We consider a free stream flow containing a combination of orthogonal stagnation-point flow with strain rate a and a shear flow along the plate having strain b. If U and V respectively are the velocity components of the power-law fluid in x and y directions, then we have

$$Q = \int_0^{\delta(x)} U(x, y)\, dy, \tag{2.1}$$

where Q is the volumetric flow rate and δ is the variable thickness of the lubricant. Assuming u, v the velocity components of the bulk fluid in x and y direction, the steady, incompressible, two-dimensional flow is governed by:

$$\frac{\partial u}{\partial x} + \frac{\partial v}{\partial y} = 0, \tag{2.2}$$

$$u\frac{\partial u}{\partial x} + v\frac{\partial u}{\partial y} = -\frac{1}{\rho}\frac{\partial p}{\partial x} + \nu \nabla^2 u, \tag{2.3}$$

$$u\frac{\partial v}{\partial x} + v\frac{\partial v}{\partial y} = -\frac{1}{\rho}\frac{\partial p}{\partial y} + \nu \nabla^2 v, \tag{2.4}$$

where $\nu = \mu/\rho$ is the kinematic viscosity. Eliminating the pressure between Eqs. (2.3) and (2.4) we obtain

$$u\frac{\partial^2 u}{\partial y \partial x} + v\frac{\partial^2 u}{\partial y^2} - u\frac{\partial^2 v}{\partial x^2} - v\frac{\partial^2 v}{\partial x \partial y} - \nu\left(\frac{\partial^3 u}{\partial y \partial x^2} + \frac{\partial^3 u}{\partial y^3} - \frac{\partial^3 v}{\partial x^3} - \frac{\partial^3 v}{\partial x \partial y^2}\right) = 0. \tag{2.5}$$

The expression for the shear stress is given by

$$\tau_{xy} = \mu\left(\frac{\partial u}{\partial y} + \frac{\partial v}{\partial x}\right). \tag{2.6}$$

The boundary conditions at the surface, interface and free stream are as follows:

At the surface the no-slip boundary conditions imply

$$U(x, 0) = 0, \quad V(x, 0) = 0 \tag{2.7}$$

Assuming that the lubricant film is very thin, we have

$$V(x, y) = 0, \quad \forall\, y \in [0, \delta(x)]. \tag{2.8}$$

The interfacial condition between the viscous fluid and the lubricant can be obtained by imposing continuity of velocity and shear stress of both the fluids. If μ_L is the apparent viscosity of the power-law fluid, the continuity of shear stress at $y = \delta(x)$ gives

$$\mu\left(\frac{\partial u}{\partial y}\right) = \mu_L \frac{\partial U}{\partial y} \tag{2.9}$$

where μ_L is defined as

$$\mu_L = k\left(\frac{\partial U}{\partial y}\right)^{n-1} \tag{2.10}$$

Assuming $U(x,y)$ varies linearly inside the lubricant, therefore

$$U(x,y) = \frac{\bar{U}(x)\,y}{\delta(x)} \tag{2.11}$$

Here $\bar{U}(x)$ denotes the velocity of both the fluids at the interface. Using Eq. (2.1), the thickness $\delta(x)$ of the lubricant can be expressed as

$$\delta(x) = \frac{2Q}{\bar{U}(x)}. \tag{2.12}$$

Substituting Eqs. (2.10) - (2.12), Eq. (2.9) suggests

$$\frac{\partial u}{\partial y} = \frac{k}{\mu}\left(\frac{1}{2Q}\right)^n \bar{U}^{2n}. \tag{2.13}$$

The continuity of horizontal velocity components of both fluids implies that

$$\bar{U} = u. \tag{2.14}$$

Therefore Eq. (2.13) leads to the following slip boundary condition

$$\frac{\partial u}{\partial y} = \frac{k}{\mu}\left(\frac{1}{2Q}\right)^n u^{2n}. \tag{2.15}$$

The continuity of vertical velocity components of both the fluids at $y = \delta(x)$ implies

$$v\left(x,\delta(x)\right) = V\left(x,\delta(x)\right). \tag{2.16}$$

By using Eq. (2.8) one gets

$$v\left(x,\delta(x)\right) = 0 \tag{2.17}$$

Assuming the lubrication layer to be very thin, we can apply boundary conditions (2.15) and (2.17) at $y = 0$. If $\bar{a}$ and $\bar{b}$ represent dimensional constants, then following Tooke and Blythe [23], the boundary conditions for the velocity components at free stream are

$$u_e = ax + b(y - \bar{b}),\ v_e = -a(y - \bar{a}). \tag{2.18}$$

To express the set of equations into dimensionless form, following dimensionless variables are introduced

$$u = axf'(\eta) + ag'(\eta),\quad v = -\sqrt{a\nu}f(\eta),\quad \eta = y\sqrt{\frac{a}{\nu}}, \tag{2.19}$$

where prime denotes the differentiation with respect to η nad f and g measure the normal and tangential components of the flow. In new variables boundary value problem takes the

form

$$f^{v} + ff''' + f'f'' - 2f'f'' = 0, \tag{2.20}$$

$$g^{v} + f'g'' + fg''' - f'g'' - g'f'' = 0, \tag{2.21}$$

$$f(0) = 0, \quad f''(0) = \lambda(f'(0))^{2n}, \quad f'(\infty) = 1, \tag{2.22}$$

$$g(0) = 0, \quad g''(0) = 2n\lambda g'(0)(f'(0))^{2n-1}, \quad g''(\infty) = \gamma. \tag{2.23}$$

The parameter λ in Eqs. (2.22) and (2.23) is given as

$$\lambda = \frac{k\sqrt{\nu}}{\mu} \frac{a^{2n} x^{2n-}}{a^{3/2}(2Q)^{n}}. \tag{2.24}$$

Equations (2.20) and (2.21) can be integrated once to give following equations upon using the free stream conditions

$$f''' - f'^2 + ff'' + 1 = 0, \tag{2.25}$$

$$g'' + fg'' - f'g' + \gamma(\alpha - \beta) = 0, \tag{2.26}$$

where $\alpha = \eta_{\infty} - f(\infty)$ and β is a free parameter.

Letting $g'(\eta) = \gamma h(\eta)$, Eq. (2.26) reduces to

$$h' + fh' - f'h + \alpha - \beta = 0, \tag{2.27}$$

where $\gamma = b/a$ represents the shear in the free stream.

The relevant boundary conditions become

$$h(0) = 2n\lambda h(0)(f'(0))^{2n-1}, \quad h'(\infty) = 1. \tag{2.28}$$

From Eq. (2.24) we note that Eqs. (2.25) - (2.27) possess a similarity solution when $n = 1/2$. The solutions for $n \neq 1/2$ are non-similar and are also included in the chapter. The parameter λ represents the ratio of viscous and lubrication length scales respectively as follows

$$\lambda = \frac{\sqrt{\frac{\nu}{a}}}{\frac{\mu}{k}\sqrt{2Q}} = \frac{L_{visc}}{L_{lub}} \tag{2.29}$$

The case when L_{lub} is small, λ becomes sufficient large and when $\lambda \to \infty$, the no-slip conditions $f'(0) = 0$, and $h(0) = 0$ are restored from Eqs. (2.22) and (2.28). The case when L_{lub} attains a large value then $\lambda \to 0$ and the full-slip boundary conditions $f''(0) = 0$ and $h'(0) = 0$ are obtained. Thus the parameter λ can be utilized to control the slip produced by the lubricant and is called slip parameter.

Employing (2.19), the dimensionless shear stress at the wall takes the form

$$\tau_w = xf''(0) + g'(0) = xf''(0) + \gamma h'(0). \tag{2.30}$$

To find the location of separation point (stagnation-point) x_s on the surface, we put $\tau_w = 0$. Therefore

$$x_s = -\frac{g''(0)}{f''(0)} = -\gamma \frac{h'(0)}{f''(0)}. \tag{2.31}$$

2.2 Numerical results and discussions

To find the impact of physical parameters λ and β on the dimensionless quantities f', f'', h and h' Eqs. (2.25) and (2.27) subject to boundary conditions (2.22) and (2.28) are solved numerically by implementing Keller-box method.

Influence of slip parameter λ on f' is demonstrated in Fig. 2.2 while Figs. 2.3-2.5 display the effects of parameters λ and β on h. The effect of flow behavior index n on f' and h is shown in the Figs. 2.6 and 2.7. Streamlines of the flow against the involved parameters are shown in Figs. 2.8-2.10. A comparison of numerical values of $\alpha, f''(0)$ and $h'(0)$ with the existing values in the literature is presented in Table 2.1. Impact of emerging parameters on $f''(0)$, α and $h'(0)$ is shown in Tables 2.2 and 2.3. Table 2.4 is devoted for the influence of parameters γ λ and β on the stagnation-point.

The variation of horizontal velocity component f' against λ is displayed in Fig. 2.2. The figure elucidates that f' accelerates by increasing slip at the surface. Hence the lubricant is forcing the fluid to flow fast at the surface. To see the effects of λ on the shear velocity h in the absence of β, Fig. 2.3 is plotted. It is noted that h decreases by increasing λ near the

surface ($\eta = 0$). More precisely h varies with λ between $\eta = 0$ and $\eta = 1$ and after this it becomes independent of η and varies linearly with η. Variation in h against λ for two different values of β is depicted in Fig. 2.4. According to this figure h increases by increasing the slip (i.e. by decreasing λ) for negative values of β. However, for the positive values of β the shear velocity decreases by increasing slip. Fig. 2.5 elucidates the variation of h for different values of β and for two different values of λ. One can observe that the shear velocity component h decreases when β increases from negative to positive. Fig. 2.6 is plotted to illustrate the behavior of f' under the influence of flow behavior index n when $\lambda = 2$. This figure shows that f' is an increasing function of n. Variation of $h(\eta)$ for different values of n when $\lambda = 2$ is displayed in Fig. 2.7. We see that h increases by increasing n when $\beta < 0$ and decreases when $\beta > 0$. Figures 2.8-2.10 show the influence of λ and β on the streamlines pattern for $\gamma = 1$ and $\gamma = 5$ respetively. It is clear from Fig. 2.8 that separation point moves to the right side along x-axis when β increases from negative to positive. Fig 2.9 shows that by increasing slip (i.e. by decreasing λ), the separation point moves towards right on the x-axis when $\gamma < 3$. However, for $\gamma \geq 3$, the separation point moves towards left by increasing slip as shown in the Fig. 2.10.

The comparison of numerical values of $f''(0)$, α and $h'(0)$ with that of already available values in the literature [54] in the limiting case is presented in Table 2.1. It is noted that our numerical values are in excellent agreement with previously published data. This fact validates the accuracy of our developed numerical solution.

Table 2.2 illustrates the numerical values of $f''(0)$ and α against λ. This table demonstrates that $f''(0)$ and α increases by increasing λ. Effects of parameter λ on $h'(0)$ for three different values of β are investigated in Table 2.3. This table indicates an increase in $h'(0)$ by increasing λ for $\beta \leq 0$. However, the values of $h'(0)$ follow a reverse trend by increasing λ for $\beta > 0$. The separation points for various values of γ, λ and for three different values of β are shown in the Table 2.4. The tabular results do confirm the observations made through Figs. 2.8-2.10.

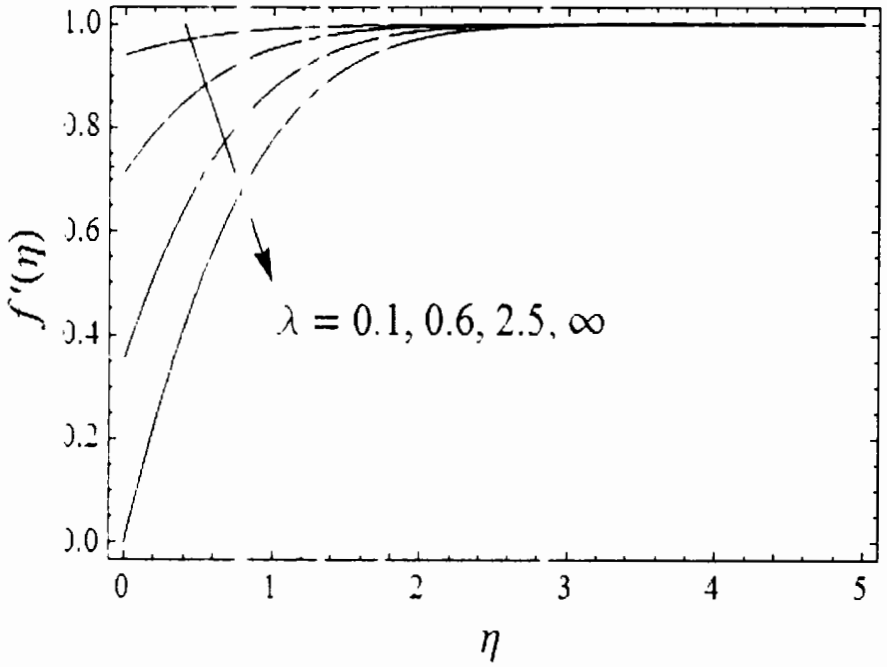

Fig. 2.2. Variation of $f'(\eta)$ against slip parameter λ.

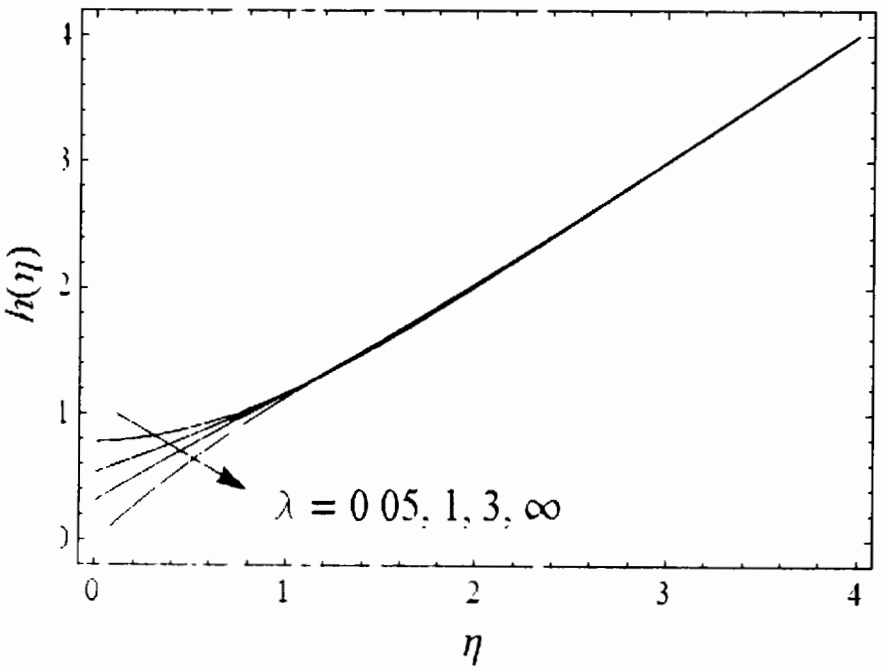

Fig. 2.3. Variation of $h(\eta)$ against slip parameter λ when $\beta = 0$.

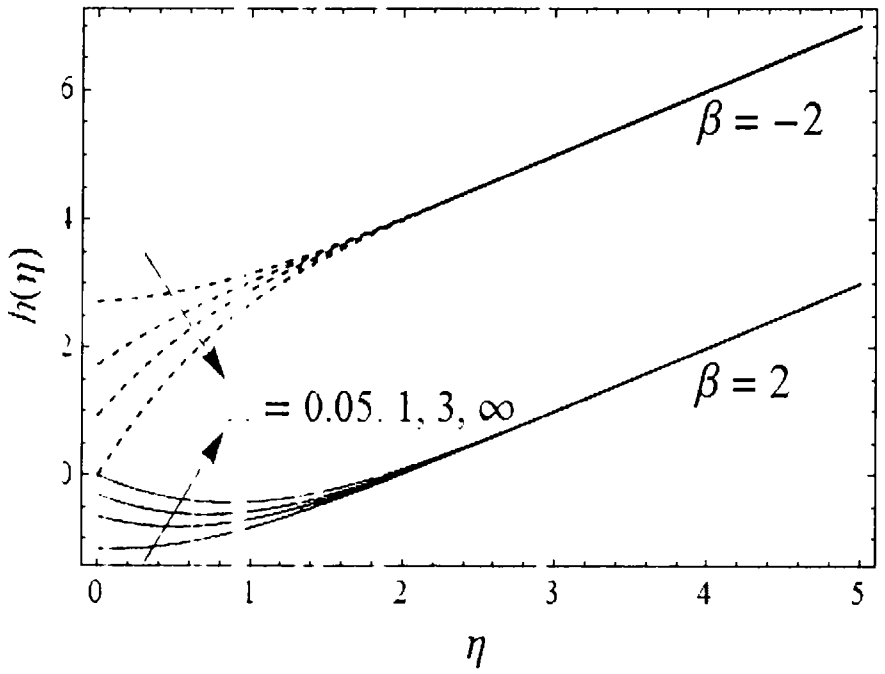

Fig. 2.4. Variation of $h(\eta)$ against slip parameter λ when $\beta = 2$ and -2.

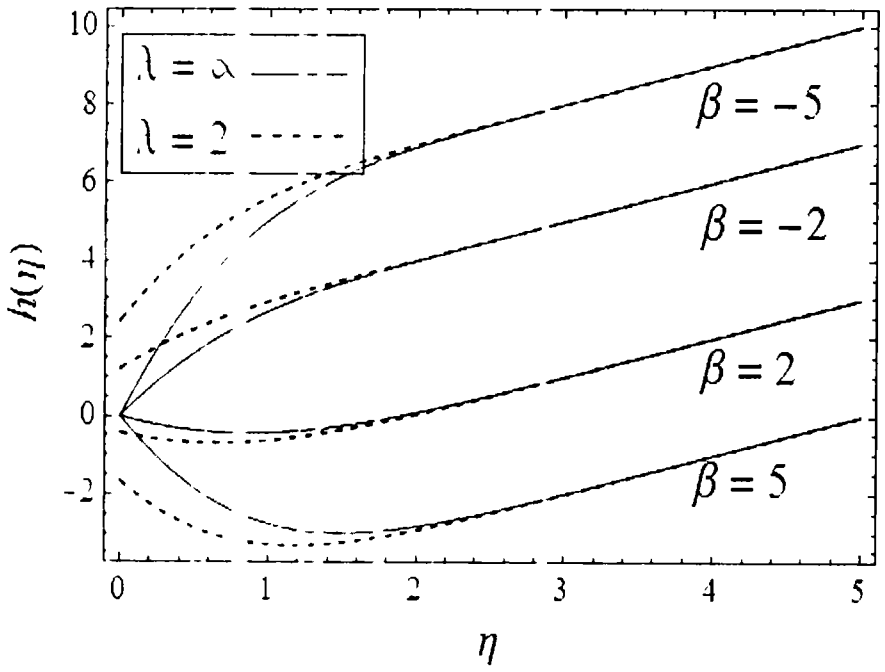

Fig. 2.5. Effects of slip parameter λ on $h(\eta)$ for various values of β.

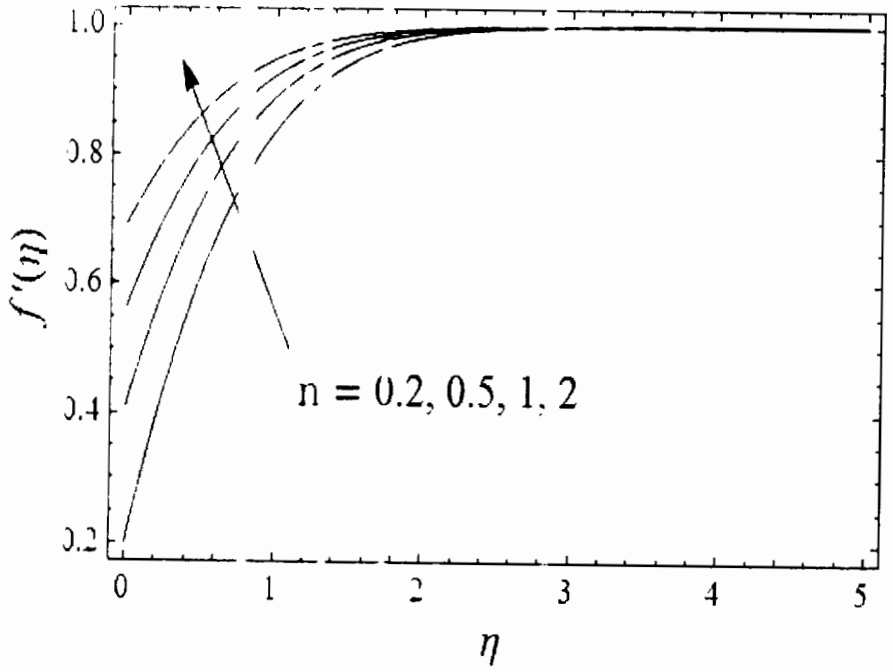

Fig. 2.6 Effects of n on $f'(\eta)$ when $\lambda = 2$.

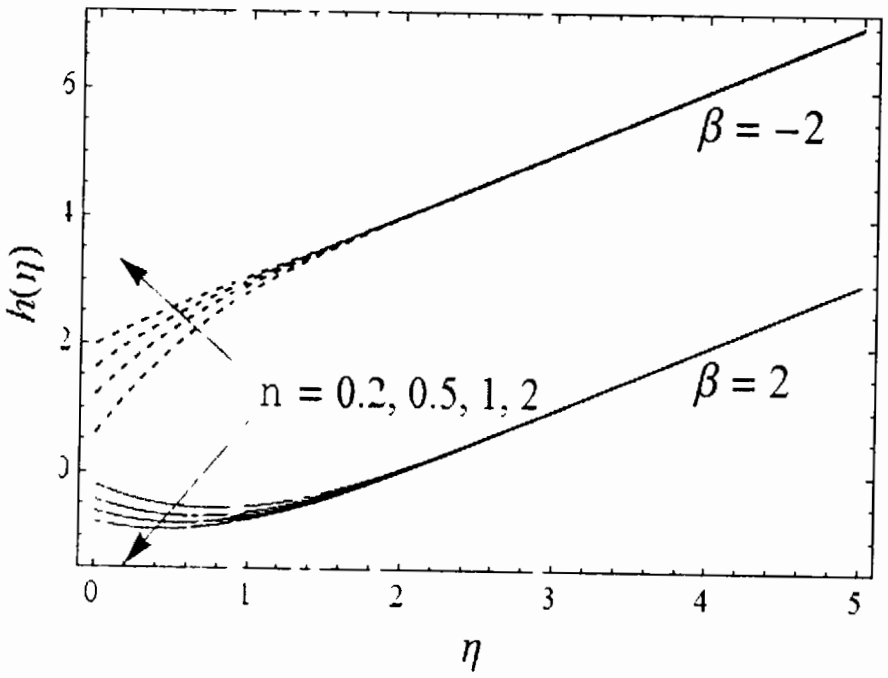

Fig. 2.7 Effects of n on $h(\eta)$ when $\lambda = 2$.

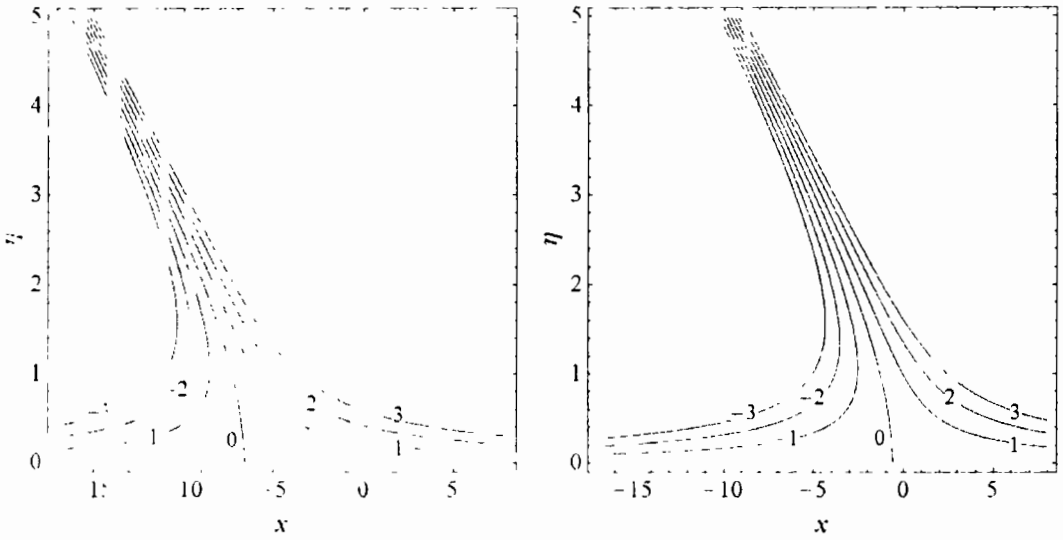

$x_s = -6.624, \lambda = 1, \beta = -3, \gamma = 5$ $x_s = -0.6242, \lambda = 1, \beta = 3, \gamma = 5$

Fig. 2.8. Streamlines showing the effects of parameter β.

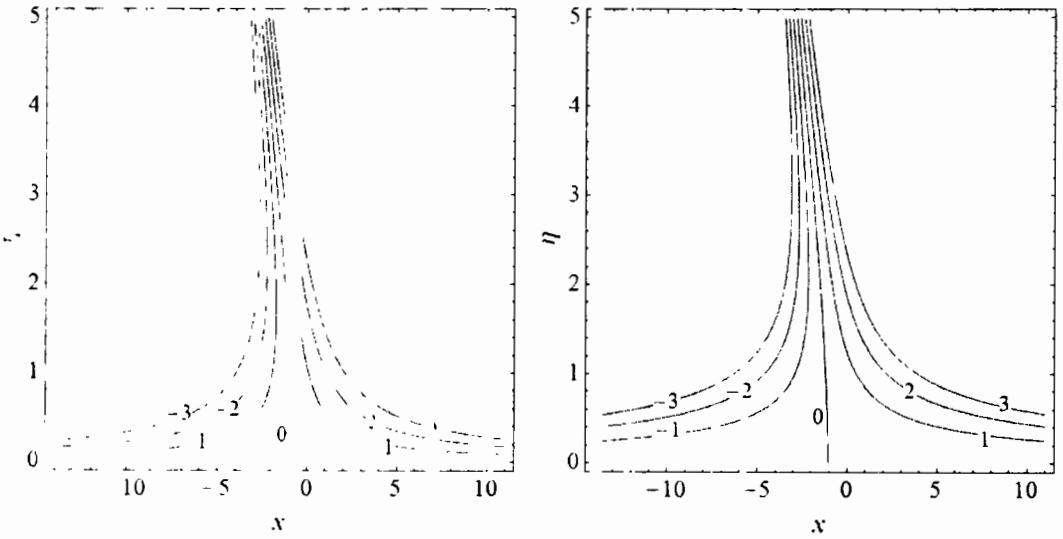

$x_s = -0.7994, \lambda = 0.01, \beta = 0, \gamma = 1$ $x_s = -1.0480, \lambda = 5, \beta = 0, \gamma = 1$

Fig. 2.9. Streamlines showing the effects of slip parameter λ.

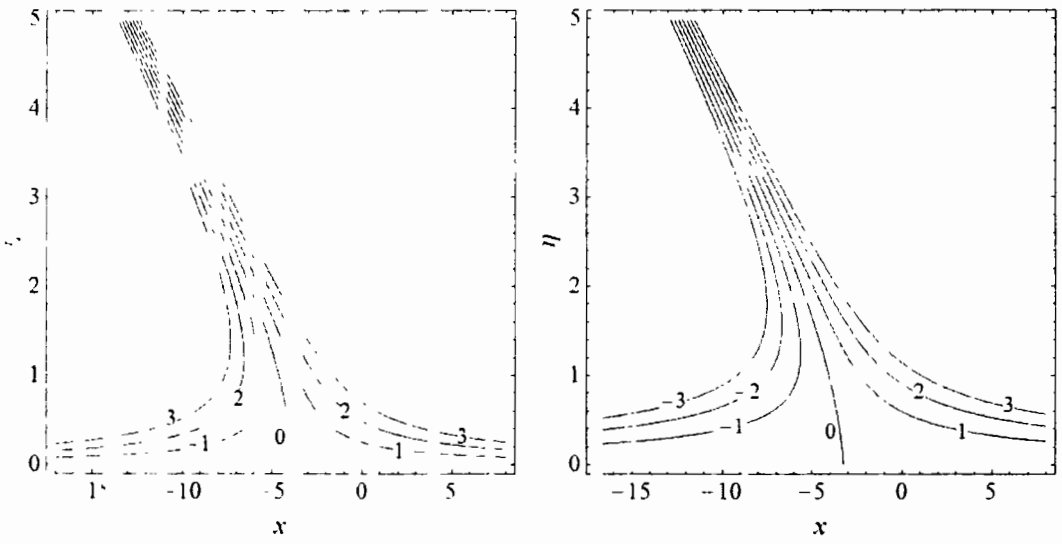

$x_s = -3.984, \lambda = 0.01, \beta = 0, \gamma = 5$ $x_s = -3.288, \lambda = 5, \beta = 0, \gamma = 5$

Fig. 2.10. Streamlines showing the effects of slip parameter λ.

Table 2.1: Comparison of numerical values of $f''(0)$, α and $h'(0)$ for no-slip case ($\lambda = \infty$) with reference [54] Li et al.

			$h'(0)$		
Comparison	$f''(0)$	α	$\beta = 0$	$\beta = 5$	$\beta = -5$
Present	1.232598	0.647903	1.406564	−4.756416	7.569314
Ref [54]	1.23259	0.64790	1.40637	−4.75656	7.56931

Table 2.2: Numerical values of $f''(0)$ and α against λ.

λ	$f''(0)$	α	λ	$f''(0)$	α
0.01	0.009938	0.0033200	3.0	0.934338	0.4151829
0.05	0.048472	0.0163362	5.0	1.042591	0.4880532
0.1	0.094036	0.0320301	10	1.134289	0.5587490
0.5	0.375887	0.1375776	20	1.182886	0.6007183
1.0	0.593464	0.2318142	100	1.222604	0.6380184
2.0	0.821483	0.3480926	∞	1.232598	0.6479025

Table 2.3: Numerical values of $h'(0)$ against λ and β when $\gamma = 1$.

λ	$\beta = 0$	$\beta = 5$	$\beta = -5$
0.01	0.0079443	-0.0417440	0.0576325
0.05	0.0390407	-0.2033187	0.2814000
0.1	0.0764260	-0.3937518	0.5466039
0.5	0.3244734	-1.5549615	2.2039084
1.0	0.5402318	-2.4270889	3.5075523
2.0	0.7976856	-3.3097286	4.9050999
3.0	0.9412541	-3.7304323	5.6129404
5.0	1.0926509	-4.1203028	6.3056047
10	1.2346924	-4.4367471	6.9061319
20	1.3228857	-4.5977831	7.2310617
100	1.3879235	-4.7250888	7.5009358
500	1.4028093	-4.7501721	7.5557906
∞	1.4065638	-4.7564167	7.5695442

Table 2.4: Influence of λ and β on stagnation-point x_s when $\gamma = 1$ and $\gamma = 5$.

γ	λ	$\beta = -3$	$\beta = 0$	$\beta = 3$
-5	0.5	0.4906	3.4906	6.4906
	5.0	-0.6882	2.3118	5.3118
-3	0.5	-2.4119	0.5881	3.5881
	5.0	-2.9281	0.0719	3.0719
1	0.5	-3.8632	−0.8632	2.1368
	5.0	-4.0480	−1.0480	1.9520
2	0.5	-4.5889	−1.5889	1.4111
	5.0	-4.6080	−1.6080	1.3920
3	0.5	-5.3145	−2.3145	0.6855
	5.0	-5.1679	−2.1679	0.8321
5	0.5	-6.7658	−3.7658	−0.7658

	5.0	-6.2879	−3.2879	−0.2879
10	0.5	-10.394	−7.3940	−4.3940
	5.0	-9.0877	−6.0877	−3.0877

2.3 Conclusion

In this chapter oblique flow of a viscous fluid towards a stagnation-point over a plate lubricated with a power-law fluid is investigated. In the present case we have solved the flow equations for $n = 1/2$ (similar solution) and $n \neq 1/2$ (non-similar solution). The solutions are developed using the Keller-box method. The motivation is to determine the effects of the parameter β and the slip parameter λ on the flow characteristics ranging from no-slip to full-slip cases. It is found that slip increases the velocity and suppress the effects of free stream velocity for large values. Moreover, the separation point moves towards and away from origin for various values of involved parameters.

Chapter 3

Non-orthogonal stagnation-point flow of a second grade fluid past a lubricated surface

The stagnation-point flow of a second-grade fluid past a power-law lubricated surface is analyzed in this chapter. It is assumed that the fluid impinges on the wall obliquely. A suitable choice of similarity transformations reduces the governing partial differential equations into ordinary differential equations. The thin lubrication layer suggests that interface conditions between fluid and lubricant can be imposed on the boundary. An implicit finite difference scheme known as Keller-box method is employed to obtain the numerical solutions. The effects of slip parameter and Weissenberg number on the fluid velocity and streamlines are discussed through graphs. The limiting cases of partial and no-slip can be deduced from the present solutions [54]

3.1 Mathematical formulation

Consider the steady oblique stagnation-point flow of a second grade fluid over an infinite plate lubricated with a thin layer of power-law fluid. The x-axis is taken along the flow, the y-axis is normal to the plate and the origin O is located at the center of the plate. We consider a free stream flow containing a combination of orthogonal stagnation-point flow with strain rate a and a shear flow along the plate having strain b. The power-law lubricant spreads on the plate with constant flow rate Q and forms a thin lubrication layer of variable thickness $h(x)$. Owing to the mass conservation principle the flow rate Q is given by Eq. (2.1). Under these assumptions, the steady two-dimensional flow of second grade fluid is governed by Eq. (2.2) and

$$u\frac{\partial u}{\partial x}+v\frac{\partial u}{\partial y}=-\frac{1}{\rho}\frac{\partial p}{\partial x}+\nu\nabla^2 u+\frac{k_0}{\rho}\left[\begin{array}{c}2\frac{\partial}{\partial x}\left\{u\frac{\partial^2 u}{\partial x^2}+v\frac{\partial^2 u}{\partial x\partial y}-2\left(\frac{\partial u}{\partial x}\right)^2-\frac{\partial u}{\partial y}\left(\frac{\partial v}{\partial x}+\frac{\partial u}{\partial y}\right)\right\}\\+\frac{\partial}{\partial y}\left\{\begin{array}{c}u\frac{\partial^2 v}{\partial x\partial y}+u\frac{\partial^2 v}{\partial x^2}+v\frac{\partial^2 u}{\partial y^2}+v\frac{\partial^2 u}{\partial x\partial y}\\-2\left(\frac{\partial u}{\partial x}\frac{\partial v}{\partial x}+\frac{\partial u}{\partial y}\frac{\partial v}{\partial y}\right)\end{array}\right\}\end{array}\right], \tag{3.1}$$

$$u\frac{\partial v}{\partial x}+v\frac{\partial v}{\partial y}=-\frac{1}{\rho}\frac{\partial P}{\partial y}+\nu\nabla^2 v+\frac{k_0}{\rho}\left[\begin{array}{c}\frac{\partial}{\partial x}\left\{u\frac{\partial^2 v}{\partial x^2}+u\frac{\partial^2 u}{\partial x\partial y}+v\frac{\partial^2 v}{\partial x\partial y}+v\frac{\partial^2 u}{\partial y^2}\right.\\ \left.-2\left(\frac{\partial u}{\partial x}\frac{\partial v}{\partial x}+\frac{\partial u}{\partial y}\frac{\partial v}{\partial y}\right)\right\}\\ +2\frac{\partial}{\partial y}\left\{u\frac{\partial^2 v}{\partial x\partial y}+v\frac{\partial^2 v}{\partial y^2}-2\left(\frac{\partial v}{\partial y}\right)^2-\frac{\partial v}{\partial x}\left(\frac{\partial v}{\partial x}+\frac{\partial u}{\partial y}\right)\right\}\end{array}\right], \tag{3.2}$$

where k_0 is the second grade fluid parameter. Elimination of pressure between Eqs. (3.1) and (3.2) gives

$$\frac{\partial(\psi,\nabla^2\psi)}{\partial(x,y)}=\nu\nabla^4\psi-\frac{k_0}{\rho}\frac{\partial(\psi,\nabla^4\psi)}{\partial(x,y)}, \tag{3.3}$$

where $u=\partial\psi/\partial y$ and $v=-\partial\psi/\partial x$

The no-slip boundary conditions are given by Eqs (2.7) and (2.8). The continuity of the shear stress at the interface $y=\delta(x)$ suggests that

$$\mu\frac{\partial u}{\partial y}+k_0\left(v\frac{\partial^2 u}{\partial y^2}+u\frac{\partial}{\partial x}\frac{u}{y}-2\frac{\partial u}{\partial y}\frac{\partial}{\partial y}\right)=\mu_L\frac{\partial U}{\partial y}. \tag{3.4}$$

Using Eqs (2.1) and (2.9) (2.14), one obtains the following slip condition

$$\frac{\partial u}{\partial y}+\frac{k_0}{\mu}\left(v\frac{\partial^2 u}{\partial y^2}+u\frac{\partial^2 u}{\partial x\partial y}-2\frac{\partial u}{\partial y}\frac{\partial v}{\partial y}\right)=\frac{k}{\mu}\left(\frac{1}{2Q}\right)^n u^{2n}. \tag{3.5}$$

The other boundary condition at the interface is represented in Eq. (2.17). The assumption of a thin lubrication layer allows us to impose boundary conditions (3.5) and (2.17) at the surface when $y=0$. The boundary conditions far away from the stagnation-point are given in Eq (2. 8). The wall shear stress is represented by the left hand side of Eq. (3.4). Substituting Eq (2.19) into Eq (3.3) and integrating the resulting equations, one yields

$$f'''+ff''-f'^2-We\left(ff^{iv}-2f'f'''+f''^2\right)+C_1=0, \tag{3.6}$$

$$g'''+fg''-f'g'-We\left(fg^{iv}-f'g'''+f''g''-f'''g'\right)+C_2=0. \tag{3.7}$$

In above equations, $We=k_0a/\rho\nu$ is the Weissenberg number. The boundary conditions in new variables take the form

$$f(0)=0 \quad f''(0)+3We\,f'(0)f''(0)=\lambda(f'(0))^{2n},\ f'(\infty)=1,\ f''(\infty)=0, \tag{3.8}$$

$$g(0)=0 \qquad g''(\infty)=\gamma,\quad g'''(\infty)=0, \tag{3.9}$$

$$g'(0)+We\left(g'(0)f''(0)+2g''(0)f'(0)\right)=2n\lambda\,g'(0)(f'(0))^{2n-1}. \tag{3.10}$$

In Eqs. (3.8) and (3.9), the boundary conditions are augmented at the free stream because the governing equations are one order higher than the Navier-Stokes equations.

Substituting the free stream conditions give $C_1 = 1$ and $C_2 = \gamma(\alpha - \beta)$. Thus Eqs. (3.6) and (3.7) yield

$$f''' + ff'' - f'^2 - We\left(ff^{iv} - 2f'f''' + f''^2\right) + 1 = 0, \tag{3.11}$$

$$g''' + fg' - f'g' - We\left(fg^{iv} - f'g''' + f''g'' - f'''g'\right) + \gamma(\alpha - \beta) = 0. \tag{3.12}$$

Assuming $g'(\eta) = \gamma h(\eta)$ Eq. (3.13) reduces to

$$h'' + fh' - f'h - We(fh''' - f'h'' + f''h' - f'''h) + C = 0, \tag{3.13}$$

in which $C = \alpha - \beta$ and the corresponding boundary conditions become

$$h'(0) + We\,(h(0)f''(0) + 2h'(0)f'(0)) = 2n\lambda\, h(0)(f'(0))^{2n-1}, \tag{3.14}$$

$$h'(\infty) = 1,\ h''(\infty) = 0. \tag{3.15}$$

Employing (2.19), the dimensionless shear stress at the wall takes the form

$$Re_x^{1/2}C_f = xf''(0)[1 + 3We\,f'(0)] + \left[g''(0) + We\left(g'(0)f''(0) + 2g''(0)f'(0)\right)\right]$$

$$= xf''(0)[1 + 3We\,f'(0)] + \gamma[h'(0) + We\,(h(0)f''(0) + 2h'(0)f'(0))], \tag{3.16}$$

$$= xRe_x^{1/2}C_{f_1} + \gamma Re_x^{1/2}C_{f_2}, \tag{3.17}$$

where $Re_x^{1/2}C_{f_1} = f''(0)\,[1 + 3We\,f'(0)]$ and

$Re_x^{1/2}C_{f_2} = h'(0) + We\,(h(0)f''(0) + 2h'(0)f'(0))$.

To find the location of separation point (stagnation-point) x_s on the surface, we put $Re_x^{1/2}C_f = 0$. Therefore

$$\lambda = -\frac{g'(0) + We\left(g'(0)f''(0) + 2g''(0)f'(0)\right)}{xf''(0)[1 + 3We\,f'(0)]} = -\gamma\frac{h'(0) + We\,(h(0)f''(0) + 2h'(0)f'(0))}{f''(0)[1 + 3We\,f'(0)]}. \tag{3.18}$$

3.2 Analysis of numerical results

Equations (3.11) and (3.13) subject to boundary conditions (3.8), (3.14) and (3.15) are solved numerically for different values of parameter λ, β and We by using Keller-box method which is already explained in detail in section 1.7. In order to see the effects of slip parameter λ and Weissenberg number We on f', Figs. 3.1 and 3.2 are plotted. Figs. 3.3-3.6 have been displayed to see the effects of λ, We and β on h while the effects of flow behaviour index n on f' and h are presented in Figs 3.7 and 3.8 The effects of parameters on the location of stagnation-point have been shown in Figs 3.9-3.11. The numerical values of $Re_x^{1/2}C_{f_1}$ and α for various values of λ and We have been shown in Table 3.1

while Tables 3.2 and 3.3 represent the numerical values of $R_{e_x}{}^{1/2}C_h$ for various values of λ, β and We. Tables 3.4 and 3.5 show comparison of numerical values of $R_{e_x}{}^{1/2}C_{f_1}, \alpha$ and $R_{e_x}{}^{1/2}C_h$ for various values of We and β for no-slip case with those of [54].

The horizontal velocity component f' for various values of slip parameter and for a fixed value of We is shown in Fig. 3.1. It is clear from the figure that f' decreases by increasing λ. This figure illustrates both full-slip and no-slip cases for $\lambda \to 0$ and $\lambda \to \infty$, respectively. The increase of velocity with increasing slip indicates the ability of the power-law lubricant to increase the velocity of the fluid impinging on the surface. The variation in the horizontal velocity component f' for different values of We and for a fixed value of λ is displayed in Fig. 3.2. It is clear from the figure that f' follows a decreasing trend by increasing We. Test computations show that such a decrease is not significant for smaller values of λ. This implies that the full-slip suppress the viscoelastic effects. Fig. 3.3 is plotted to show the variation of tangential velocity component h for different values of λ when $We = 0.5$ and $\beta = 0$. It is noted that h increases by increasing the slip at the surface. Fig. 3.4 shows the variation of h against λ and β when $We = 0.5$. Here two interesting situations occur. For negative values of β, h decreases by increasing λ. On the contrary, it follows a converse trend by increasing λ for positive values of β. The later case also confirms the appearance of distinct regions of reversed flow corresponding to positive values of β. The variation of h for different values of β and for a fixed value of We both for partial and no-slip cases is depicted in Fig. 3.5. In either case it is observed that the tangential velocity component increases by varying β from -5 to 5. Moreover, the lubricant enhances the tangential velocity. Fig. 3.6 shows the effects of We on the shear velocity h for different values of β when $\lambda = 4$. We observe that h follows a similar trend by varying β as observed in Fig. 3.5. Moreover, a decrease in Weissenberg number We enhances the magnitude of tangential velocity. Thus enhancement in the magnitude of tangential velocity component owes to a decrease in We or a decrease in λ. Variation of f' for different values of n when $\lambda = 2$ and for two different values of We is depicted in Fig. 3.7. It is clear from this figure that f' increases by increasing n. This increase is more rapid for lower values of We. Fig. 3.8 is plotted to illustrate the behavior of h under the influence of flow behavior index n when $\lambda = 2$. We see that h increases by increasing n for negative

values of β and decreases for positive values of β. Figs. 3.9 and 3.10 elucidate the effects of parameters λ and β on the streamlines. It is evident from these figures that the stagnation point moves towards right on the x-axis by increasing the slip at the surface for $\beta = 0$ or by increasing β keeping λ fixed, respectively. Fig. 3.11 shows that the stagnation point moves towards left on the x-axis by increasing We for fixed value of slip parameter when $\beta = 0$

The change in numerical values of ${R_{e_x}}^{1/2}C_{f_1}$ and α for various values of λ when $We = 0.5$ and $We = 0.05$ is displayed in Table 3.1. It is clear from the Table 3.1 that the numerical values of both ${R_{e_x}}^{1/2}C_{f_1}$ and α increase by varying λ from 0 to ∞. Table 3.2 shows the change in ${R_{e_x}}^{1/2}C_h$ for different values of λ and β when $We = 0.5$. It is clear from the Table 3.2 that an increase in the value of λ from 0 to ∞ results in increase in ${R_{e_x}}^{1/2}C_h$ when $\beta \leq 0$. However, for the case when $\beta > 0$, ${R_{e_x}}^{1/2}C_h$ decreases by increasing λ. Table 3.3 elucidates the change in ${R_{e_x}}^{1/2}C_h$ for various values of We and β when $\lambda = 5$. We see that for $\beta > 0$, ${R_{e_x}}^{1/2}C_h$ increases with an increase in We. On the contrary, ${R_{e_x}}^{1/2}C_h$ decreases when $\beta \leq 0$. Tables 3.4 and 3.5 show comparison of numerical values of ${R_{e_x}}^{1/2}C_{f_1}$, α and ${R_{e_x}}^{1/2}C_h$ respectively for various values of We and β when there is no-slip with those calculated by Li et al [54]. It is observed that the numerical values of ${R_{e_x}}^{1/2}C_{f_1}$ and ${R_{e_x}}^{1/2}C_h$ in the limiting case when there is no-slip agrees well with the values already reported in the literature.

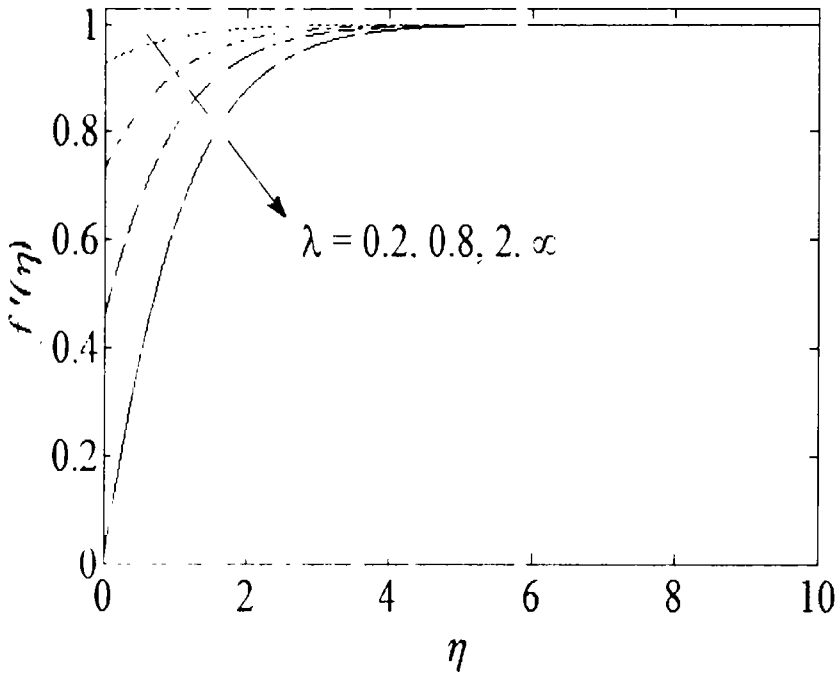

Fig.3.1. Variation in $f'(\eta)$ for different values λ when $We = 0.5$.

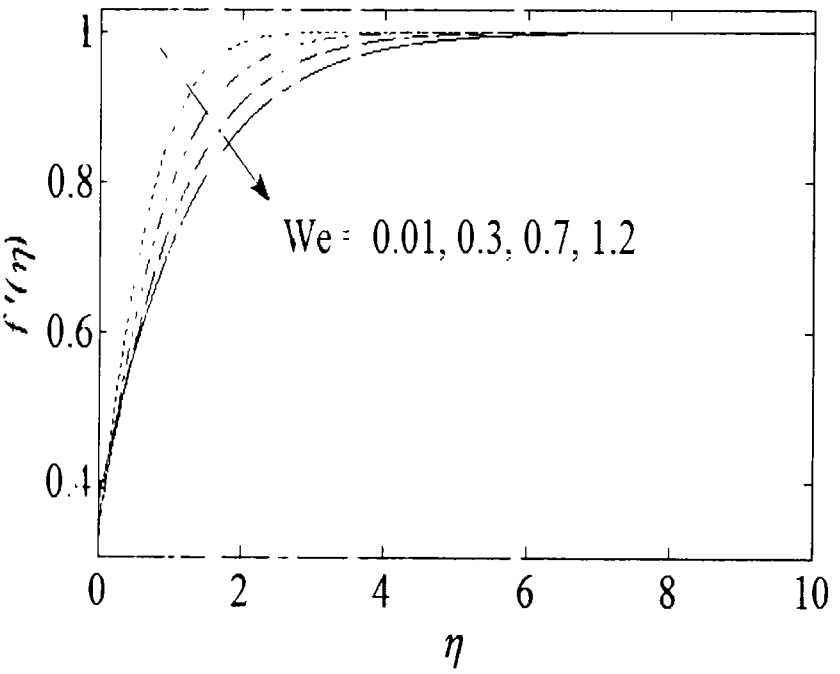

Fig.3.2. Variation in $f'(\eta)$ for different values of We when $\lambda = 3$.

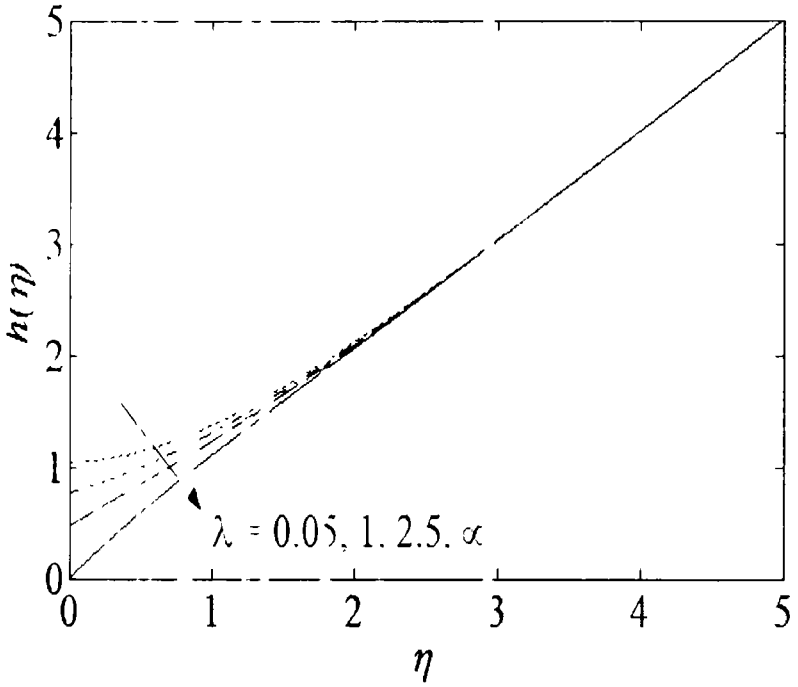

Fig.3 3. Variation in $h(\eta)$ for different values of λ when $\beta = 0$ and $We = 0.5$.

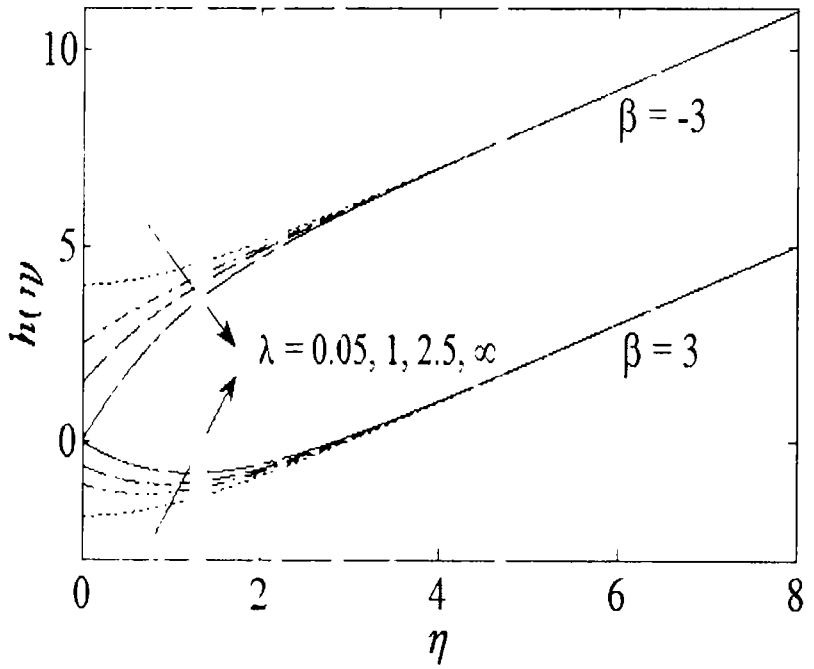

Fig 3.4 Variation in $h(\eta)$ for different values of λ and β when $We = 0.5$.

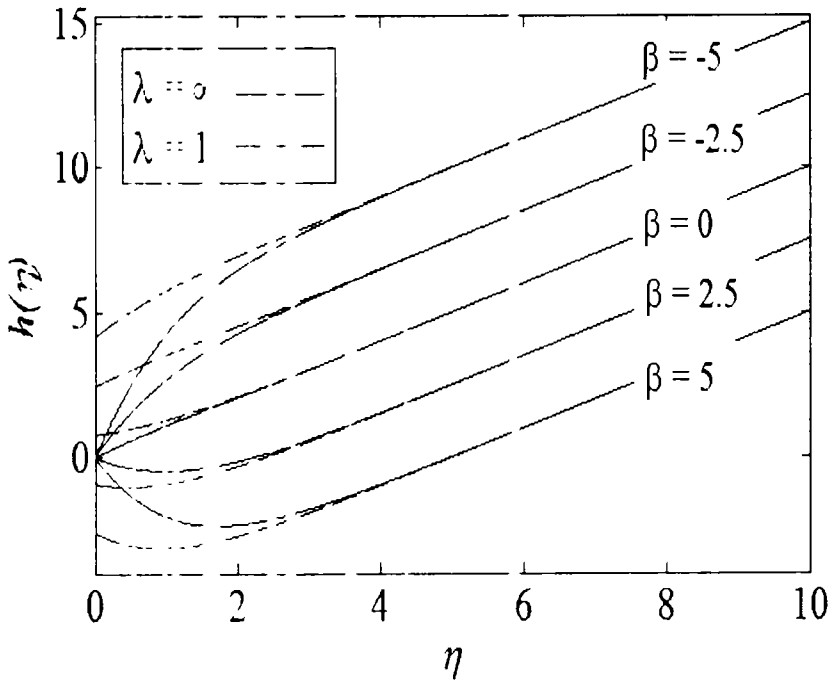

Fig.3.5. Effect of slip on $h(\eta)$ for different values of β when $We = 0.5$.

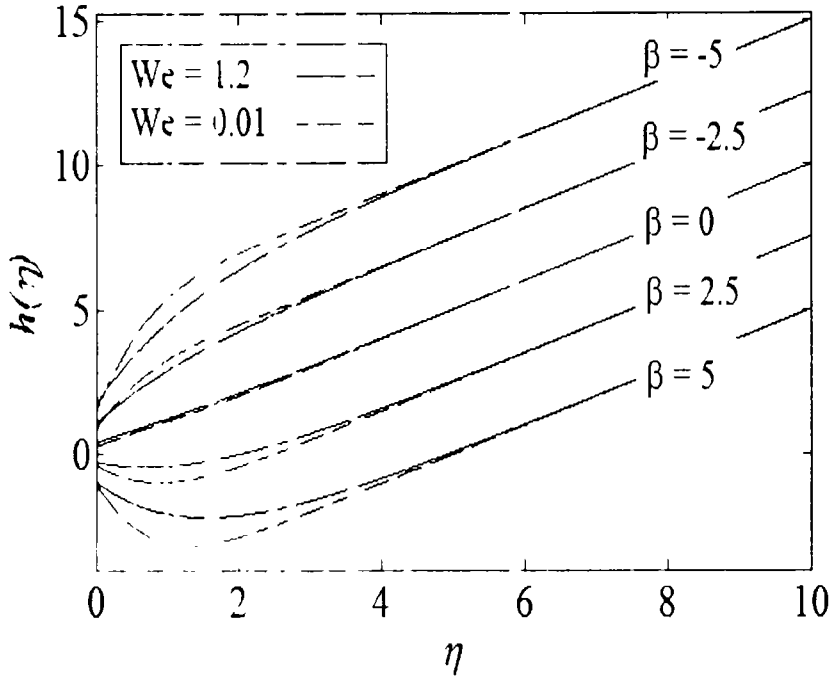

Fig.3.6. Effect of We on $h(\eta)$ for different values of β when $\lambda = 4$.

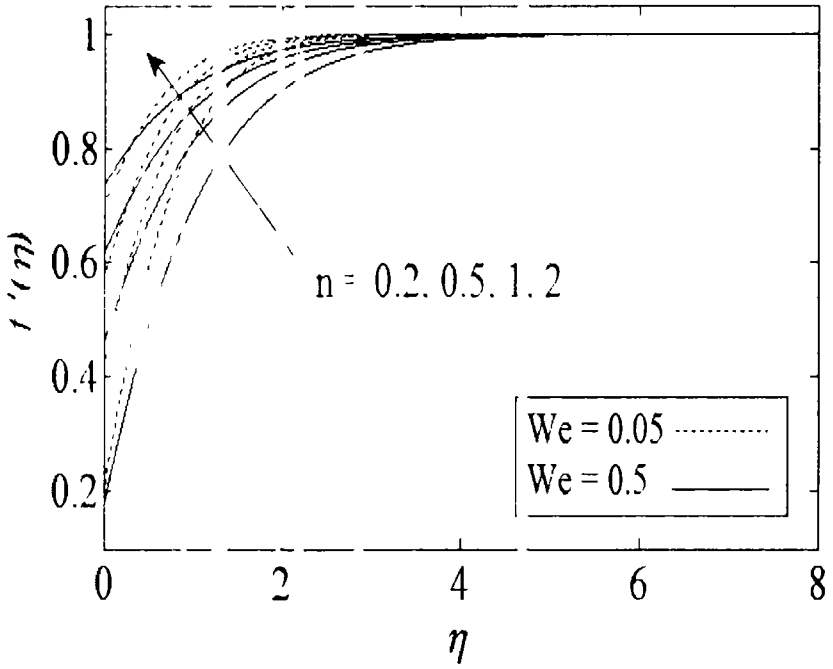

Fig. 7. Effect of flow behavior index n on $f'(\eta)$ when $\lambda = 2$ and $We = 0.5$.

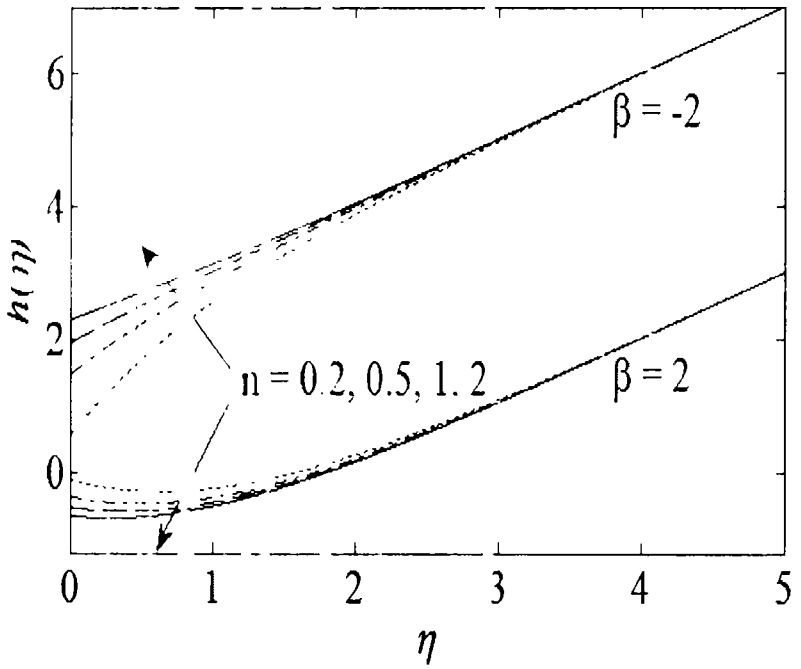

Fig. 8. Effect of flow behavior index n on $h(\eta)$ when $\lambda = 2$ and $We = 0.5$.

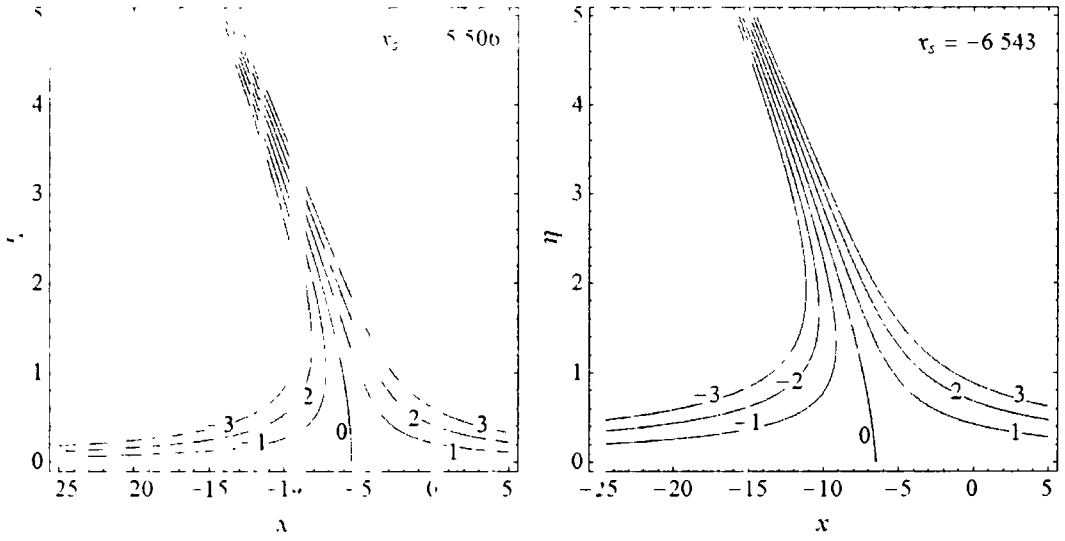

$\lambda = 0.5$ $\lambda = 5$

Fig.3 9. Streamlines showing the effects of slip when $We = 0.5, \beta = 0, \gamma = 5$.

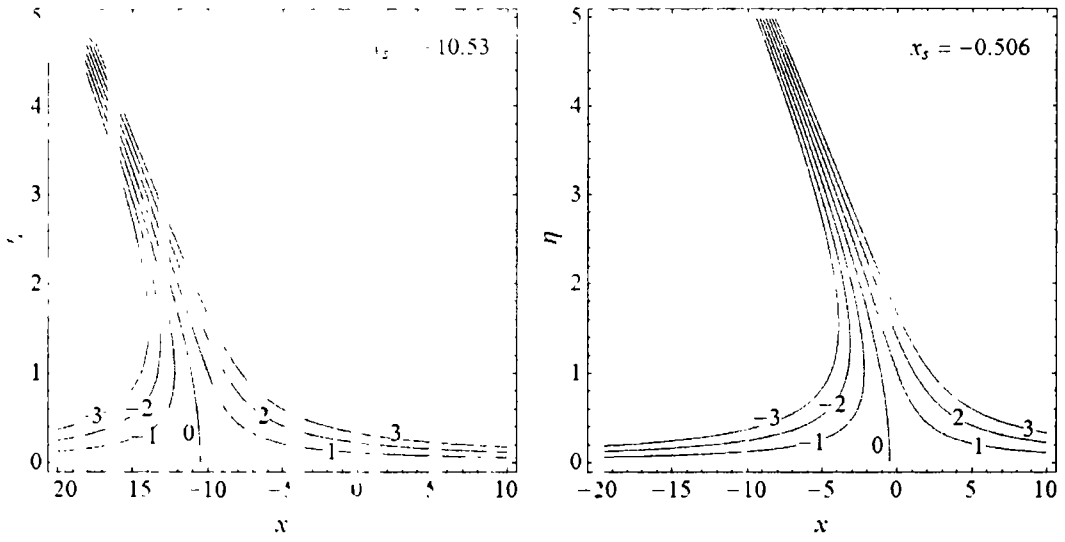

$\beta = -$ $\beta = 1$

Fig 3.10. Streamlines showing the effects of parameter β when $We = \lambda = 0.5, \gamma = 5$.

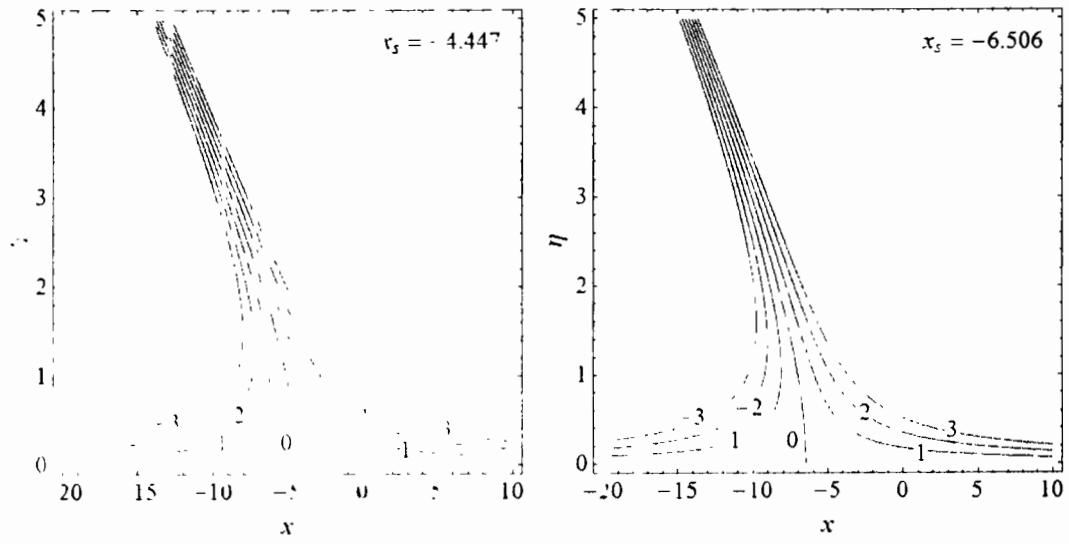

Fig.3 11. Streamlines showing the effects of We when $\lambda = 0.5, \beta = 0, \gamma = 5$.

Table 3.1: Impact of slip parameter λ on $R_{e_x}{}^{1/2}C_{f_1}$ and α.

$We = 0.5$			$We = 0.05$		
λ	$R_{e_x}{}^{1/2}C_{f_1}$	α	λ	$R_{e_x}{}^{1/2}C_{f_1}$	α
0.05	0.0198423	0.0165893	0.05	0.0424031	0.0164028
0.1	0.0393910	0.0330210	0.1	0.0827249	0.0322846
0.5	0.1841689	0.1581293	0.5	0.3419276	0.1420064
1.0	0.3348054	0.2958945	1.0	0.5523375	0.2433985
2.0	0.5406256	0.5018014	2.0	0.7788879	0.3706274
5.0	0.7597807	0.7587700	5.0	0.9981635	0.5223289
10	0.8363330	0.8649429	10	1.0869816	0.5967908
50	0.8903610	0.9487069	50	1.1612002	0.6681064

100	0.8965048	0.9588520	100	1.1705256	0.6778271
500	0.9013107	0.9668995	500	1.1779773	0.6857377
∞	0.9025014 [54]	0.9638954 [54]	∞	1.179839 [54]	0.687734 [54]

Table 3.2: Impact of λ and β on $R_{e_x}^{1/2}C_h$ when $We = 0.5$.

λ	$\beta = 0$	$\beta = 5$	$\beta = -5$
0.05	0.0211315	−0.078110	0.1203731
0.1	0.0420940	−0.154856	0.2390438
0.5	0.2027522	−0.718091	1.1235950
1.0	0.3818285	−1.292183	2.0558402
2.0	0.6533382	−2.049776	3.3564525
5.0	0.9957851	−2.803089	4.7946595
10	1.1366289	−3.045024	5.3182823
50	1.2465143	−3.205243	5.6982719
100	1.2597150	−3.222766	5.7421960
500	1.2701666	−3.236373	5.7767065
∞	1.272780 [54]	−3.239720 [54]	5.785280 [54]

Table 3.3: Impact of We and β on $R_{e_x}^{1/2}C_h$ when $\lambda = 5$.

We	$\beta = 0$	$\beta = 5$	$\beta = -5$
0.01	1.0895978	−4.243463	6.2554636
0.05	1.0781991	−4.080050	6.0690204
0.1	1.0654379	−3.899551	5.8627391
0.5	0.9957851	−2.972068	4.7946691
1.0	0.9419525	−2.360739	4.0712972
1.5	0.9001453	−1.979875	3.6009434
2.0	0.8626899	−1.525316	3.2506969

Table 3.4: Comparison showing effects of We and β on ${R_{e_x}}^{1/2}C_{f_1}$ and α for the no-slip case. The values written in the brackets are calculated by Li et al. [54].

We	${R_{e_x}}^{1/2}C_{f_1}$	α
0	1.232594 (1.23259)	0.6479022 (0.64790)
0.1	1.134251 (1.13425)	0.725040 (0.72504)
0.2	1.058179 (1.05818)	0.793784 (0.79378)
0.3	0.996890 (0.99689)	0.856403 (0.85640)
0.4	0.945882 (0.94588)	0.914558 (0.91456)
0.5	0.902485 (0.902485)	0.968899 (0.96890)
1.0	0.752764 (0.752763)	1.202033 (1.20203)
2.0	0.596775 (0.596775)	1.566224 (1.56622)

Table 3.5: Comparison showing effects of We and β on ${R_{e_x}}^{1/2}C_h$ for the no-slip case ($\lambda = \infty$). The values written in the brackets are calculated by Li et al. [54].

We	$\beta = 0$	$\beta = 5$	$\beta = -5$
0	1.406368 (1.40637)	-4.756558 (-4.75656)	7.569314 (7.56931)
0.1	1.366218 (1.36622)	-4.304363 (-4.30436)	7.036803 (7.03680)
0.2	1.335391 (1.33539)	-3.955234 (-3.95523)	6.626002 (6.62600)
0.3	1.310462 (1.31046)	-3.673611 (-3.67360)	6.294509 (6.29451)
0.4	1.289708 (1.28971)	-3.439634 (-3.43963)	6.019047 (6.01905)
0.5	1.272168 (1.27217)	-3.240309 (-3.24031)	5.784649 (5.78465)
1.0	1.211672 (1.21167)	-2.551788 (-2.55179)	4.975144 (4.97514)
2.0	1.151269 (1.15127)	-1.832512 (-1.83250)	4.135046 (4.13505)

3.3 Concluding remarks

In this chapter, we have investigated the non-orthogonal flow of a second grade fluid near a stagnation-point over a plate lubricated with power-law fluid. The governing equations along with boundary conditions are transformed to ordinary differential equations by a suitable choice of transformations. The governing equations possess a similarity solution when $n = 1/2$. The numerical solutions are developed using Keller-box method. Some findings of the investigation are

(i) The increase in horizontal velocity f' with increasing slip indicates the ability of the power law lubricant to increase the velocity of the fluid. Moreover, f' decreases by increasing We and increases by increasing n.

(ii) Tangential velocity component h decreases by increasing λ for $\beta \leq 0$ and it increases when $\beta > 0$. Furthermore, h is a decreasing function of We.

(iii) h increases by increasing n for negative values of β and decreases for positive values of β.

(iv) The stagnation-point moves towards right on the x-axis by increasing the slip or by increasing β and it moves towards left by increasing We.

(v) ${Re_x}^{1/2}C_{f_1}$ and α increase by increasing λ while ${Re_x}^{1/2}C_{f_1}$ decreases and α increases by augmenting We. It is also noted that ${Re_x}^{1/2}C_h$ increases by increasing λ when $\beta \leq 0$ and it reduces for $\beta > 0$. An opposite behavior is observed for ${Re_x}^{1/2}C_h$ against We.

Chapter 4

Oblique stagnation-point flow of a couple stress fluid over a lubricated surface

In this chapter steady two-dimensional oblique flow of a couple stress fluid towards a stagnation-point on a flat plate is investigated numerically by implementing Keller-box method. The plate is lubricated with a slim coating of power-law fluid. Governing partial differential equations of a couple stress fluid are converted into ordinary differential equations using similarity transformations. Analysis has been performed by imposing continuity of velocity and shear stress of both the fluids at the interface. Influence of slip and couple stress parameters on the horizontal and shear velocity components, wall shear stress and location of the stagnation-point are presented graphically and in the tabular form. The limiting cases for the viscous fluid and no-slip condition have been deduced from the present solutions. The results are compared and found in excellent agreement with already recorded results in the existing research articles [28, 54].

4.1 Mathematical formulation

Consider the steady, two dimensional, oblique flow of a couple stress fluid towards a stagnation-point over a lubricated plate. A power-law fluid is used as lubricant. The plate is fixed in xz-plane such that it is symmetric with respect to the origin. The fluid impinges on the plate with an angle γ in the domain $y > 0$. (Fig. 2.1). We assume that power-law lubricant spreads on the plate forming a thin coating with the flow rate given by Eq. (2.1). The flow problem is governed by the following equations along with continuity Eq. (2.2).

$$u\frac{\partial u}{\partial x} + v\frac{\partial u}{\partial y} = -\frac{1}{\rho}\frac{\partial P}{\partial x} - \nu\left(\frac{\partial^2 u}{\partial x^2} + \frac{\partial^2 u}{\partial y^2}\right) - \nu_1\left(\frac{\partial^4 u}{\partial x^4} + 2\frac{\partial^4 u}{\partial x^2 \partial y^2} + \frac{\partial^4 u}{\partial y^4}\right), \tag{4.1}$$

$$u\frac{\partial v}{\partial x} + v\frac{\partial v}{\partial y} = -\frac{1}{\rho}\frac{\partial P}{\partial y} + \nu\left(\frac{\partial^2 v}{\partial x^2} + \frac{\partial^2 v}{\partial y^2}\right) - \nu_1\left(\frac{\partial^4 v}{\partial x^4} + 2\frac{\partial^4 v}{\partial x^2 \partial y^2} + \frac{\partial^4 v}{\partial y^4}\right), \tag{4.2}$$

where ν_1 represents the ratio of couple stress viscosity to the density. Eliminating the pressure between Eqs. (4.1) and (4.2) one obtains

$$u\frac{\partial^2 u}{\partial y \partial x} + v\frac{\partial^2 u}{\partial y^2} - u\frac{\partial^2 v}{\partial x^2} - v\frac{\partial^2 v}{\partial x \partial y} - \nu\left(\frac{\partial^3 u}{\partial y \partial x^2} + \frac{\partial^3 u}{\partial y^3} - \frac{\partial^3 v}{\partial x^3} - \frac{\partial^3 v}{\partial x \partial y^2}\right) +$$

$$\nu_1\left(\frac{\partial^5 u}{\partial y \partial x^4} + 2\frac{\partial^5 u}{\partial x^2 \partial y^3} + \frac{\partial^5 u}{\partial y^5} - \frac{\partial^5 v}{\partial x^5} - 2\frac{\partial^5 v}{\partial x^3 \partial y^2} - \frac{\partial^5 v}{\partial x \partial y^4}\right) = 0. \tag{4.3}$$

The expression for the wall shear stress is given as

$$\tau_w = \mu\left(\frac{\partial u}{\partial y}\right)\Big|_{y=0} - \eta^*\left(\frac{\partial}{\partial}\frac{u}{3}\right)\Big|_{y=0}. \tag{4.4}$$

Boundary conditions at the solid lubricant interface are given by Eqs. (2.7) and (2.8). The continuity of shear stress at the interface $y = \delta(x)$ implies

$$\mu\frac{\partial u}{\partial y} - \eta^*\frac{\partial^3 u}{\partial y^3} = \mu_L\frac{\partial U}{\partial y}, \tag{4.5}$$

in which μ represents the viscosity of the lubricant defined in Eq. (2.10).

Substituting Eqs. (2.11)-(2.14) into Eq. (4.5) we get

$$\frac{\partial u}{\partial y} - \frac{\eta^*}{\mu}\frac{\partial^3 u}{\partial y^3} = \frac{k}{\mu}\left(\frac{1}{2Q}\right)^n x^{2n}. \tag{4.6}$$

The rest of the boundary conditions are the same as mentioned in Eqs. (2.17) and (2.18). Following Santra et al. [148] the boundary conditions (4.6) and (2.17) can be imposed at the fluid-solid interface. Boundary conditions at free stream have been mentioned in equation (2.18).

Using transformations given in Eq. (2.19), the governing Eqs. (4.3), (2.7), (4.6), and (2.17) reduce to

$$f^{iv} + ff''' - f'f'' - Kf^{vi} = 0, \tag{4.7}$$

$$g'' + fg'' + fg''' - f'g'' - g'f' - Kg^{vi} = 0 \tag{4.8}$$

$$f(0) = 0,\ f'''(0) = 0,\ f''(0) - Kf^{iv}(0) = \lambda(f'(0))^{2n},$$

$$f'(\infty) = 1,\ f''(\infty) = 0, \tag{4.9}$$

$$g(0) = 0,\quad g'''(0) = 0,\quad g''(0) - Kg^{iv}(0) = 2n\lambda\, g'(0)\left(f'(0)\right)^{2n-1}, \tag{4.10}$$

$$g''(\infty) = \gamma,\quad g'''(\infty) = 0, \tag{4.11}$$

where $K = \nu_1 a^2/\nu^2$ is called the couple stress parameter. The parameter λ given in Eqs. (4.9) and (4.10) is defined in Eq. (2.24). The boundary conditions $f'''(0) = 0$ and $g'''(0) = 0$ are consequences of the vanishing of couple stress tensor at the fluid-solid interface. Integrating Eqs. (4.7) and (4.8) and using free stream conditions, we get

$$f''' - f' + ff'' + 1 - Kf^v = 0, \tag{4.12}$$

$$g''' + fg'' - f'g' - Kg^{iv} = \gamma(\beta - \alpha). \tag{4.13}$$

In order to eliminate γ from Eq. (4.13) we let $g'(\eta) = \gamma h(\eta)$ to obtain

$$h'' + fh' - f'h - Kh^{iv} = \beta - \alpha. \tag{4.14}$$

The boundary conditions in new variables become

$$h'(0) = 1,\ h'(0) - Kh''(0) = 2n\lambda h(0)\left(f'(0)\right)^{2n-1},\ h'(\infty) = 1,\ h''(\infty) = 0. \tag{4.15}$$

Equation (2.24) suggests that to obtain similar solution, one should have $n = 1/2$. The parameter λ given in Eq. (2.24) measures slip produced by the lubricant on the surface. Employing (2.19), the dimensionless wall shear stress is given by

$$Re_x^{1/2} C_f = x\left(f''(0) - Kf^{iv}(0)\right) + \left(g''(0) - Kg^{iv}(0)\right)$$

$$= x\left(f''(0) - Kf^{iv}(0)\right) + \gamma\left(h'(0) - Kh'''(0)\right), \tag{4.16}$$

$$= xRe_x^{1/2} C_{f_1} + \gamma Re_x^{1/2} C_h, \tag{4.17}$$

where $Re_x^{1/2} C_{f_1} = f''(0) - Kf^{iv}(0)$ and $Re_x^{1/2} C_h = h'(0) - Kh'''(0)$.

To find the stagnation-point x_s on the surface, we set $Re_x^{1/2} C_f = 0$ to get

$$x_s = -\frac{g'(0) - Kg'''(0)}{f'(0) - Kf^{iv}(0)} = \gamma \frac{h'(0) - Kh'''(0)}{f'(0) - Kf^{iv}(0)}. \tag{4.18}$$

4.2 Discussions of the numerical results

Equations (4.12) and (4.15) are highly nonlinear and coupled along with nonlinear and coupled boundary conditions (4.9) and (4.15). Exact solution of such a system of equations is not possible. To handle this system of equations numerically, we have employed the Keller-box method which is based on an implicit finite difference approach. Using this scheme, the values of f' and h' are displayed graphically for different values of λ, K and β in Figs. 4.1-4.5. The influences of pertinent parameters on the streamlines have been shown in Figs. 4.6 and 4.7 while the impact of these parameters on $Re_x^{1/2} C_{f_1}$, α, $Re_x^{1/2} C_h$ and stagnation-points is displayed in Tables 4.1-4.5. A comparison of numerical values of $Re_x^{1/2} C_{f_1}$, α and $Re_x^{1/2} C_h$ in the special cases with that of existing in the literature is presented in Tables 4.6-4.7.

Fig. 4.1 displays the variation in horizontal velocity component under the influence of slip parameter λ. Dashed lines show the results for viscous and solid lines for the couple stress

fluid. We observe that f' decreases by decreasing λ. Moreover, couple stress parameter enhances the effects of slip parameter. Analysis showing the impact of couple stress parameter K on f' for fixed λ is presented in Fig. 4.2. It is clear from this figure that f' is a decreasing function of K. One can observe some alteration inside the boundary layer. However, the curve becomes smooth at the free stream. Effects of slip parameter λ on h' for two values of β when $K = 0.5$ have been provided in Fig. 4.3. According to this figure h' decreases for positive values of β and increases for negative values of β. Fig. 4.4 is displayed to analyze the behavior of h' under the influence of β both for the no-slip and partial slip cases. It is noted that an increment in the value of β results in the decrease of h'. This decrease is more significant on the rough surface (when $\lambda \to \infty$). Influence of parameter β on h' for two values of K when $\lambda = 2$ is presented in Fig. 4.5. The analysis shows that h' decreases by increasing β. This decrease is diminished by enlarging couple stress parameter K.

The stream lines explored in Fig. 4.6 show the influence of β on the stagnation-point in the presence of slip when $\gamma = 8$ and $K = 0.5$. It has been observed that the stagnation-point moves towards left by increasing β. Streamlines showing the impact of slip and couple stress parameters are expressed in Fig. 4.7. It is evident that stagnation-point shifts towards right by increasing λ as well as K when $\beta = 0$.

Influence of parameters λ and K on the skin friction coefficient ${R_{e_x}}^{1/2}C_{f_1}$ and boundary layer displacement α has been provided through Table 4.1. It is observed through Table 4.1 that ${R_e}^{1/2}C_{f_1}$ increases by increasing λ and decreases by increasing K. Likewise, α is increased by enhancing λ and K independently. Impact of λ on ${R_{e_x}}^{1/2}C_h$ is shown in Table 4.2. It has been observed that ${R_{e_x}}^{1/2}C_h$ gains the magnitude by enhancing λ for $\beta \leq 0$ and loses for $\beta > 0$. Data showing ${R_{e_x}}^{1/2}C_h$ for various values of K is represented through Table 4.3. It is observed that ${R_{e_x}}^{1/2}C_h$ gains the magnitude as K is accelerated for $\beta \geq 0$ and loses its values for $\beta < 0$. The movement of the stagnation-point under the influence of increasing λ, K and β is demonstrated through Tables 4.4 and 4.5. We observe that stagnation point moves towards right on the x-axis by raising both λ and K while it shifts leftwards by augmenting β. The tabular results shown in Tables 4.4 and 4.5 do confirm the investigations made through Figs. 4.6 and 4.7.

The numerical data regarding $R_{e_x}{}^{1/2}C_f$, α and $R_{e_x}{}^{1/2}C_h$ in the limiting case (when $\lambda \to \infty$) acknowledges the values already recorded in the research articles [28, 54]. This evidence certifies the correctness of our investigation.

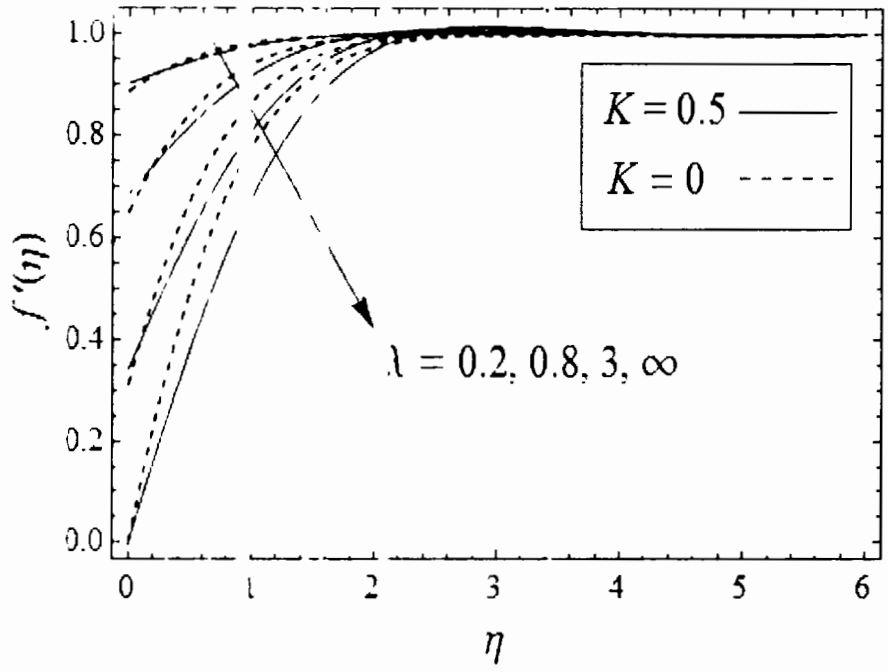

Fig. 4. . Effects of slip parameter λ on $f'(\eta)$ for viscous and couple stress fluids.

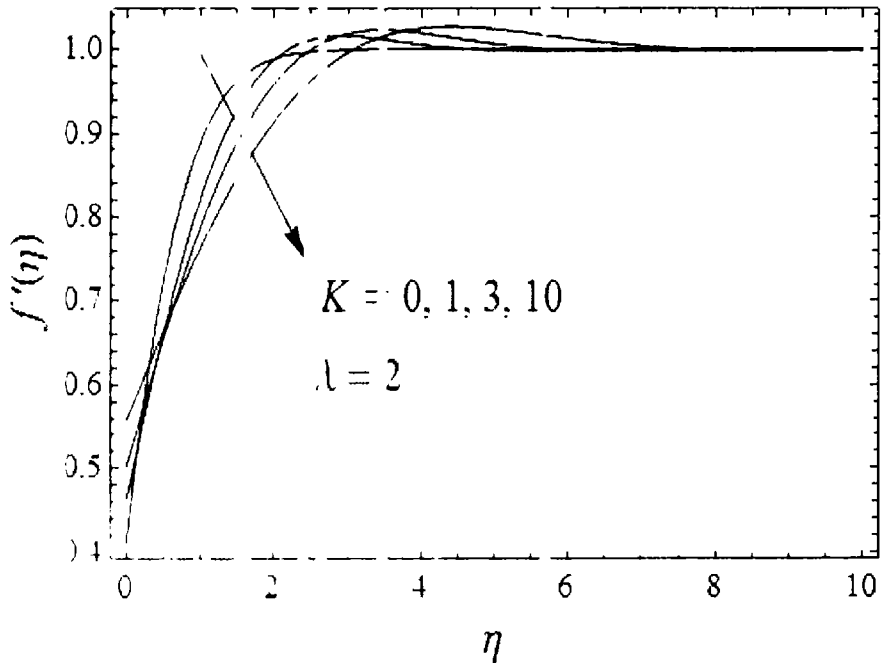

Fig. 4.2. Impact of couple stress parameter K on $f'(\eta)$ when $\lambda = 2$.

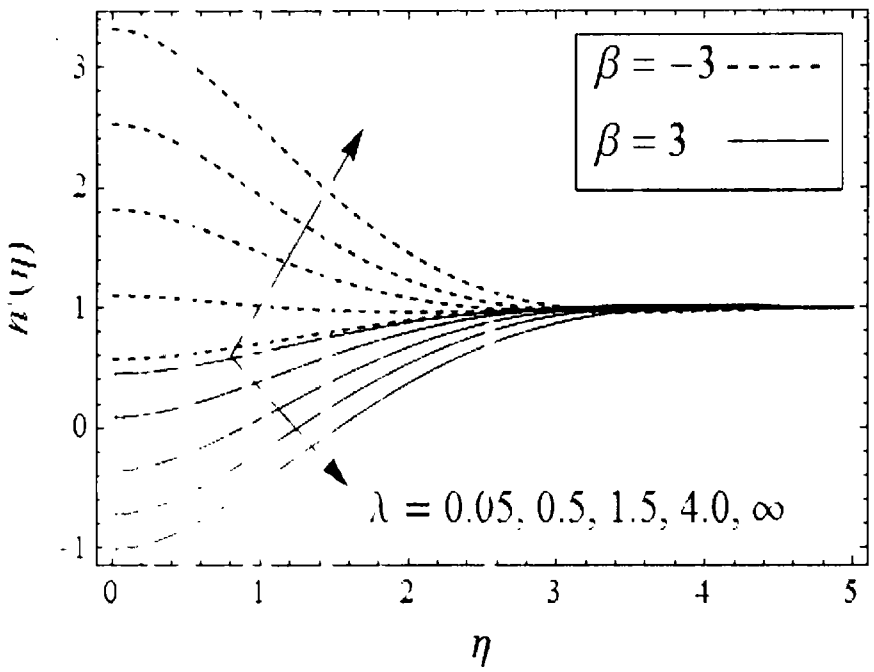

Fig. 4.3 Influence of slip parameter λ on $h'(\eta)$ when $K = 0.5$ for various values of β.

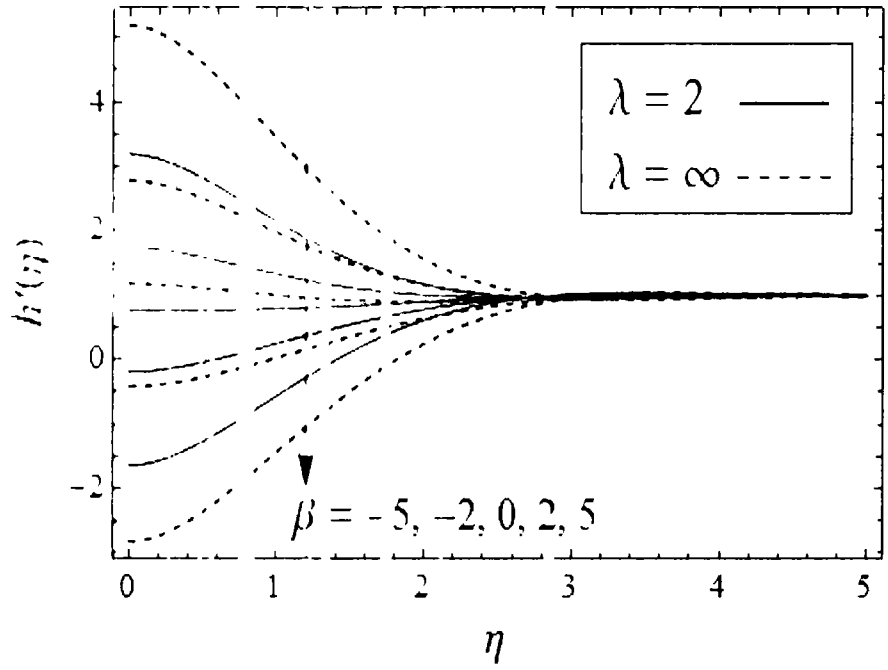

Fig. 4.4 Influence of parameter β on $h'(\eta)$ when $K = 0.5$, for two different values of λ.

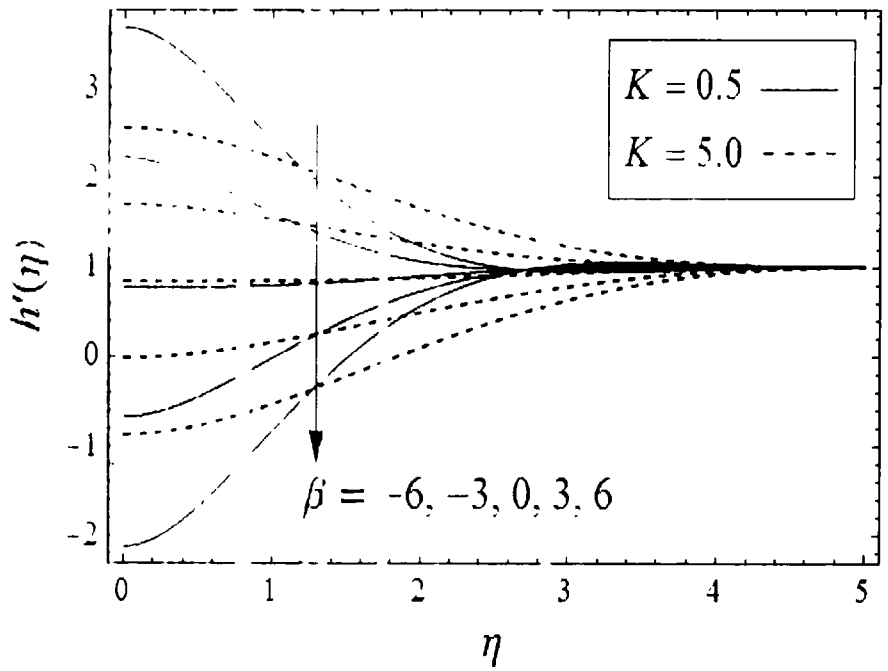

Fig. 4.5 Influence of parameter β on $h'(\eta)$ when $\lambda = 2$, for different values of K.

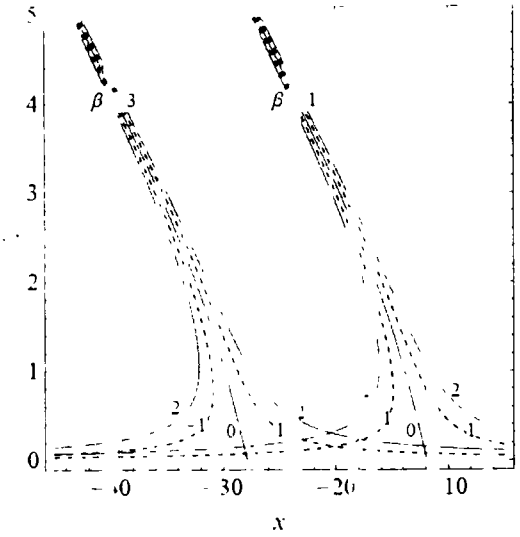

Fig 4.6(a) $\gamma = 8, K = 0.5, \lambda = 0.5$

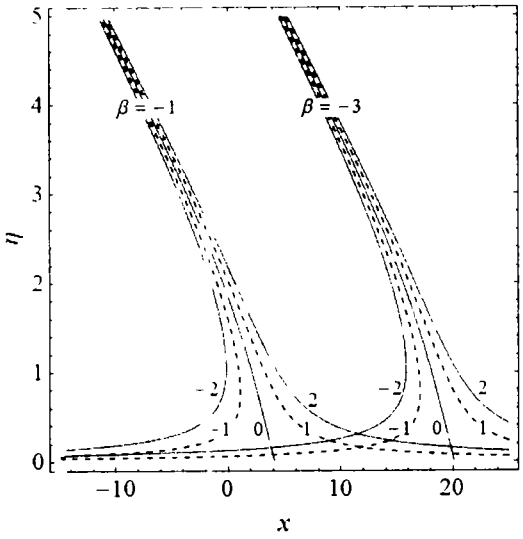

Fig. 4.6(b) $\gamma = 8, K = 0.5, \lambda = 0.5$

Fig. 6 Streamlines showing the effects of parameter β.

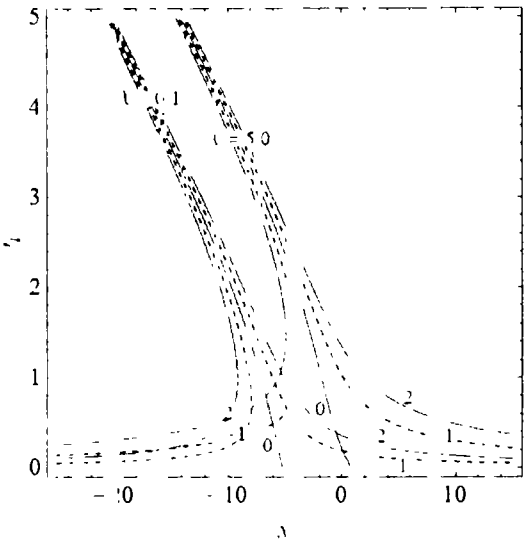

Fig. 4.7(a) $\gamma = 8, K = 0.5, \beta = 0$

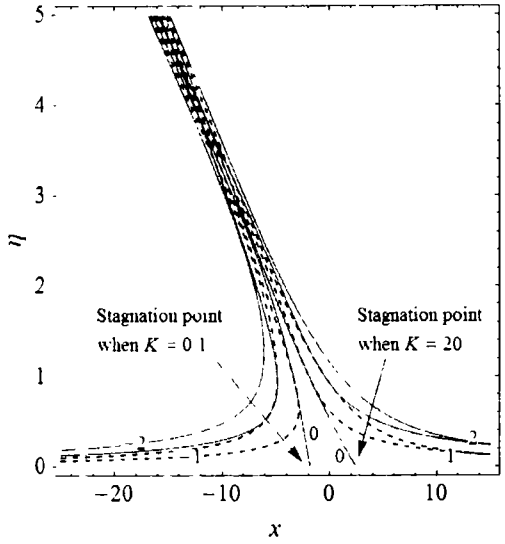

Fig. 4.7(b) $\gamma = 10, \lambda = 2, \beta = 0$

Fig. 4.7 Influence of slip parameter λ (Fig. 4.7(a)) and couple stress parameter K (Fig. 4.7(b)) on streamlines.

Table 4.1: Variation in $R_{e_x}{}^{1/2}C_{f_1}$ and α under the influence of λ.

	$K = 0.5$		$K = 5$		$K = 10$	
λ	$R_{e_x}{}^{1/2}C_{f_1}$	α	$R_{e_x}{}^{1/2}C_{f_1}$	α	$R_{e_x}{}^{1/2}C_{f_1}$	α
0.05	0.024513	0.016329	0.011422	0.018947	0.008514	0.020793
0.1	0.047914	0.032162	0.022481	0.037498	0.016793	0.041183
0.5	0.201357	0.142545	0.099287	0.172333	0.075344	0.1903459
1.0	0.331885	0.241714	0.171830	0.310541	0.132596	0.345523
2.0	0.482678	0.384176	0.266567	0.510465	0.210874	0.575286
5.0	0.645204	0.559482	0.385209	0.801933	0.315692	0.923349
10	0.717872	0.651212	0.444105	0.969866	0.370759	1.130525
50	0.782587	0.742733	0.498917	1.145315	0.423622	1.350408
100	0.791011	0.755479	0.506158	1.170181	0.430701	1.381723
500	0.797793	0.765898	0.511999	1.190562	0.436424	1.407399
∞	0.799494	0.768534	0.513465	1.195725	0.437862	1.413905

Table 4.2: Variation in $R_{e_x}{}^{1/2}C_{f_1}$ under the influence of λ and β when $K = 0.5$.

	$\beta = 0$	$\beta = 5$	$\beta = -5$
0.05	0.4[illegible]9505	0.307015	0.551994
0.1	0.4[illegible]3315	0.203884	0.682746
0.5	0.5[illegible]2598	−0.463751	1.548947
1.0	0.6[illegible]1277	−1.017849	2.300403
5.0	0.9[illegible]8302	−2.270844	4.187448
10	1.0[illegible]6333	−2.537892	4.650558
50	1.1[illegible]5641	−2.764100	5.075382

00	1.1[illegible]9566	−2.792576	5.131708
00	1.1[illegible]0963	−2.815420	5.177246
∞	1.1[illegible]3848	−2.820999	5.188695

Table 4.3: Variation in $R_e^{1/2}C_h$ under the influence of K and β when $\lambda = 1$.

K	$\beta = 0$	$\beta = 5$	$\beta = -5$
0	0.5[illegible]0232	−2.427089	3.507552
0.5	0.6[illegible]1277	−1.017849	2.300403
1	0.6[illegible]0213	−0.749052	2.089478
5	0.7[illegible]0745	−0.152261	1.693750
10	0.8[illegible]4636	0.138111	1.531161
50	0.9[illegible]9295	0.709083	1.189507
00	0.9[illegible]2800	0.840434	1.105165
00	0.9[illegible]4183	0.965210	1.023155
000	0.9[illegible]9406	0.996439	1.002374

Table 4.4: Variation in the stagnation point (x_s) under the influence of parameters of λ, β and γ when $K = 1$.

γ	λ	$\beta = -3$	$\beta = 0$	$\beta = 3$
1	0.5	[illegible].558763	−0.4412284	−3.441220
	5.0	[illegible].197895	0.1979019	−2.802092
2	0.5	[illegible].117527	−0.8824568	−6.882440
	5.0	[illegible].395791	0.3958038	−5.604183
5	0.5	[illegible]2.79382	−2.2061420	−17.20610
	5.0	[illegible]5.98948	0.9895095	−14.01046
8	0.5	[illegible]0.47011	−3.5298270	−27.52976
	5.0	5.58316	1.5832150	−22.41673

Table 4.5: Variation in the stagnation point (x_s) against K, β and γ when $\lambda = 1$.

γ	K	$\beta = -3$	$\beta = 0$	$\beta = 3$
1	0.5	.667206	−0.3327937	−3.332794
	5.0	.870132	−0.1293493	−3.128831
2	0.5	.334413	−0.6655873	−6.665587
	5.0	.740265	−0.2586985	−6.257662
5	0.5	3.33603	−1.6639680	−16.66397
	5.0	4.35066	−0.6467463	−15.64415
8	0.5	1 33765	−2 6623490	−26.66235
	5.0	2.96106	−1.0347940	−25.03065

Table 4 6: Comparison of computed results of $R_{e_x}{}^{1/2}C_{f_1}$ and α with that of Labropulu et al [28] for no-slip case ($\lambda = \infty$)

$R_{e_x}{}^{1/2}C_{f_1}$		α	
Present result when $K = 0$	Result by [28] when $\varepsilon = 0$	Present result when $K = 0$	Result by [28] when $\varepsilon = 0$
1.232594	1.23259	0.6479025	0.64790

Table 4 7: Comparison of computed results of $R_{e_x}{}^{1/2}C_h$ with that of Labropulu et al. [28] and Li et a [54] for no-slip case ($\lambda = \infty$)

$R_{e_x}{}^{1/2}C_f$	$\beta = 5$	$\beta = 0$	$\beta = \alpha$	$\beta = -\alpha$
Present results when $K = 0$	−4.75621"	1.406514	2.205136	0.607917
Results by [28] when $\varepsilon = 0$	−4 7562	1.4065	2.2051	0.6079
Results by [54] when $We = 0$	−4.756	1.4063	2.2049	0.6077

4.3 Conclusions

In this chapter, oblique flow of a couple stress fluid near stagnation-point over a lubricated plate is investigated. A power law fluid has been used as a lubricant. To obtain similar solution of the flow problem, we have fixed $n = 1/2$. The Keller-box method is employed to solve the flow problem numerically. Our interest is to figure out the effects of free parameter β and couple stress parameter K on the flow characteristics on the lubricated surface. It has been concluded that:

(i) Slip produced on the surface increases the velocity of the bulk fluid and abolishes the effects of free stream velocity for large values.

(ii) The stagnation-point is shifted towards right and left along x-axis under the influence of physical parameters in the presence of lubrication.

(iii) The skin friction coefficient ${R_{e_x}}^{1/2}C_{f_1}$ increases by increasing λ and decreases by increasing K. However, boundary layer displacement α is increased by enhancing λ and/or K

(iv) It has been observed that ${R_{e_x}}^{1/2}C_h$ gains the magnitude by enhancing λ for $\beta \leq 0$ and loses for $\beta > 0$. Data showing ${R_{e_x}}^{1/2}C_h$ for various values of K is represented through Table 3. It is observed that ${R_{e_x}}^{1/2}C_h$ gains the magnitude as K is accelerated for $\beta \geq 0$ and loses its values for $\beta < 0$.

Chapter 5

Slip flow of a second grade fluid past a lubricated rotating disc

The chapter deals with the study of slip flow of a second-grade fluid past a lubricated rotating disc. The disc is lubricated with a power-law fluid. The interfacial conditions between fluid and lubricant are imposed on the surface of disc by assuming a thin lubrication layer. A highly accurate technique, the Keller-box method is used to obtain numerical solutions. The effects of Weissenberg number and slip parameter on three components of the fluid velocity and pressure are analyzed graphically while effects on both components of skin friction are demonstrated through tables. The obtained solutions agree well in the special case with those of Andersson and Rousselet [147].

5.1 Problem statement

Consider the steady, axisymmetric flow of a second grade fluid over a rotating disc lubricated with a slim coating of power-law fluid. The disc is rotating with a uniform velocity ω about z-axis which is taken normal to the disc. The origin O is located at the center of the disc as shown in Fig. 5.1.

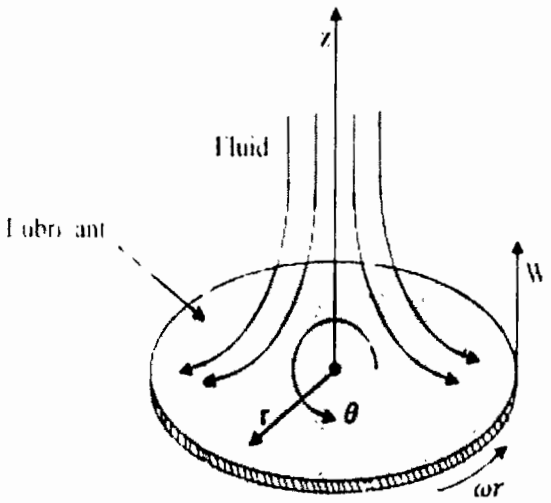

Figure 5.1 A sketch of considered flow situation

If U, V, W are the velocity components of the power-law fluid, then its volume flow rate is given by [47]

$$Q = \int_0^{S(r} U(r,z)\, 2\pi r\, dz, \tag{5.1}$$

in which s is the thickness of the power-law lubricant. The equations governing the rotational flow are

$$\frac{\partial}{\partial} + \frac{u}{r} + \frac{w}{z} = 0, \tag{5.2}$$

$$\rho\left(\frac{\partial u}{\partial t} + u\frac{u}{r} + \frac{v}{r}\frac{\partial u}{\partial \theta} - \frac{v^2}{r} + w\frac{\partial u}{\partial z}\right) = -\frac{\partial P}{\partial r} + \left(\frac{1}{r}\frac{\partial(r\tau_{rr})}{\partial r} - \frac{\tau_{\theta\theta}}{r} + \frac{\partial \tau_{zr}}{\partial z}\right), \tag{5.3}$$

$$\rho\left(\frac{\partial v}{\partial t} + u\frac{v}{r} + \frac{v}{r}\frac{\partial v}{\partial \theta} + \frac{uv}{r} + w\frac{\partial v}{\partial z}\right) = -\frac{1}{r}\frac{\partial P}{\partial \theta} + \left(\frac{1}{r^2}\frac{\partial(r^2\tau_{r\theta})}{\partial r} + \frac{\partial \tau_{z\theta}}{\partial z} + \frac{\tau_{\theta r} - \tau_{r\theta}}{r}\right), \tag{5.4}$$

$$\rho\left(\frac{\partial w}{\partial t} + u\frac{w}{r} + \frac{v}{r}\frac{\partial w}{\partial \theta} + w\frac{w}{z}\right) = -\frac{\partial P}{\partial z} + \left(\frac{1}{r}\frac{\partial(r\tau_{rz})}{\partial r} + \frac{\partial \tau_{zz}}{\partial z}\right), \tag{5.5}$$

in which

$$\tau_{rr} = 2\mu u + k_0\left[\frac{3v^2}{r^2} + v_z^2 - \frac{2vv_r}{r} - v_r^2 + 2wu_{rz} + 2uu_{rr}\right],$$

$$\tau_{r\theta} = \tau_{\theta r} = \mu\left(v_r - \frac{v}{r}\right) + k_0\left[-\frac{2uv}{r^2} - \frac{wv_z}{r} + \frac{3vu_r}{r} - \frac{2uv_r}{r} + u_z v_z + u_r v_r + wv_{rz} + uv_{rr}\right],$$

$$\tau_{rz} = \tau_{zr} = \mu u_z + k_0\left[-\frac{vv_z}{r} + u_z w_r - u_z u_r + wu_{zz} - v_z v_r + uu_{rz}\right],$$

$$\tau_{\theta\theta} = -\frac{2\mu v}{r} + \frac{k_0}{r^2}[-2u^2 - 3v^2 + 2ru_r + 2rvv_r + 2rwu_z + r^2 v_z^2 + r^2 v_r^2],$$

$$\tau_{\theta z} = \tau_{z\theta} = \mu v_z + \frac{k_0}{r}[2u_z - uv_z + rv_z w_z + rwv_{zz} + ruv_{rz}],$$

$$\tau_{zz} = 2\mu w_z + k_0[-u_z^2 - v_z^2 + 2ww_{zz}],$$

where $[u, v, w]$ is the velocity vector of the second grade fluid and k_0 is the second grade fluid parameter. The boundary condition at the surface are

$$U(r,0) = 0, \quad V(r,0) = \omega r, \quad W(r,0) = 0, \quad P(r\ 0) = 0. \tag{5.6}$$

As the lubrication layer is very slim, therefore

$$w(r,z) = 0 \quad \forall\ 0 \le z \le \delta. \tag{5.7}$$

The continuity of the shear stress at the interface $z = \delta(r)$ for both the fluids suggests

$$\mu\left(\frac{\partial u}{\partial z}\right) + k_0\left(\begin{array}{c} -\frac{v}{r}\frac{\partial v}{\partial z} - \frac{\partial}{\partial}\cdot\frac{\partial w}{\partial z} + \frac{\partial u}{\partial z}\frac{\partial u}{\partial r} + \frac{\partial v}{\partial z}\frac{\partial v}{\partial r} + \frac{\partial w}{\partial z}\frac{\partial w}{\partial r} - \frac{\partial u}{\partial r}\frac{\partial w}{\partial r} \\ + u\frac{\partial^2 u}{r\partial z} + w\frac{\partial^2}{\partial z} + w\frac{\partial^2 w}{\partial r\partial z} + u\frac{\partial^2 w}{\partial r^2} \end{array}\right) = \mu_L\frac{\partial U}{\partial z}, \tag{5.8}$$

$$\mu\left(\frac{\partial v}{\partial z}\right) + k_0\left(\frac{u}{r}\frac{\partial v}{\partial z} - \frac{\partial v}{\partial z}\frac{\partial}{\partial} + w\frac{\partial^2 v}{\partial z^2} + \frac{v}{r}\frac{\partial w}{\partial r} - \frac{\partial v}{\partial r}\frac{\partial w}{\partial r} + u\frac{\partial^2 v}{\partial r\partial z}\right) = \mu_L\frac{\partial V}{\partial z}, \tag{5.9}$$

in which μ_L represents the viscosity of the lubricant. If we assume $\frac{\partial U}{\partial r} \ll \frac{\partial U}{\partial z}$ and $\frac{\partial V}{\partial r} \ll \frac{\partial V}{\partial z}$, then

$$\mu_L = k\left[\left(\frac{\partial U}{\partial z}\right)^2 + \left(\frac{\partial V}{\partial z}\right)^2\right]^{\frac{n-1}{2}}. \tag{5.10}$$

It is assumed that U and V are nearly proportional to z where $0 \le z \le \delta$. Thus following [117], we have

$$u(r,z) = \frac{\tilde{U}(r)z}{\delta(r)}, \tag{5.11}$$

$$v(r,z) = \omega r - \frac{(\omega r - \tilde{V}(r))z}{\delta(r)}, \tag{5.12}$$

where $\tilde{U}$ and $\tilde{V}$ are the velocity components of both fluids at the interface. Solving Eqs. (5.11) and (5.11), we get

$$\delta(r) = \frac{Q}{\pi\tilde{U}(r)}. \tag{5.13}$$

Like the shear stress, the radial and azimuthal velocity components of both fluids are also continuous at the interface. Therefore

$$\tilde{U} = u, \tilde{V} = v. \tag{5.14}$$

Substituting Eqs. (5.10)-(5.14) into Eqs. (5.8) and (5.9), one gets the following boundary conditions known as slip conditions.

$$\mu\left(\frac{\partial u}{\partial z}\right) + \frac{k_0}{\mu}\left(\begin{array}{c} \frac{v}{r}\frac{\partial v}{\partial z} - \frac{\partial u}{\partial z}\frac{\partial w}{\partial z} + \frac{\partial u}{\partial z}\frac{\partial u}{\partial r} + \frac{\partial v}{\partial z}\frac{\partial v}{\partial r} \\ + \frac{\partial w}{\partial z}\frac{\partial w}{\partial r} - \frac{\partial u}{\partial r}\frac{\partial w}{\partial r} + u\frac{\partial^2 u}{\partial r\partial z} \\ + w\frac{\partial^2 u}{\partial z^2} + w\frac{\partial}{\partial}\frac{w}{\partial z} + u\frac{\partial^2 w}{\partial r^2} \end{array}\right) = \frac{k}{\mu}\left(\frac{\pi}{Q}\right)^n u(ru)^n[u^2 + (\omega r - v)^2]^{\frac{n-1}{2}}, \tag{5.15}$$

$$\frac{\partial v}{\partial z} + \frac{k_0}{\mu}\left(\begin{array}{c} \frac{u}{r}\frac{\partial v}{\partial z} - \frac{\partial v}{\partial z}\frac{\partial w}{\partial z} + w\frac{\partial^2 v}{\partial z^2} \\ \frac{v}{r}\frac{\partial w}{\partial r} - \frac{\partial v}{\partial r}\frac{\partial w}{\partial r} + u\frac{\partial^2 v}{\partial r \partial z} \end{array}\right) = -\frac{k}{\mu}\left(\frac{n}{Q}\right)^n (\omega r - v)(rv)^n [v^2 + (\omega r - v)^2]^{\frac{n-1}{2}}. \quad (5.16)$$

Using the continuity of axial velocity components of both fluids and Eq. (5.7), we have

$$w(r, \delta(r)) = W(r, \delta(r)) = 0. \quad (5.17)$$

Following [47], we can impose boundary conditions (5.15)-(5.17) at the surface of disc. Furthermore

$$u(r, \infty) = 0 \text{ and } v(r, \infty) = 0. \quad (5.18)$$

The radial shear stress τ_r and tangential shear stress τ_θ at the wall are respectively given by

$$\tau_r = \mu\left(\frac{\partial u}{\partial z}\right)_{z=0} + k_0\left(\begin{array}{c} -\frac{\partial v}{\partial z}\frac{\partial u}{\partial z}\frac{\partial w}{\partial z} + \frac{\partial u}{\partial z}\frac{\partial u}{\partial r} + \frac{\partial v}{\partial z}\frac{\partial v}{\partial r} + \frac{\partial w}{\partial z}\frac{\partial w}{\partial r} - \frac{\partial u}{\partial r}\frac{\partial w}{\partial r} \\ + u\frac{\partial^2 u}{\partial r \partial z} + w\frac{\partial^2 u}{\partial z^2} + w\frac{\partial^2 w}{\partial r \partial z} + u\frac{\partial^2 w}{\partial r^2} \end{array}\right)_{z=0},$$

$$\tau_\theta = \mu\left(\frac{\partial v}{\partial z}\right)_{z=0} + k_0\left(\frac{u}{r}\frac{\partial v}{\partial z} - \frac{v}{r}\frac{\partial w}{\partial z} + w\frac{\partial^2 v}{\partial z^2} + \frac{v}{r}\frac{\partial u}{\partial r} - \frac{\partial v}{\partial r}\frac{\partial w}{\partial r} + u\frac{\partial^2 v}{\partial r \partial z}\right)_{z=0}. \quad (5.19)$$

To solve the Eqs. (5.3)-(5.5), we introduce the following dimensionless variables

$$\eta = z\sqrt{\frac{\omega}{\nu}}, \quad u = \omega r f(\eta), \quad v = \omega r g(\eta), \quad w = \sqrt{\omega\nu}\, h(\eta), \quad P = \omega\mu\, p(\eta). \quad (5.20)$$

The resulting system in new variables is given by

$$h' = -2f, \quad (5.21)$$

$$f'' - hf' - f^2 + g^2 + We(hf'' + 4ff'' + 2g'^2) = 0, \quad (5.22)$$

$$g'' - hg' - 2fg + We(hg''' + 4fg'' - 2f'g') = 0, \quad (5.23)$$

$$p' + 2f'' - 2fh + We(4ff' + 2f'h) = 0. \quad (5.24)$$

The corresponding boundary conditions take the form

$$h(0) = 0, \quad p(0) = 0, \quad (5.25)$$

$$f(0) + We[2f(0)f'(0) - f'(0)h'(0) + h(0)f''(0)]$$
$$= \lambda(f(0))^{\frac{4}{3}}[(f'(0))^2 + (1 - g(0))^2]^{-1/3}, \quad (5.26)$$

$$g(0) + We[2f(0)g'(0) - g'(0)h'(0) + h(0)g''(0)]$$
$$= -\lambda(f(0))^{\frac{1}{3}}(1 - g(0))[f(0))^2 + (1 - g(0))^2]^{-1/3}, \quad (5.27)$$

$$f(\infty) = 0, \quad g(\infty) = 0, \quad (5.28)$$

where $We = k_0\omega/\rho\nu$ is the Weissenberg number and λ is the slip parameter defined as

$$\lambda = \frac{k_1 \bar{\nu}}{\mu}\left(\frac{\pi}{2}\right)^{\frac{1}{3}} \frac{\omega^{\frac{2}{3}}}{\omega^{\frac{1}{2}}}. \tag{5.29}$$

It is worth mentioning that we have used $n = 1/3$ in Eqs. (5.21)-(5.24) in order to obtain similarity solution. The constant λ given in Eq. (5.29) may be rewritten as

$$\lambda = \frac{\sqrt{\frac{\nu}{\omega}}}{\frac{\mu}{k}\left(\frac{2\omega}{\pi}\right)^{\frac{1}{3}}} = \frac{L_{visc}}{L_{lub}}. \tag{5.30}$$

According to Eq. (5.30), the constant λ defines the ratio of L_{visc} (viscous length) to the L_{lub} (lubrication length). For highly viscous lubricant and small L_{lub}, the parameter λ achieves a huge value. When $\lambda \to \infty$, one gets $f(0) = 0$ and $g(0) = 1$, from Eqs. (5.26) and (5.27) commonly known as no-slip conditions. Conversely when $\lambda \to 0$, we obtain $f'(0) = 0$ and $g'(0) = 0$ called full-slip boundary conditions. Thus λ measures the slip produced by the lubricant. The non-dimensional forms of both the components of skin friction coefficients are given as

$$Re_r^{1/2} C_f = f'(0) + We(h(0)f''(0) + 2f(0)f'(0) - f'(0)h'(0)), \tag{5.31}$$

$$Re_r^{1/2} C_{f_\theta} = g'(0) + We(h(0)g''(0) + 2f(0)g'(0) - g'(0)h'(0)) \tag{5.32}$$

where $Re_r = \alpha r^2/\nu$, C_{fr} and $C_{f\theta}$ respectively at the wall are defined as

$C_{fr} = \tau_r/\rho V^2$, $C_{f\theta} = \tau_\theta/\rho V^2$,

where $V = \omega r$

5.2 Numerical results and discussions

To analyze the behaviour of parameters λ and We on velocity and pressure profiles, the Eqs. (5.21)-(5.24) together with boundary conditions (5.25)-(5.28) are solved numerically using Keller-box method.

Figs. 5.2-5.6 are plotted to see the effects of slip parameter λ on velocity profiles f, g, h and pressure p for some fixed values of Weissenberg number while the effects of We in the presence of slip are shown in Figs. 5.7-5.11. Dashed lines shown in Figs. 5.2-5.6 corresponds to the results already calculated by Andersson and Rousselet [147] through Keller-box method for the case of Newtonian fluid (i.e. $We = 0$). Numerical computations for both the components of skin friction coefficients under the influence of pertinent

parameters are presented in Tables 5.1 and 5.2.

Fig. 5.2 is displayed to show the effects of slip parameter λ on axial velocity when $We = 1$. It is important to mention here that as we increase the numerical values of λ, an increase in the value of $-h$ is observed. Also the thickness of boundary layer region is increased by increasing the numerical value of λ. Fig. 5.3 shows the variation in the radial velocity f caused by the centrifugal force under the influence of slip parameter. It is clear from Fig. 5.3 that by increasing slip on the surface, f decreases. The variation in radial velocity has the same behaviour as observed for the viscous fluid (dashed lines) except the peak value which was near 0.18 at $\eta = 0.90$ for the viscous fluid when there is no-slip [147] and is now near 0.225 when η is about 1.1 (near unity) for the second grade fluid. The gradual increase in the radial velocity in Fig. 5.4 with increasing value of λ is directly related with the distributions of the h-profile shown in Fig. 5.2. This is due to the direct relation between f and h shown in Eq. (5.21).

Effect of slip parameter on the azimuthal velocity component g in the circumferential direction is depicted in Fig. 5.4. It is obvious from Fig. 5.4 that by increasing λ, the numerical value of g is increased. The torque required to maintain steady rotation of the disc is controlled by this component of the velocity. The imposed torque decreases monotonically by increasing slip on the surface. It is evident from Figs. 5.2-5.4 that the variation in the three velocity components is more significant for smaller values of λ showing that power-law lubricant increases the fluid velocity at the surface.

The variation in the pressure under the influence of slip parameter when $We = 1$, is observed in Figs. 5.5 and 5.6. It is clear from Fig. 5.6 that pressure increases by decreasing slip. However, the behaviour of pressure distribution near the full-slip is different as shown in the Fig. 5.5. For $\lambda \leq 1$ the disc pressure is less than the ambient pressure $-p(\infty)$, which means that the flow is driven towards the disc by the axial pressure gradient in this particular range of λ.

Effect of We on h-profile when $\lambda = 1.5$ is shown in Fig. 5.7. It is obvious from this figure that by increasing We, the axial velocity component is increased. The velocity profile shown by dashed line is for viscous fluid i.e. when $We = 0$. Fig. 5.8 shows the variation in radial velocity component f when We ranges from 0 to 5 and $\lambda = 1.5$. It is evident from this figure that f increases with an increase in Weissenberg number. We observe some

reverse effects on the peak for higher values of We. The azimuthal velocity component g is presented in Fig. 5.9. It is evident from this figure that g increases by increasing the value of We when λ is fixed. An opposite behaviour in the shear component of velocity is observed near the surface. Figs. 5.10 and 5.11 are plotted for the pressure distribution using various values of We when $\lambda = 1.5$. It is clear from these figures that $-p$ increases when $0 \leq We < 0.8$. After this pressure profile shows an increase near the surface and then decreases dramatically.

Table 5.1 elucidates the change in numerical values of $Re_r^{1/2}C_{fr}$ and $Re_r^{1/2}C_{f\theta}$ for various values of λ when $We = 0.05$ and $We = 1$. It is clear from the Table 5.1 that as λ increases from 0 to ∞, the numerical values of $Re_r^{1/2}C_{fr}$ increase. However, the numerical values of $Re_r^{1/2}C_{f\theta}$ initially increase and then start decreasing. The numerical values of $Re_r^{1/2}C_{fr}$ and $Re_r^{1/2}C_{f\theta}$ for different values of We when $\lambda = 0.05$ and $\lambda = 1.5$ are presented in Table 5.2. According to this table as the numerical value of We increases, the numerical values of $Re_r^{1/2}C_{fr}$ increase while those of $Re_r^{1/2}C_{f\theta}$ decrease.

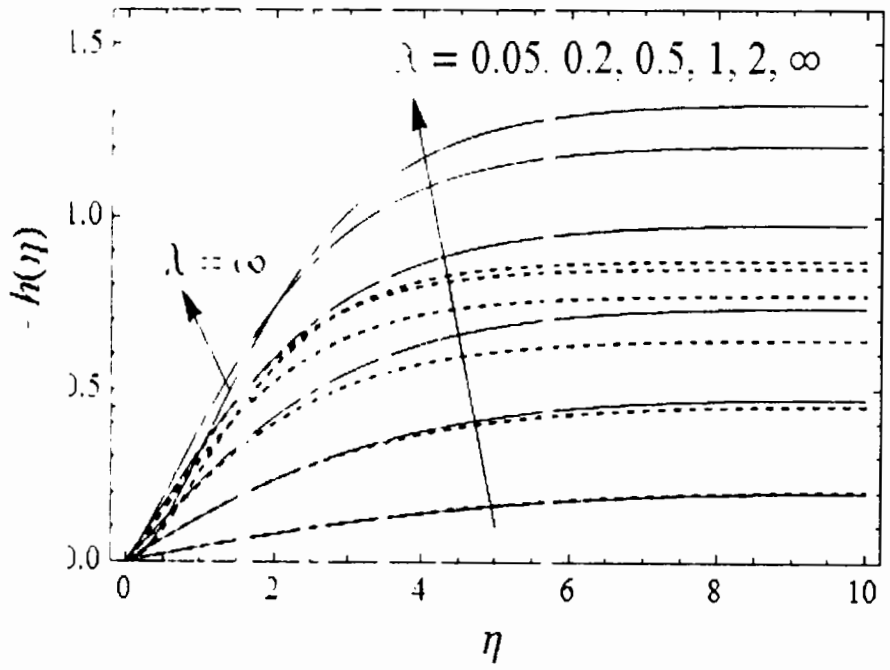

Fig. 5.2 Variation in $-h(\eta)$ against λ when $We = 1$. Dashed lines are calculated by [147].

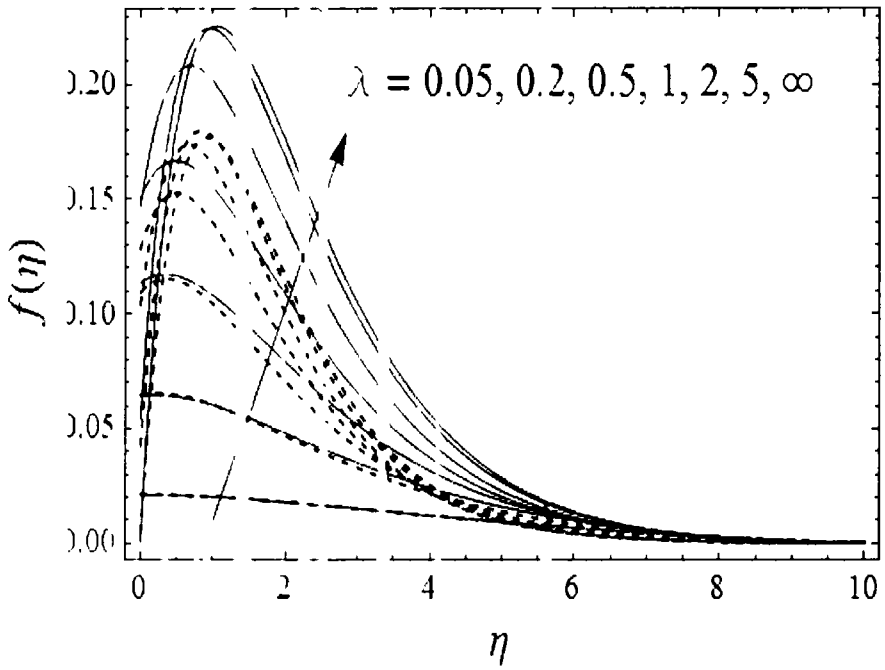

Fig. 5.3 Variation in $f(\eta)$ against λ when $We = 1$ Dashed lines are calculated by [147].

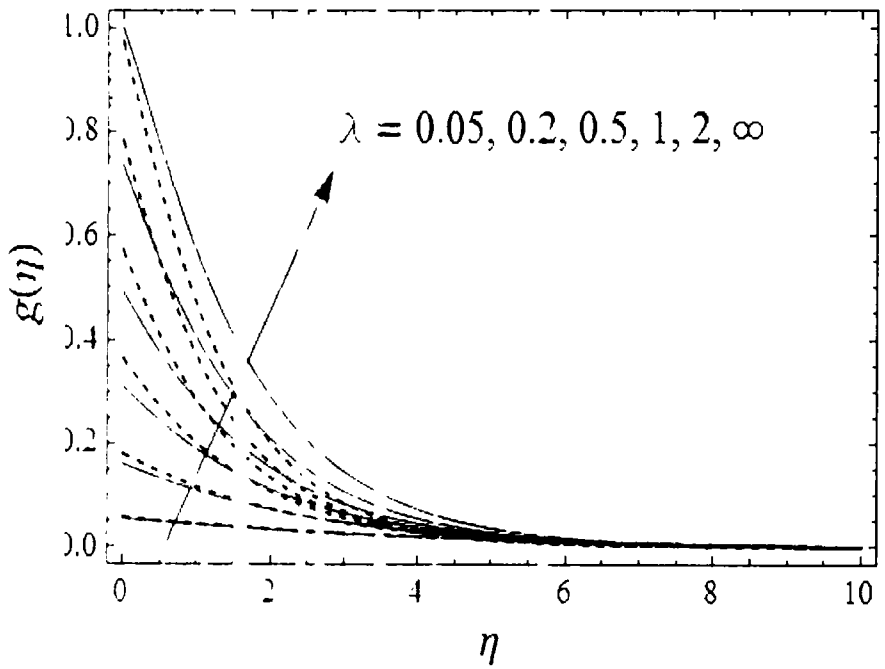

Fig. 5.4 Variation in $g(\eta)$ against λ when $We = 1$ Dashed lines are calculated by [147].

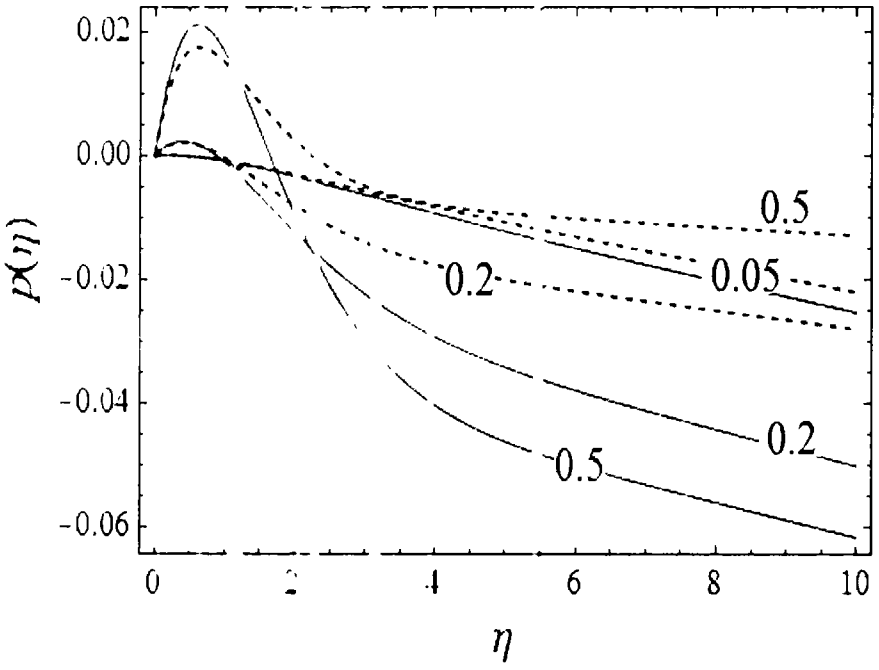

Fig. 5 5. Effect of slip on pressure when $We = 1$.

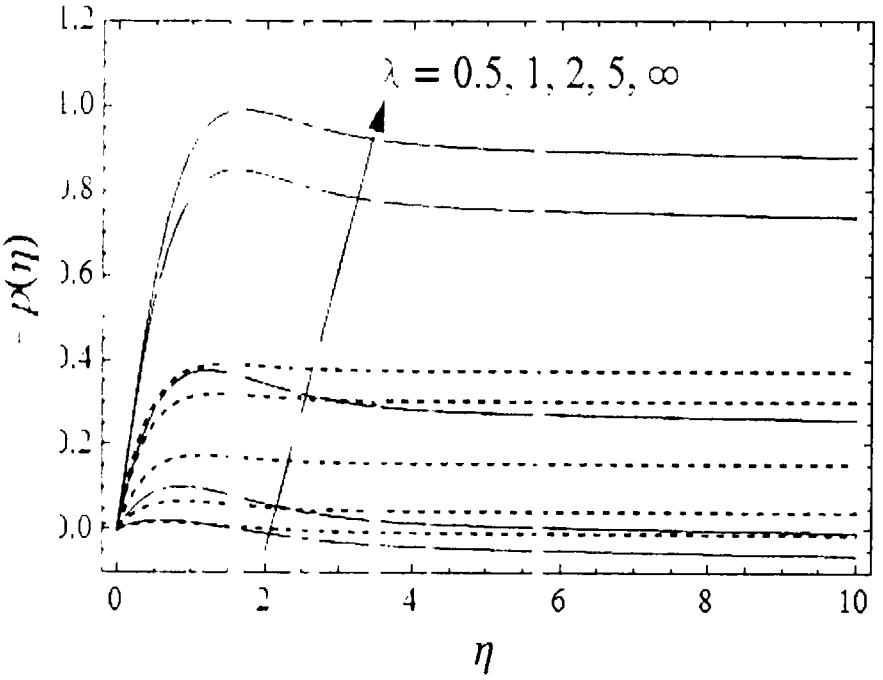

Fig. 5 6. Effect of slip on pressure when $We = 1$.

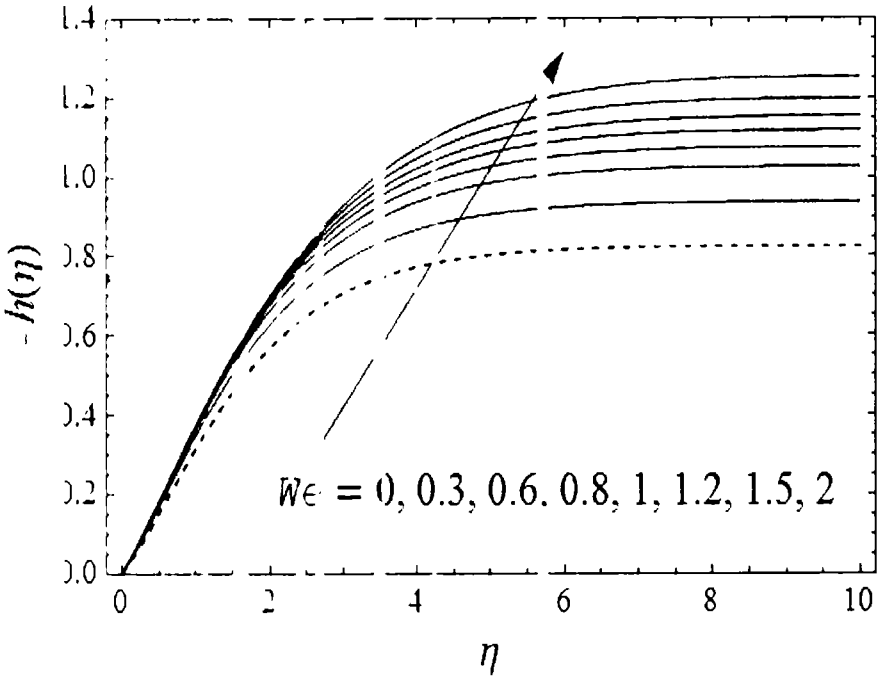

Fig. 5.7. Variation in $-h(\eta)$ for different values of We when $\lambda = 1.5$.

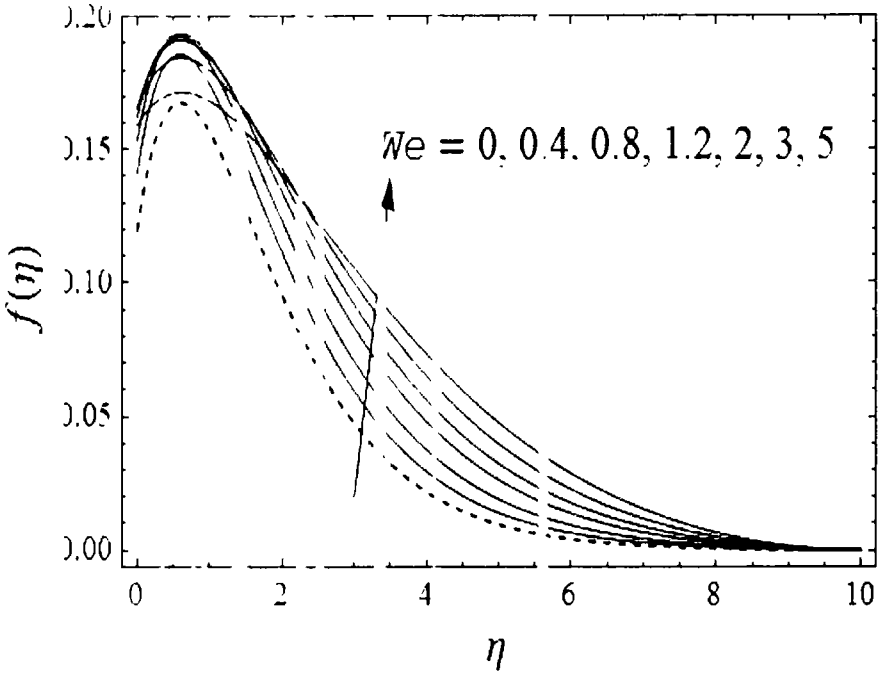

Fig. 5.8 Variation in $f(\eta)$ for different values of We when $\lambda = 1.5$.

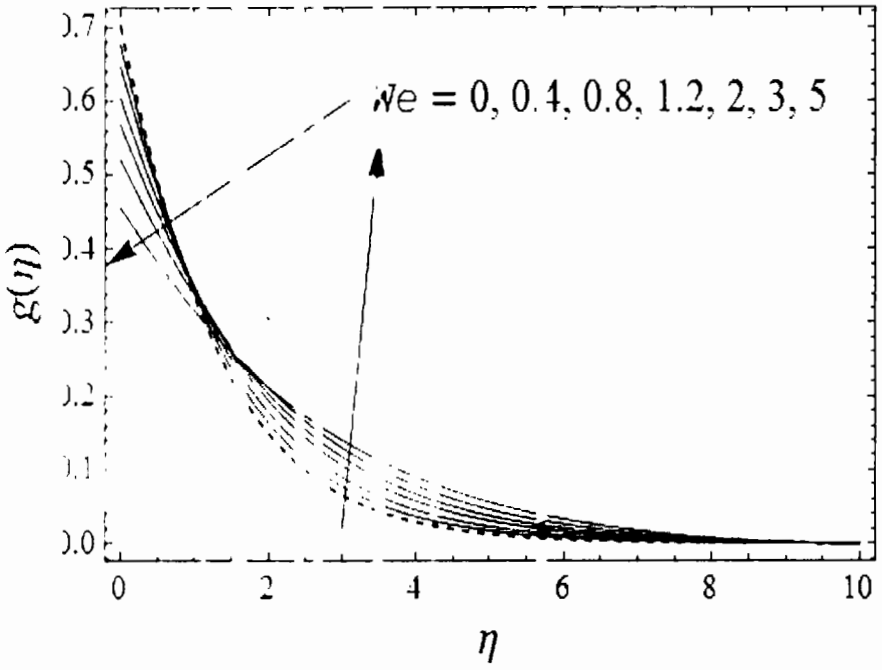

Fig. 5.9. Variation in $g(\eta)$ for different values of We when $\lambda = 1.5$.

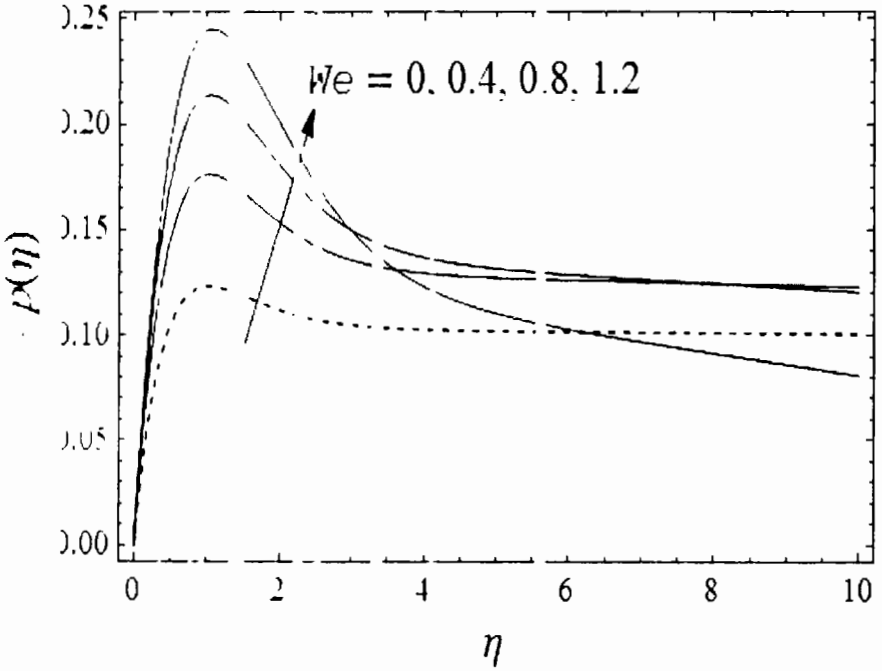

Fig. 5.10. Variation in $-p(\eta)$ for different values of We when $\lambda = 1.5$.

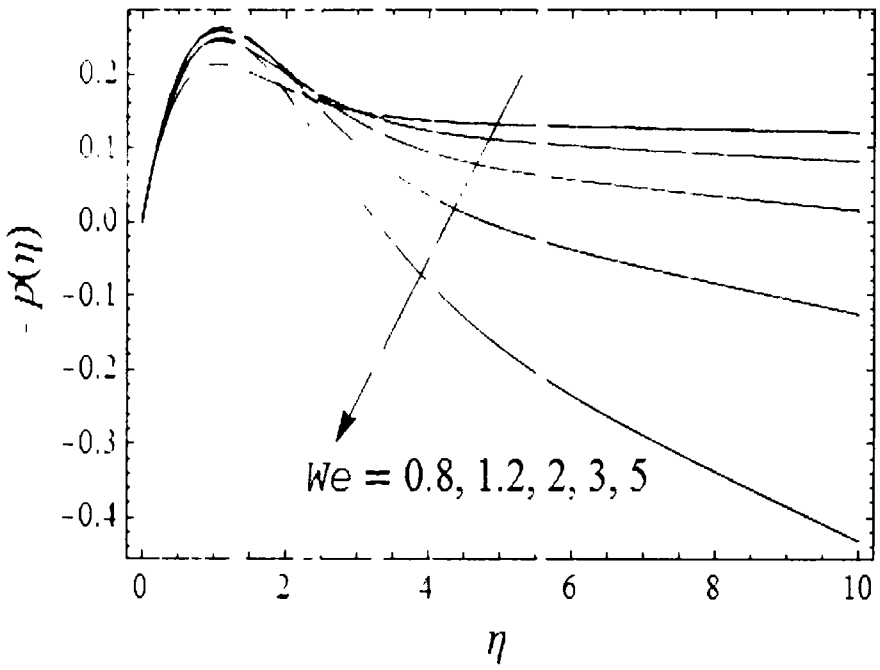

Fig. 5.11. Variation in $-p(\eta)$ for different values of We when $\lambda = 1.5$.

Table 5.1: Numerical values of $Re_r^{1/2}C_{fr}$ and $Re_r^{1/2}C_{f\theta}$ for various values of λ.

$We = 0.05$			$We = 1$		
λ	$Re_r^{1/2}C_{fr}$	$Re_r^{1/2}C_{f\theta}$	λ	$Re_r^{1/2}C_{fr}$	$Re_r^{1/2}C_{f\theta}$
0.01	−0.000119	0.000056	0.01	−0.000119	0.000055
0.05	−0.002743	0.002407	0.05	−0.002556	0.002074
0.1	−0.008848	0.007504	0.1	−0.007839	0.006160
0.5	−0.119575	0.077270	0.5	−0.086636	0.043736
1.0	−0.311114	0.141201	1.0	−0.220373	0.068210
2.0	−0.614639	0.152593	2.0	−0.518510	0.029763
5.0	−0.908031	0.056128	5.0	−1.053342	−0.261694

10	−0.990542	0.004268	10	−1.232311	−0.406746
50	−1.032491	-0.028260	50	−1.320843	−0.484123
100	−1.035151	-0.030489	100	−1.326394	−0.489068
500	−1.036475	-0.031607	500	−1.329053	−0.491426
∞	−1.036605	-0.031717	∞	−1.329155	−0.491531

Table 5.2: Numerical values of $Re_r^{1/2}C_{fr}$ and $Re_r^{1/2}C_{f\theta}$ for various values of We.

$\lambda = 0.5$			$\lambda = 1.5$		
We	$Re_r^{1/2}C_{fr}$	$Re_r^{1/2}C_{f\theta}$	We	$Re_r^{1/2}C_{fr}$	$Re_r^{1/2}C_{f\theta}$
0	−0.002753	0.002427	0	−0.478938	0.168179
0.001	−0.002753	0.002427	0.001	−0.479043	0.168021
0.01	−0.002751	0.002423	0.005	−0.479498	0.167321
0.05	−0.002743	0.002407	0.01	−0.480046	0.166445
0.1	−0.002733	0.002388	0.05	−0.483640	0.159458
0.6	−0.002635	0.002206	0.1	−0.486222	0.150860
1.0	−0.002556	0.002074	0.5	−0.453483	0.096387
1.5	−0.002461	0.001925	1	−0.368705	0.062445
2	−0.002370	0.001791	1.5	−0.294832	0.046572
3	−0.002202	0.001565	2	−0.239556	0.037693
5	−0.001922	0.001230	3	−0.168367	0.027724
10	−0.001462	0.000766	5	−0.100475	0.018027

5.3 Final remarks

In this chapter, we have examined the slip flow of a second grade fluid over a rotating disc lubricated with power-law fluid. The governing equations are transformed to ordinary differential equations by a suitable choice of transformation. Self-similarity is achieved in the governing equations for $n = 1/3$. The numerical solutions are computed using Keller-Box method. The motivation is to determine the effects of the slip parameter λ and We on the flow characteristics. The main findings are summarized as under.

(i) The computed results show that spin-up by second grade bulk fluid near the rotating disc is reduced by increasing slip.

(ii) Numerical value of all velocity components is decreased as We is decreased.

(iii) An unexpected reversal in the pressure gradient has been observed for the smaller values of λ and We

(iv) The numerical values of $Re_r^{1/2} C_{fr}$ increase as λ increases from 0 to ∞. However, the numerical values of $Re_r^{1/2} C_{f\theta}$ initially increase and then start decreasing.

(v) As Weissenberg number We increase, the numerical values of $Re_r^{1/2} C_{fr}$ increase while those of $Re_r^{1/2} C_{f\theta}$ decrease.

Chapter 6

Heat transfer analysis in the time-dependent slip flow over a lubricated rotating disc

In this chapter, we have performed an analysis to study characteristics of heat transfer in unsteady flow past a lubricated rotating disc. A generalized Newtonian fluid obeying power-law constitutive equation is employed to model the lubricant. A set of dimensionless coordinates is utilized to convert given partial differential equations into nonlinear coupled ordinary differential equations. Interfacial conditions have been derived with the help of continuity of shear stress and velocity of the lubricant and core fluid. The obtained boundary value problems are numerically solved with the help of Keller-box method. Impact of physical parameters in the presence of lubrication on fluid velocity, temperature and pressure is displayed graphically. The skin friction coefficients and the local Nusselt number are examined through tables. Comparison of the present results with the existing results in the literature [1-7] is also provided.

6.1 Formulation of the problem

Consider time-dependent incompressible three dimensional flow due to a rotating disc which is lubricated by a thin coating of a power-law fluid. Core fluid strikes the disc at right angle and spreads all around in the radial direction as shown in Fig. 5.1. The disc is assumed to be rotating about z-axis with angular velocity ω with center at origin. The viscous fluid at the free stream moves with a velocity $U_\infty = \omega r/(1 - \gamma_0 t)$ such that $\gamma_0 t < 1$ where the parameter γ_0 has dimension (t^{-1}). The time-dependent temperature T_w of the disc is given as

$$T_w = T_\infty + T_0(1 - \gamma_0 t)^{3/2}, \tag{6.1}$$

where T_0 and T_∞ measure the temperatures along the disc and at free stream respectively. The volume flow rate of power-law fluid is given by Eq. (5.1). The equations governing the rotational flow and heat transfer are represented by Eq. (5.2) and

$$\frac{\partial u}{\partial t} + u\frac{\partial u}{\partial r} - \frac{v^2}{r} + w\frac{\partial u}{\partial z} = -\frac{1}{\rho}\frac{\partial P}{\partial r} + \nu\left(\frac{\partial^2 u}{\partial r^2} + \frac{\partial}{\partial r}\left(\frac{u}{r}\right) + \frac{\partial^2 u}{\partial z^2}\right), \tag{6.2}$$

$$\frac{\partial v}{\partial t} + u\frac{\partial v}{\partial r} + \frac{uv}{r} + w\frac{\partial v}{\partial z} = \nu\left(\frac{\partial^2 v}{\partial r^2} + \frac{\partial}{\partial r}\left(\frac{v}{r}\right) + \frac{\partial^2 v}{\partial z^2}\right), \tag{6.3}$$

$$\frac{\partial w}{\partial t} + u\frac{\partial w}{\partial r} + w\frac{\partial w}{\partial z} = -\frac{1}{\rho}\frac{\partial P}{\partial z} + \nu\left(\frac{\partial^2 w}{\partial r^2} + \frac{1}{r}\frac{\partial w}{\partial r} + \frac{\partial^2 w}{\partial z^2}\right), \tag{6.4}$$

$$\frac{\partial T}{\partial t} + u\frac{\partial T}{\partial r} + w\frac{\partial T}{\partial z} = \alpha^*\left(\frac{\partial^2 T}{\partial r^2} + \frac{1}{r}\frac{\partial T}{\partial r} + \frac{\partial^2 T}{\partial z^2}\right), \tag{6.5}$$

where α^* is thermal diffusivity. The boundary conditions at fluid-solid interface are represented by Eqs (5.6) and (5.7). At the interface, radial and tangential components of shear stress must be continuous. Therefore, according to [147]

$$\mu\left(\frac{\partial u}{\partial z}\right) = \mu_L\frac{\partial U}{\partial z}, \tag{6.6}$$

$$\mu\left(\frac{\partial v}{\partial z}\right) = \mu_L\frac{\partial V}{\partial z}, \tag{6.7}$$

in which μ is represented by Eq (5.10). The continuity of radial and azimuthal velocities of both fluids is given by Eq. (5.14). Substituting Eqs. (5.10)-(5.14) into Eqs. (6.6) and (6.7), we get the following slip boundary conditions

$$u = \frac{k}{\mu}\left(\frac{\pi}{Q}\right)^n u(ru)^n[u^2 + (U_\infty - v)^2]^{\frac{n-1}{2}}, \tag{6.8}$$

$$\frac{\partial w}{\partial z} = -\frac{k}{\mu}\left(\frac{\pi}{Q}\right)^n (U_\infty - v)(ru)^n[u^2 + (U_\infty - v)^2]^{\frac{n-1}{2}}. \tag{6.9}$$

The continuity of axial velocity components of both fluids is displayed in Eq. (5.17). Following [147], we can impose boundary conditions (6.8), (6.9) and (5.17) at the surface of disc. The boundary conditions at the free stream are given in Eq. (5.18). The temperature profile satisfies the following boundary conditions

$$T(r,0) = T_w \text{ and } T(r,\infty) = T_\infty. \tag{6.10}$$

The rate of heat transfer q at the wall is given by

$$q = -K\left(\frac{\partial T}{\partial z}\right)_{z=0}, \tag{6.11}$$

in which K denotes the thermal conductivity. To transform Eqs (6.2)-(6.5) into ordinary differential equations, the following new variables are utilized.

$$\eta = \sqrt{\frac{\omega}{\nu(1-\gamma_0 t)}}\,z,\ u = U_\infty f(\eta),\ v = U_\infty g(\eta),\ w = \sqrt{\frac{\omega\nu}{(1-\gamma_0 t)}}\,h(\eta), \tag{6.12}$$

$$P = \frac{\mu}{r}U_\infty p(\eta),\quad T - T_\infty = (T_w - T_\infty)\,\theta(\eta). \tag{6.13}$$

The resulting system in new variables is given by continuity Eq (5.21) and

$$f''' - hf'' - f'^2 - A\left(f' + \frac{\eta}{2}f''\right) + g^2 = 0, \tag{6.14}$$

$$g'' - hg' - 2fg - A\left(g + \frac{\eta}{2}g'\right) = 0, \tag{6.15}$$

$$p' - 2fh + 2f'' - \frac{A}{2}(\eta h' + h) = 0, \tag{6.16}$$

$$\theta'' - Pr\left\{h\theta' + \frac{A}{2}(3\theta + \eta\theta')\right\} = 0, \tag{6.17}$$

$$h(0) = 0 \qquad p(0) = 0, \quad \theta(0) = 1 \tag{6.18}$$

$$f''(0) = \lambda|f(0)|^{\frac{4}{3}}\left[(f'(0))^2 + (1 - g(0))^2\right]^{-1/3}, \tag{6.19}$$

$$g(0) = -\lambda|f(0)|^{\frac{1}{3}}[1 - g(0)]\left[(f(0))^2 + (1 - g(0))^2\right]^{-1/3}, \tag{6.20}$$

$$f(\infty) = 0, \qquad g(\infty) = 0, \qquad \theta(\infty) = 0, \tag{6.21}$$

where $A = \gamma_0/\omega$ denotes the unsteadiness parameter, $Pr = \nu/\alpha^*$ is the Prandtl number. For $A = 0$ equations (6.14)-(6.17) represent the steady case. The parameter λ introduced in Eqs. (6.19)-(6.20) is defined as

$$\lambda = \frac{k\sqrt{\nu}}{\mu}\left(\frac{c}{\omega}\right)^{\frac{1}{3}}\frac{\omega^{\frac{3}{2}}}{\omega^{\frac{2}{3}}}, \tag{6.22}$$

where $\omega = \omega/(1 - \gamma_0 t)$. The constant λ given in Eq. (6.22), is called slip parameter discussed in detail earlier in chapter 5. The non-dimensional forms of local Nusselt number is given as

$$Re_x^{-1/2}Nu = -\theta'(0). \tag{6.23}$$

6.2 Numerical results and analysis

Equations Eqs (6.14)-(6.17) subject to boundary conditions (6.18)-(6.21) are solved numerically with the help of highly accurate technique, the Keller-box method.

To see the flow behaviour against the physical parameters Figs. 6.1-6.12 are plotted. Tables 6.1 and 6.2 show the numerical values of radial shear stress, tangential shear stress and heat transfer coefficient under the influence of emerging parameters.

Figs. 6.1-6.4 are displayed to observe the variation in velocity components and pressure against the slip parameter λ. Influence of λ on axial velocity $-h$ is depicted in Fig. 6.1. This figure shows that axial flow is increased by reducing the amount of lubrication on

the surface of disc. A steady case (when $A = 0$) is illustrated by dashed lines. Increase in the axial velocity is lesser for the unsteady case. It is due to the fact that parameter A depends upon angular velocity ω which intern is a function of time. As the time ticks away, ω is decreased causing the reduction in the axial in flow. However, h-curves tends to overlap for both cases in the absence of slip. Fig. 6.2 shows the impact of slip parameter on the radial velocity f. This figure shows that f is augmented on increasing λ. An increment in the axial inward flow automatically gives rise to radial outward flow according to continuity equation (5.21). The increase in f is more prominent for the steady case ($A = 0$). A decrement in the peak value of radial velocity with increasing amount of lubrication is observed in the figure depending upon axial inward flow (Eq. 5.21). Fig. 6.3 illustrates the variation in the shear velocity g showing that it is an increasing function of λ. Acceleration in the value of g is more significant for the steady case. It is worth noting that this component of velocity determines the torque which is responsible for the steady rotation of the disc. As the slip on the disc surface is decreased, the imposed torque decreases and accordingly the shear velocity reduces. Effects of λ on the pressure profile is presented in Fig. 6.4. According to this figure, pressure increases by reducing slip on the surface when $A = 0$ and $A > 0$. An extensive enhancement in the pressure is observed for the unsteady case while moving no-slip to full-slip regime. However, a small deviation is observed near full-slip (for smaller values of λ) for the steady case as shown in Fig. 6.4(b). The reason for this surprising behaviour is that for lowest values of slip parameter, ambient pressure exceeds the disc pressure which drives the flow towards the disc.

Variation in the velocity components and pressure against the parameter A is depicted in Figs. 6.5-6.8 for partial ($\lambda = 0.2$) and no-slip ($\lambda = 0$) cases. Fig. 6.5 provides that axial in flow $-h$ is inversely related with unsteadiness parameter A. It is due to the fact that A depends upon time and the axial velocity decreases with time. The decrease in the axial velocity is more prominent on the lubricated disc. The radial velocity f shows the same behaviour as that of axial velocity $-h$ as shown in the Fig. 6.6. It is due to the mass conservation formula (5.21) as discussed earlier. Variation in the circumferential velocity g with respect to parameter A is analyzed in Fig. 6.7 both for partial and no-slip cases. It is evident that g reduces by enhancing A. A lubricated surface appreciates this decrement in the value of g as compared to the rough surface. Impact of unsteadiness parameter A on

the pressure is presented in Fig. 6.8. One can observe that pressure is an increasing function of A. The reason is that by increasing A, angular velocity of disc reduces and thus the pressure on the surface increases. It is also clear from this figure that increase in the pressure is more prominent on the lubricated surface.

Fig. 6.9 elaborates the variation in the temperature θ by augmenting λ when $Pr = 1$ both for steady ($A = 0$) and unsteady ($A = 0.1$) cases. It is concluded from this figure that θ decreases by decreasing amount of lubrication. This figure also shows that unsteadiness appreciates the lubrication effects (solid lines). Influence of unsteadiness parameter A on θ when $Pr = 1$ for both no-slip (dashed lines) and partial slip (solid lines) cases is elaborated in Fig. 6.10. According to this figure θ increases by increasing A. This increase can be enhanced by applying the lubrication on the surface ($\lambda = 0.5$). Temperature variations with Prandtl number Pr are shown in Fig. 6.11 when $\lambda = 1$. The dashed lines show the steady case. It has been observed that θ reduces by enlarging Pr. This reduction is more eminent for the steady case. The reason is that thermal diffusivity decreases by increasing Pr and as a result temperature is reduced. Fig. 6.12 is devoted for the effects of Pr on temperature profile θ both for steady and unsteady cases respectively. It is obvious from this figure as Pr is increased, a decrease in the value of θ is observed which further depreciates on the lubricated surface (solid lines). Influence of λ and A on the magnitudes of the radial shear stress $f''(0)$ tangential shear stress $-g'(0)$ is illustrated in Table 6.1. According to this table both radial and tangential shear stresses reduce by decreasing λ (increasing slip) as well as increasing unsteadiness parameter A. However numerical value of tangential shear stress enhances by increasing A for the no-slip case. The variation in heat transfer coefficient against the different parameters is elaborated in Table 6.2. We observe that $-\theta'(0)$ increases first and then decreases by increasing slip parameter for the different values of A and Pr. It is also obvious from this table that $-\theta'(0)$ decreases by increasing unsteadiness parameter. This table also shows that heat transfer coefficient gains the magnitude as Pr is increased. Tables 6.3-6.4 show the comparison of $f''(0), -g'(0)$ and $-\theta'(0)$ respectively with available results in the special case [147].

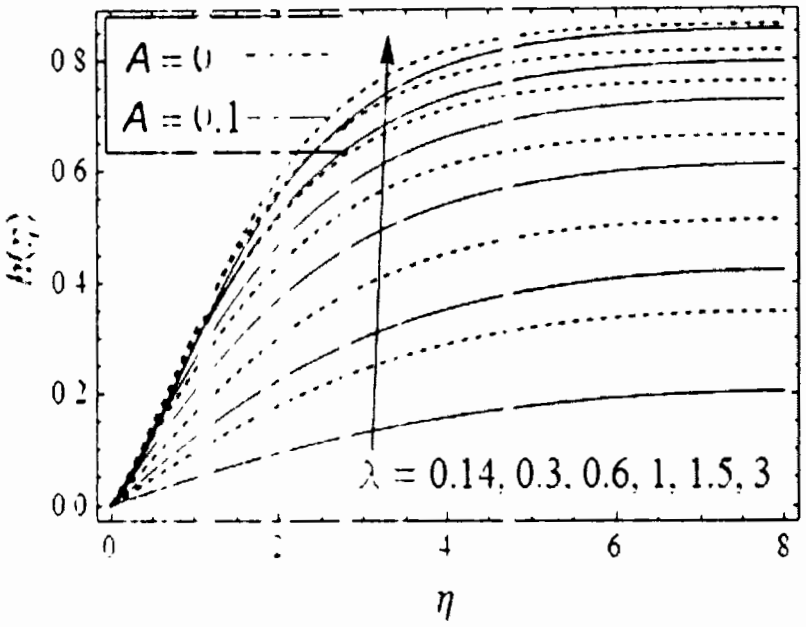

Fig. 6.1 Axial velocity $h(\eta)$ plotted against the slip parameter λ. Dashed lines are calculated by [147]

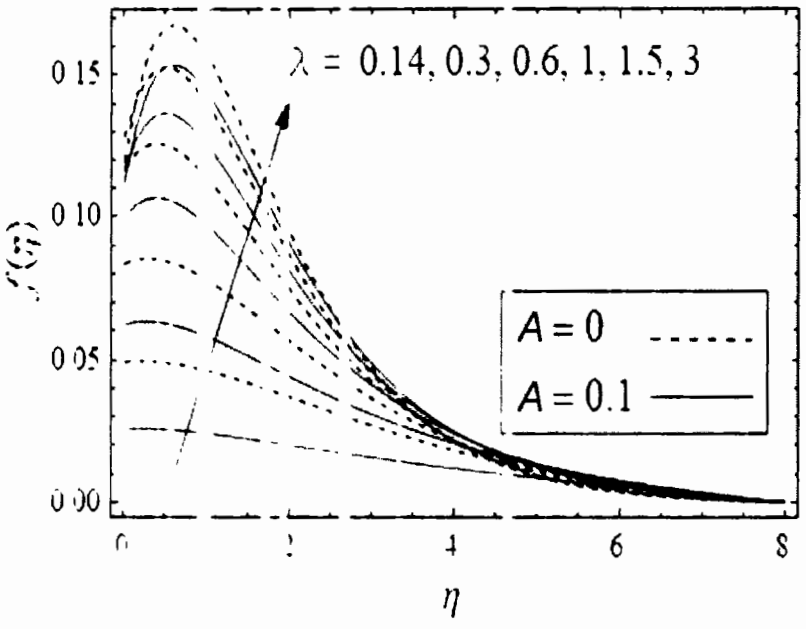

Fig. 6.2 Radial velocity $f(\eta)$ plotted against λ. Dashed lines are calculated by [147].

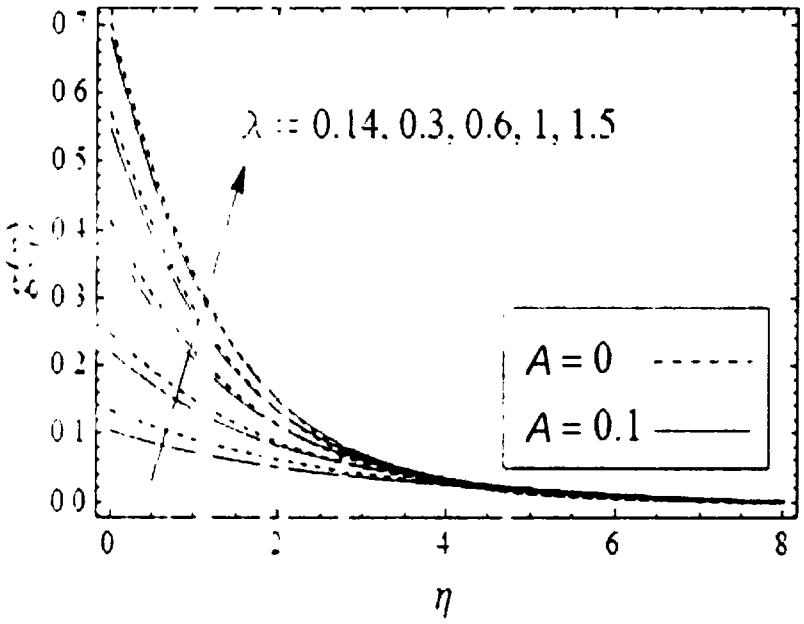

Fig. 6.3 Circumferential velocity $g(\eta)$ plotted against λ. Dashed lines are calculated by [147]

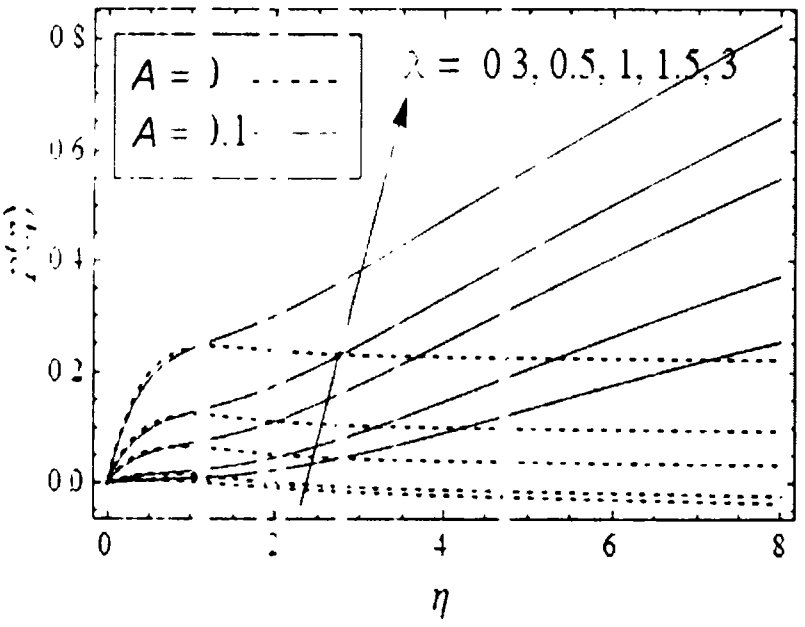

Fig. 6.4.(a)

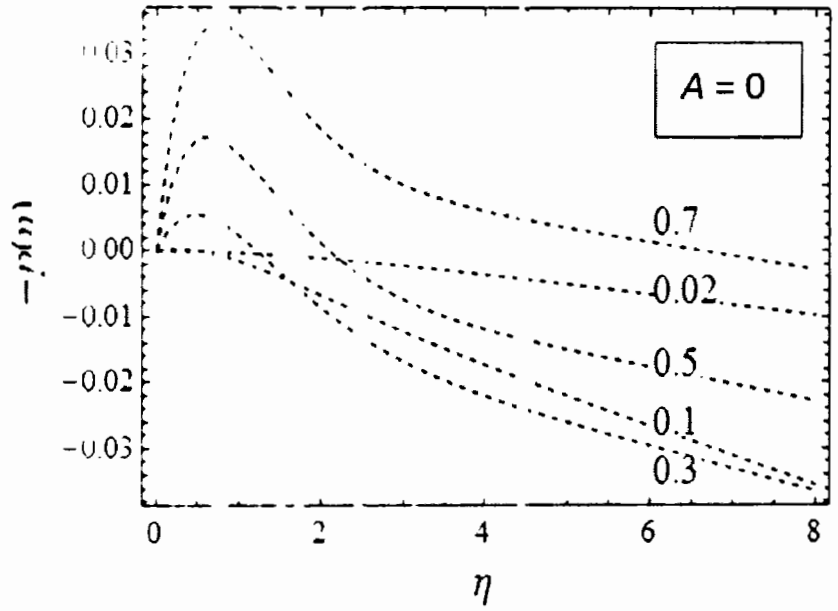

Fig 6.4.(b)

Fig. 6.4 Pressure profile plotted against the slip parameter λ. Dashed lines are calculated by [147]

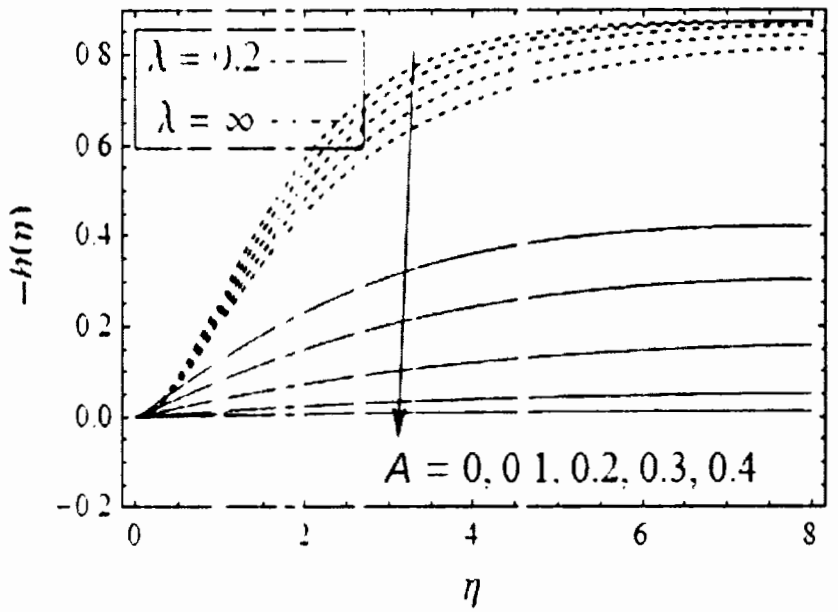

Fig. 6.5 $-h(\eta)$ plotted against the unsteadiness parameter A. Dashed lines show the no-slip case.

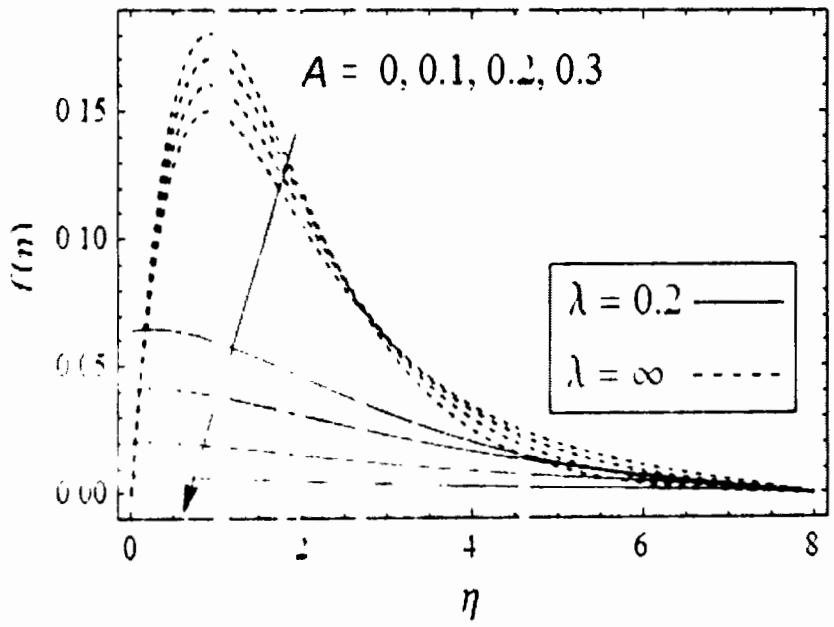

Fig. 6.6 $f'(\eta)$ plotted against the unsteadiness parameter A. Dashed lines show the no-slip case.

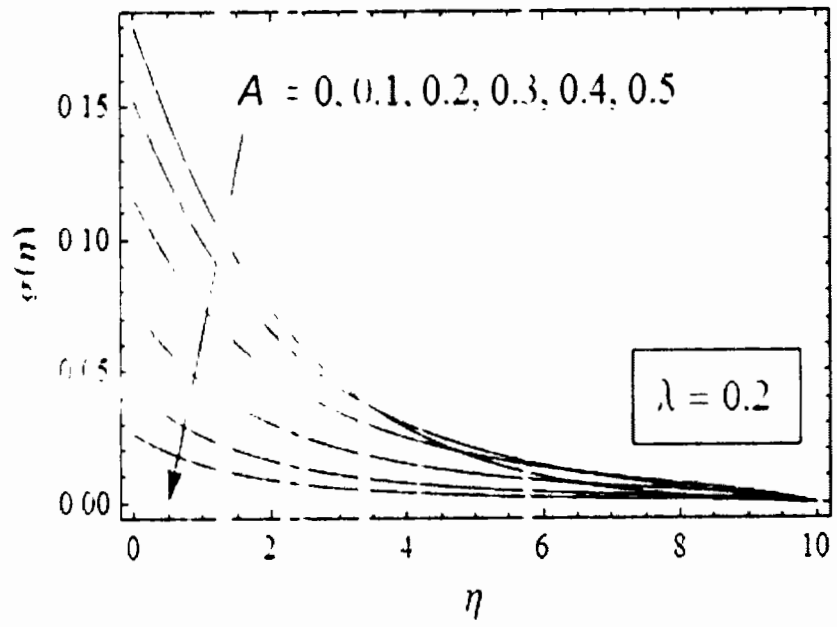

Fig. 6.7 (a)

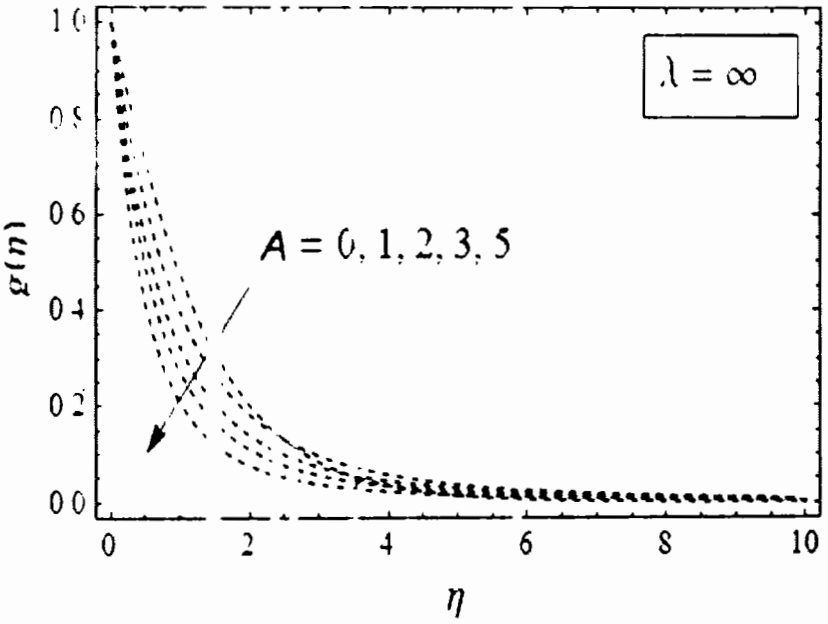

Fig. 6.7 (b)

Fig. 6.7 $g(\eta)$ plotted against the unsteadiness parameter A. Dashed lines show the no-slip case.

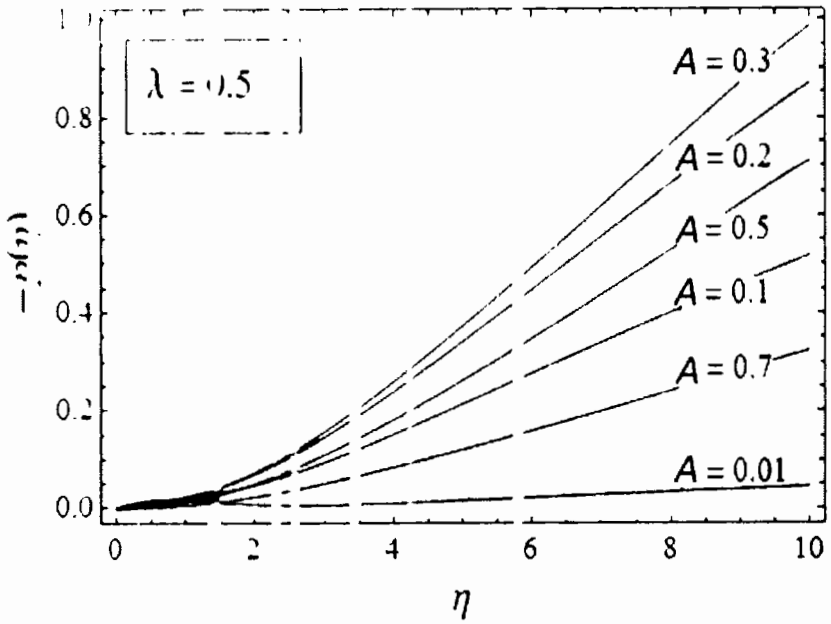

Fig. 6.8 (a)

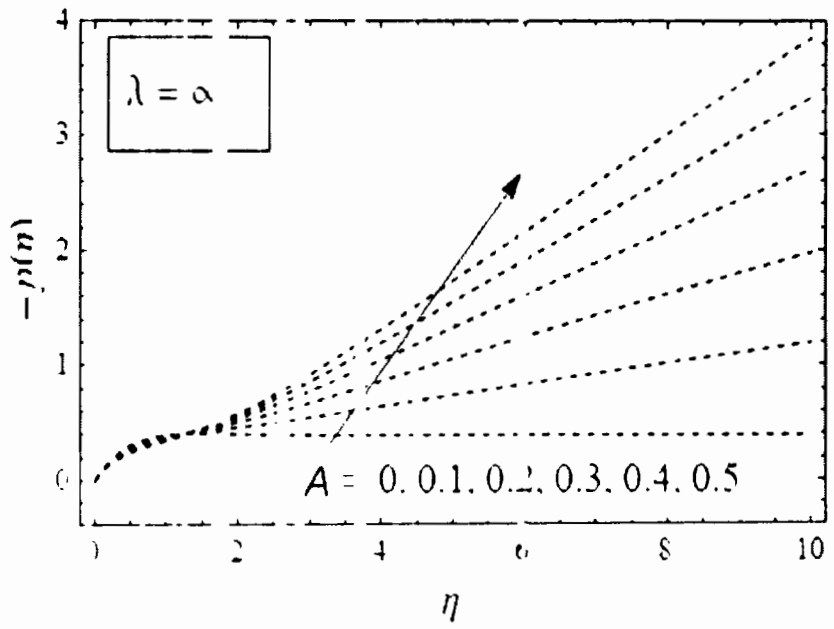

Fig. 6.8 (b)

Fig. 6.8 Pressure profile plotted against the parameter A. Dashed lines show the no-slip case.

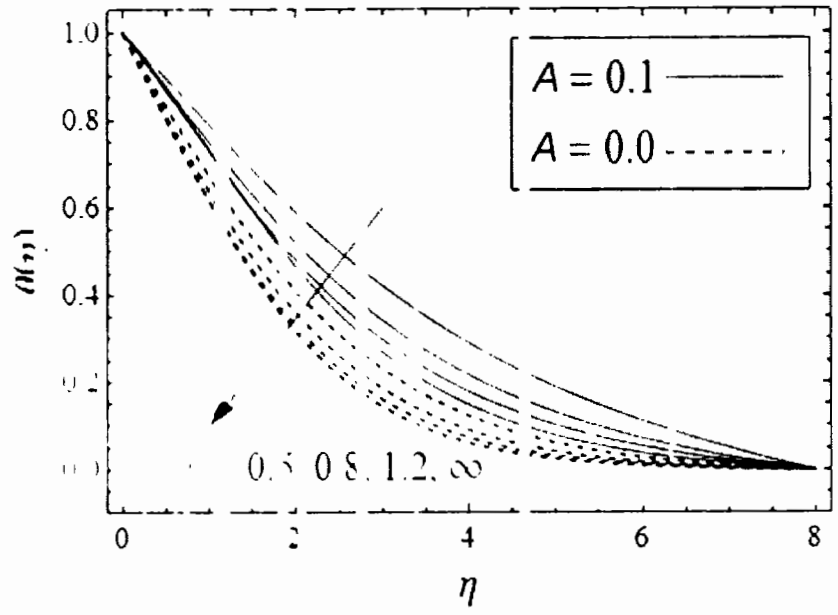

Fig. 6.9 Temperature profile plotted against λ for different values of A when $Pr = 1$.

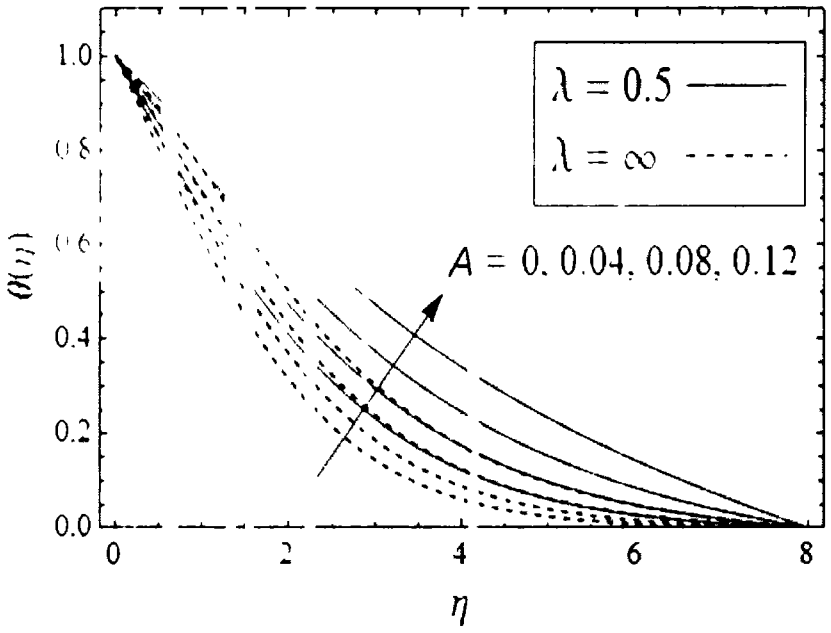

Fig. 6.10: Temperature profile plotted against A for different values of λ when $Pr = 1$.

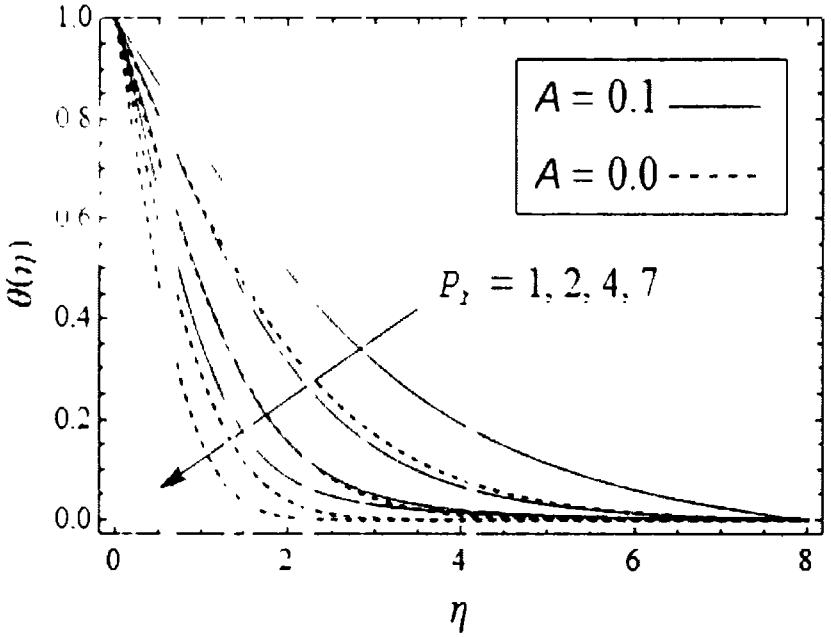

Fig. 6.11: Temperature profile plotted against Pr when $\lambda = 1$. Dashed lines show steady case.

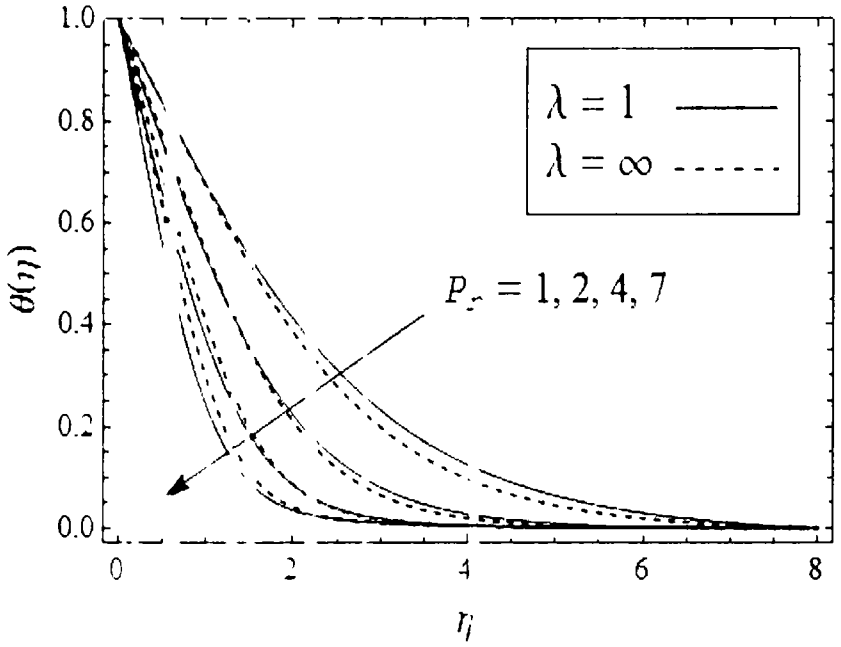

Fig. 6.1: Temperature profile plotted against Pr when $A = 0.05$. Dashed lines show no-slip case.

Table 6.1: Numerical data representing radial shear stress $f'(0)$ and tangential shear stress $-g'(0)$ under the influence of λ and A. Numerical data for the steady case is calculated by [147]

A	$f'(0)$			$-g'(0)$		
	$\lambda = 0.5$	$\lambda = 1$	$\lambda = \infty$	$\lambda = 0.5$	$\lambda = 1$	$\lambda = \infty$
0	0.0349916	0.1087184	0.5102327	0.2035352	0.3691274	0.6159221
0.1	0.0267485	0.0946545	0.4897258	0.1946088	0.3661441	0.6526113
0.2	0.0191817	0.0790946	0.4697303	0.1833526	0.3611589	0.6891521
0.4	0.0076478	0.0513263	0.4317947	0.1532713	0.3448532	0.7618598
0.7	0.0010026	0.0215[illegible]	0.3824878	0.0986576	0.3051776	0.8700152
1	0.0001113	0.0078366	0.3429943	0.0590016	0.2531332	0.9752703
1.5	0.0000058	0.0011661	0.2945197	0.0287541	0.1697148	1.1400861
2	0.0000005	0.0001948	0.2605667	0.0166259	0.1127152	1.2906812

Table 6.2: Numerical data representing heat transfer coefficient $-\theta'(0)$ under the influence of λ, A and Pr

A	λ	$Pr = 0.1$	$Pr = 0.5$	$Pr = 1$	$Pr = 3$	$Pr = 10$	$Pr = 50$
0	0.5	0.1453511	0.2317090	0.3390227	0.6352724	1.1941080	2.6764945
	1	0.1509776	0.2617037	0.3928786	0.7303140	1.3519010	2.9779919
	2	0.1539612	0.2780405	0.4155070	0.7556897	1.3600160	2.8867569
	5	0.1541503	0.2771062	0.4084500	0.7190101	1.2373179	2.4431712
	∞	0.1534816	0.2771265	0.3967034	0.6823829	1.1339601	2.0908651
0.05	0.5	0.1383725	0.1973339	0.2739340	0.5098213	0.9402619	1.9939607
	1	0.1430042	0.2240405	0.3243281	0.5955467	1.0597740	2.1395281
	2	0.1449088	0.2348962	0.3411682	0.6042143	1.0179513	1.8656158
	5	0.1443032	0.2307425	0.3290773	0.5537606	0.8574734	1.2886016
	∞	0.1433198	0.2245784	0.3152027	0.5116052	0.7401919	0.8924005
0.1	0.5	0.1314763	0.1608910	0.2028204	0.3616739	0.6513216	1.2208393
	1	0.1351181	0.1863787	0.2500794	0.4485049	0.7455582	1.2352766
	2	0.1359066	0.1897997	0.2614036	0.4423211	0.6544020	0.7740992
	3	0.1353352	0.1871110	0.2547855	0.4130926	0.5576946	0.6160532
	∞	0.1331045	0.1747750	0.2277805	0.3288278	0.3697265	0.3918378

Table 6.3: Comparison of $f''(0)$ and $-g'(0)$ with those of [147], [102] and [105] when $A = 0$

	$f''(0)$			$-g'(0)$		
	$\lambda = 0.5$	$\lambda = 1$	$\lambda = \infty$	$\lambda = 0.5$	$\lambda = 1$	$\lambda = \infty$
Current	0.0349915	0.1108785	0.51023261	0.2035353	0.3691273	0.61592202
By [147]	0.0349915	0.1108785	0.5102326	0.2035353	0.3691273	0.6159220
By [102]	-		0.5102326	-	-	0.6159220
By [105]	-		0.51023262	-	-	0.61592201

Table 6.4: Comparison of numerical values of heat transfer coefficient $-\theta'(0)$ with those of [105] when $A = 0$ and $\lambda = \infty$

	$Pr = 0.72$	$Pr = 6$
Current	0.53285011	0.92118502
By [105]	0.53285010	0.92118503

6.3 Conclusion

Heat transfer analysis in the time-dependent flow past a lubricated rotating disc is investigated in this manuscript. The required lubrication is provided by a power-law fluid. To obtain the similar solution, we have set $n = 1/3$. The problem is solved numerically by Keller-box method. Our aim is to figure out the effects of emerging parameters on the flow characteristics in the presence of lubrication. Some findings of the investigation are as under:

(i) The lubricant enhances the velocity and pressure of bulk fluid. This increase is more rapid for the unsteady case.

(ii) A reduction in the fluid velocity is observed with an increase in the unsteadiness parameter A. The lubrication enhances the reduction.

(iii) An increase in the value of A causes an increase in the pressure distribution. This fact is true for both steady and unsteady cases.

(iv) The components of radial and tangential shear stress augment by enlarging λ and decrease by enhancing A. However, tangential shear stress is an increasing function of A in the absence of slip.

(v) The heat transfer coefficient $-\theta'(0)$ increases first and then decreases by increasing slip parameter for the various values of A and Pr.

(vi) $-\theta'(0)$ decreases by increasing unsteadiness parameter and increases with increasing Prandtl number. However, an unexpected behaviour is observed for the higher values of Pr and A at and near no slip ($\lambda \to \infty$).

Chapter 7

Heat transfer analysis in the time-dependent axisymmetric stagnation-point flow over a lubricated surface

In this chapter time-dependent, two-dimensional, axisymmetric flow and heat transfer of a viscous incompressible fluid impinging orthogonally on a disc is examined. The disc is lubricated with a thin layer of power-law fluid of variable thickness. It is assumed that surface temperature of the disc is time-dependent. Continuity of velocity and shear stress at the interface layer between the fluid and the lubricant has been imposed to obtain the solution of the governing partial differential equations. The set of partial differential equations is reduced into ordinary differential equations by suitable transformations and are solved numerically by using Keller-box method Solutions are presented in the form of graphs and tables in order to examine the influence of pertinent parameters on the flow and heat transfer characteristics. An increase in lubrication results in the reduction of surface shear stress and consequently viscous boundary layer becomes thin. However, the thermal boundary layer thickness increases by increasing lubrication. It is further observed that surface shear stress and heat transfer rate at the wall grow due to unsteadiness. The results for the steady case are deduced from the present solutions and are found in good agreement with the existing results in the literature [148].

7.1 Mathematical formulation

Let us assume the unsteady, two-dimensional, axisymmetric stagnation-point flow and heat transfer of an incompressible viscous fluid past a disc lubricated by a thin layer of non-Newtonian power-law fluid. The origin O is located at the center of the disc (Fig. 7.1).

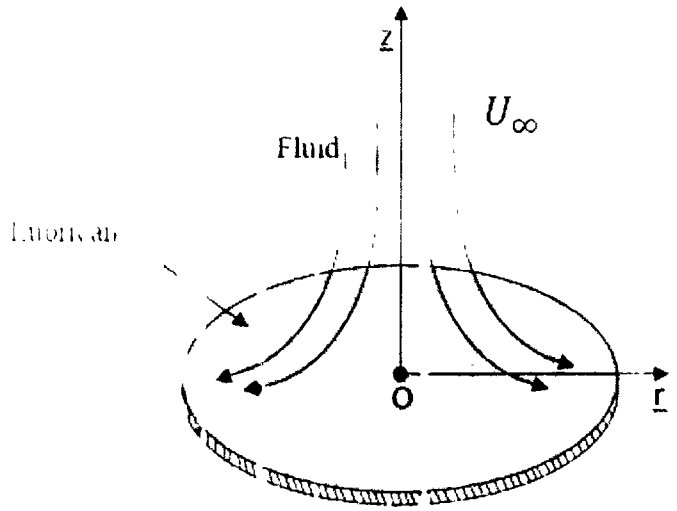

Fig. 7.1: Diagram showing stagnation-point flow problem

The flow rate Q of the lubricant coming out of a small point source at the center of the disc is given by Eq. (5.1). The stagnation flow velocity of the viscous fluid is of the form $U_\infty(r, z, t) = ar/(1 - \gamma_0 t)$, where $a > 0$ and $\gamma_0 \geq 0$ are constants with dimensions t^{-1}. The time-dependent temperature T_w of the disc is defined in Eq. (6.1). Under these assumptions, the unsteady two-dimensional, axisymmetric flow of bulk fluid is governed by the continuity Eq. (5.2), heat eq. (6.5) and the following momentum equations

$$\frac{\partial u}{\partial t} + u\frac{\partial u}{\partial r} + w\frac{\partial u}{\partial z} = -\frac{\partial P}{\partial r} + \nu\left(\frac{\partial^2 u}{\partial r^2} + \frac{\partial}{\partial r}\left(\frac{u}{r}\right) + \frac{\partial^2 u}{\partial z^2}\right), \tag{7.1}$$

$$\frac{\partial w}{\partial t} + u\frac{\partial w}{\partial r} + w\frac{\partial w}{\partial z} = -\frac{1}{\rho}\frac{\partial P}{\partial z} + \nu\left(\frac{\partial^2 w}{\partial r^2} + \frac{1}{r}\frac{\partial w}{\partial r} + \frac{\partial^2 w}{\partial z^2}\right). \tag{7.2}$$

At free stream, $u = U_\infty(r, z, t)$ and therefore Eq. (7.1) reduces to

$$\frac{\partial u}{\partial t} + u\frac{\partial u}{\partial r} + w\frac{\partial u}{\partial z} = \frac{\partial U_\infty}{\partial t} + U_\infty\frac{\partial U_\infty}{\partial r} + \nu\left(\frac{\partial^2 u}{\partial r^2} + \frac{\partial}{\partial r}\left(\frac{u}{r}\right) + \frac{\partial^2 u}{\partial z^2}\right). \tag{7.3}$$

The appropriate boundary conditions at $z = 0$ for the present flow situation is discussed in detail by Sahoo et al. [149] and are

$$\frac{\partial u}{\partial z} = \frac{k}{\mu}\left(\frac{a}{\nu}\right)^n r^n (ru)^{2n} \quad P(r, \delta(r), t) = -\frac{\rho r^2}{2}\left(\frac{a}{1-\gamma_0 t}\right)^2, \quad w(r, \delta(r), t) = 0. \tag{7.4}$$

The boundary conditions far away from the stagnation-point in the present case are given by

$$u(r,z,t) = U_\infty = \frac{ar}{(1-\gamma_0 t)}, \qquad w(r,z,t) = -\frac{2az}{(1-\gamma_0 t)}. \tag{7.5}$$

The boundary conditions to be satisfied by the temperature are presented in Eq. (6.10). Introducing the dimensionless variables

$$\eta = \sqrt{\frac{a}{\nu(1-\gamma_0 t)}}\, z, \quad u = U_\infty f'(\eta), \quad w = -2\sqrt{\frac{a\nu}{(1-\gamma_0 t)}}\, f(\eta), \tag{7.6}$$

$$p = \frac{\rho a^2 r^2}{(1-\gamma_0 t)^2} P(\eta) \quad \frac{\rho a^2}{2(1-\gamma_0 t)^2}\left(r^2 - \frac{a}{\gamma_0 t}\right)^2, \quad T - T_\infty = (T_w - T_\infty)\theta(\eta), \tag{7.7}$$

the flow is governed by

$$f''' + 2ff'' - (f')^2 + A\left(1 - f' - \frac{\eta}{2}f''\right) + 1 = 0, \tag{7.8}$$

$$P' + 4f f' + 2f'' - A(\eta f' + f) = 0, \tag{7.9}$$

$$\theta'' + Pr\left\{2f\theta' - \frac{A}{2}(3\theta + \eta\theta')\right\} = 0, \tag{7.10}$$

$$f(0) = 0, \quad P(0) = 0, \quad f''(0) = \lambda\left(f'(0)\right)^{\frac{2}{3}}, \quad f'(\infty) = 1, \tag{7.11}$$

$$\theta(0) = 1, \quad \theta(\infty) = 0 \tag{7.12}$$

where $A = \gamma_0/a$ is the unsteadiness parameter and n has been taken $1/3$ to obtain similar solution

For $A = 0$ the problem reduces to the steady state case discussed by Santra et al. [148]. The parameter λ given in Eq. (7.11) is slip parameter defined as

$$\lambda = \frac{k_1}{\mu}\left(\frac{\pi}{Q}\right)^{\frac{1}{3}} b^{\frac{2}{3}}. \tag{10.13}$$

in which $b = a/(1-\gamma_0)$.

7.2 Discussion of numerical results

To see the influence of pertinent parameters on the velocity components, pressure and temperature, Eqns. (7.8)-(7.10) subject to boundary conditions (7.11) and (7.12) are solved numerically by using Kelder-box method. The numerical results are validated through the comparison of the present solution with the existing results in the literature in the special cases.

Figures. 7.2-7.11 are plotted to observe the effects of emerging parameters on velocity components, pressure distribution and temperature profile. Numerical computations for surface shear stress and heat transfer rate showing the influence of parameters λ, A and Pr are presented in Tables 7.1 and 7.2.

To see the effects of slip parameter λ on f, f' and $-p$, Figs. 7.2-7.4 have been plotted. The dashed lines in each case are the investigations of Santra et al. [148] when $A = 0$. Figure 7.2 is displayed to show the effects of λ on axial velocity component f. From this figure, it is clear that as we increase the slip on the surface (λ is decreased), an increase in the value of f is observed. f becomes proportional to η as $\lambda \to 0$ i.e. when full-slip is applied on the surface. Figure 7.3 is displayed to see the influence of slip parameter λ on the radial velocity component f'. We see that f' decreases by increasing λ. It is due to the fact that lubricant reduces the friction on the surface. It is also clear from Figs. 7.2 and 7.3 that power-law lubricant enhances the velocity of fluid at the surface. The variation in the pressure profiles $-p$ with η is presented in Fig. 7.4. For the case of no-slip (classical Homann flow), the pressure increases towards the surface in the stagnation zone and it obtains a minimum value at $\eta = 0$. The pressure variation across the boundary layer is increased with increasing slip, and the maximum pressure build-up is observed for full-slip. The pressure increase is slightly slow in the boundary layer region for the no-slip case. As we increase the slip on the surface, the boundary layer thickness reduces and pressure seems to increase rapidly. It is clear from Fig. 7.4 that the pressure curves intersect slightly beyond $\eta = 1$ when $A = 0$. If we inspect the graph closely, we notice that the crossings of the different curves do not occur in one single point. It is evident from Eq. (7.9) that the pressure is function of both the radial and the axial velocity components, which in turn depends upon the slip. The point of inflection produced by pressure distribution is observed

somewhat above the surface for the no-slip case. As we increase the slip on the surface, this inflection point seems to shift towards the surface. But when $A = 1$, the point of inflection moves beyond $\eta = 1.57$ (solid lines) showing that boundary layer thickness increases by increasing the numerical value of parameter A.

Effect of parameter A both for no-slip and partial-slip cases on the velocity components and pressure profile is illustrated in Figs. 7.5-7.7. Figure 7.5 shows that magnitude of axial velocity f increases by increasing A for both cases. It is also evident from this figure that lubrication appreciates the effects of A (solid lines). Figure 7.6 elucidates the effects of parameter A on the radial velocity component f' both for no-slip (dashed lines) and partial-slip (solid lines) cases. It is observed from this figure that as A increases, f' increases. Moreover, the lubricated surface enhances the effect of A (solid lines). i.e. Increase in the radial velocity becomes more rapid by lubricating the surface. The effects of unsteadiness parameter A on pressure profile is depicted in Fig. 7.7. The dashed lines are for no-slip case and solid lines for partial-slip case. This figure shows that the pressure increases by decreasing A and is maximum when $A = 0$. It has also been observed that the increase in the pressure becomes more significant by applying slip on the surface.

Variation of θ for different values of A when $Pr = 1$ both for no-slip (dashed lines) and partial slip (solid lines) cases is elaborated in Fig. 7.8. It is evident from this figure that θ decreases by increasing A. This decrease can be enhanced by applying the lubrication on the surface ($\lambda = 1$). Figure 7.9 depicts the variation in the magnitude of θ for different values of slip parameter λ when $Pr = 1$ both for steady ($A = 0$) and unsteady ($A = 2$) cases. It is concluded from this figure that θ increases with an increase in the value of λ (by decreasing amount of lubrication). This figure also shows that unsteadiness depreciates the effects of lubrication (solid lines). The influence of Pr on temperature profile is elucidated in Fig. 7.10 when $A = 1$ both for no-slip and partial slip cases. According to this figure as Pr is increased, a decrease in the numerical value of θ is observed which further depreciates on the lubricated surface (solic lines). Figure 7.11 is devoted for the effects of Pr on temperature θ by considering steady and unsteady cases respectively. It has been noted from this figure that θ decreases by increasing Pr. It is also clear from this figure that as unsteadiness increases, more decrease in the magnitude of temperature is seen.

Numerical values of the skin friction coefficient at the surface for various values of λ and A are illustrated in the Table 7.1 and are compared with [148] when $A = 0$. It is evident from this table that $f''(0)$ decrease by increasing slip on the surface and increase by increasing unsteadiness parameter A. Hence the slip on the surface causes a decrease in the value of skin friction coefficient as expected. The variation in local Nusselt number under the influence of different parameters is presented in Table 7.2. It is clear from the Table 7.2 that $-\theta'(0)$ decreases by increasing slip parameter and increases by increasing unsteadiness parameter and Prandtl number.

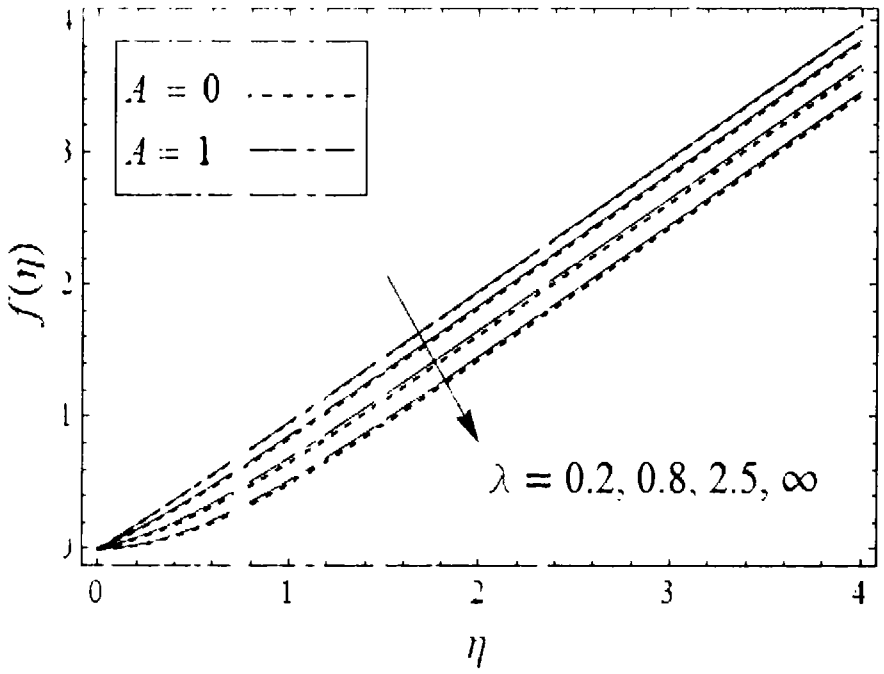

Fig. 7.2 Variation in $f(\eta)$ for different values of λ when $A = 0$ and $A = 1$.

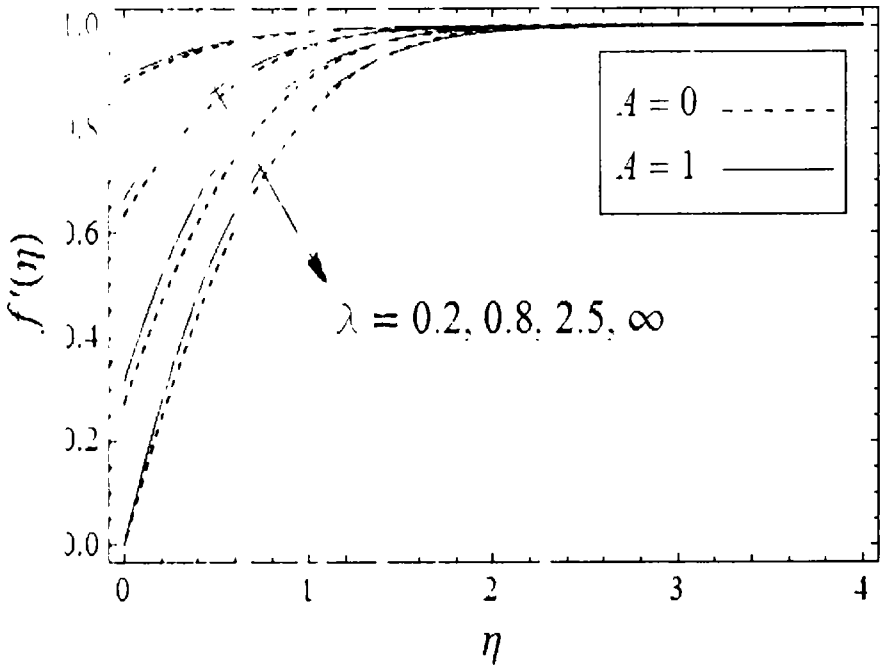

Fig. 7.3. Variation of $f'(\eta)$ for different values of λ when $A = 0$ and $A = 1$.

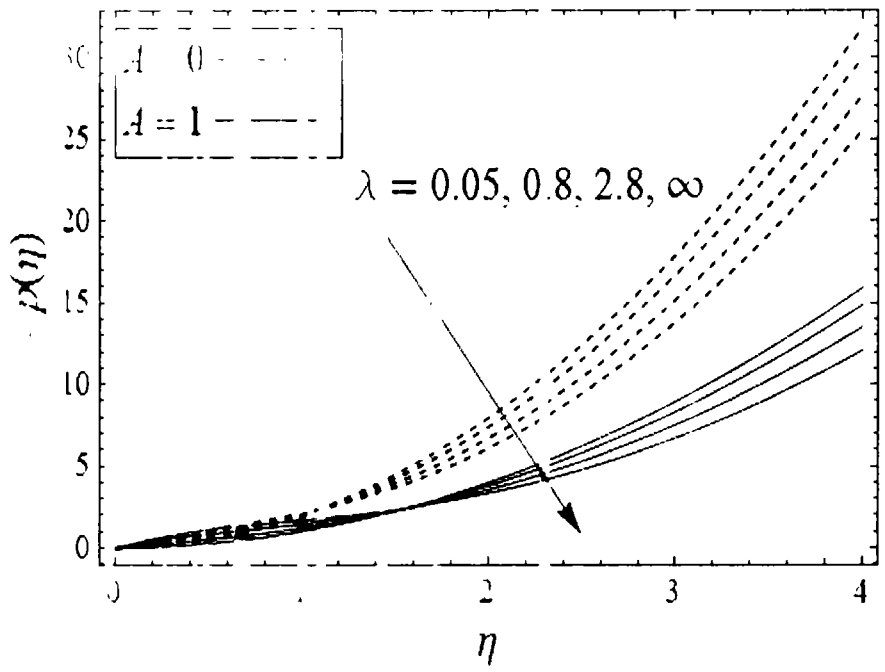

Fig. 7.4 Variation of $-p(0)$ for different values of λ when $A = 0$ and $A = 1$.

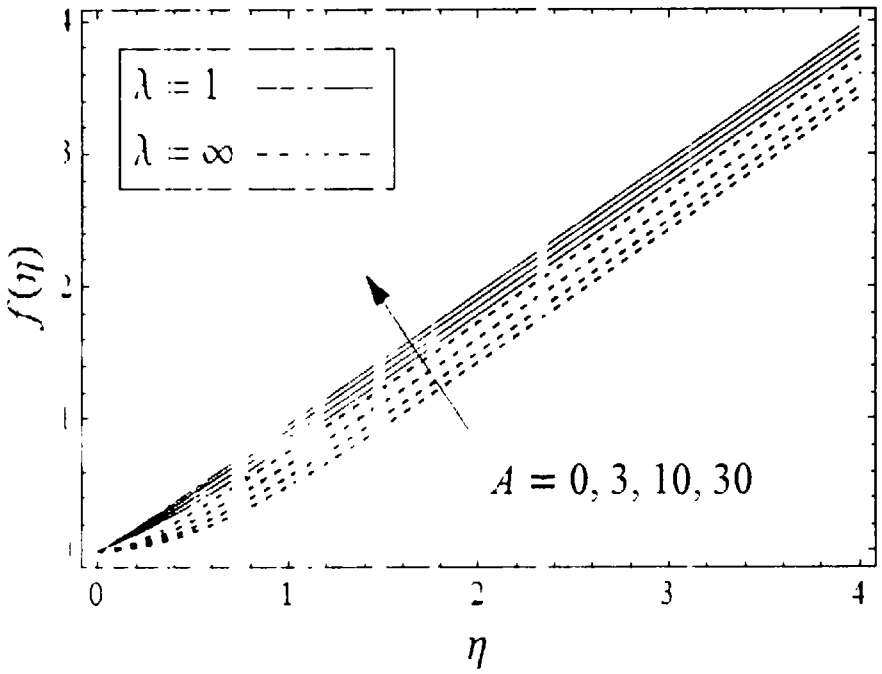

Fig. 7.5. Variation of $f(\eta)$ for different values of A when $\lambda = 1$ and $\lambda = \infty$.

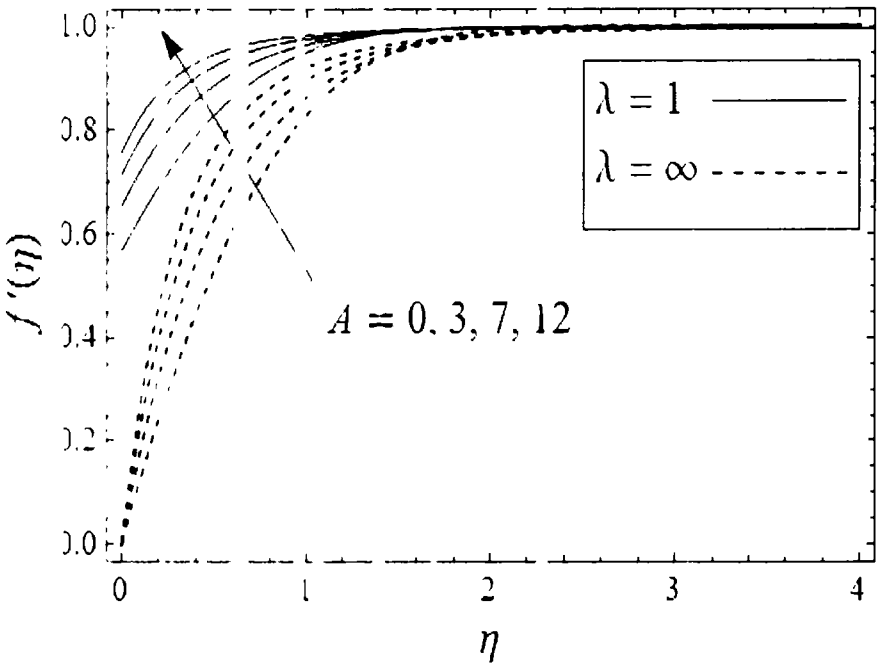

Fig. 7.6. Variation of $f'(\eta)$ for different values of A when $\lambda = 1$ and $\lambda = \infty$.

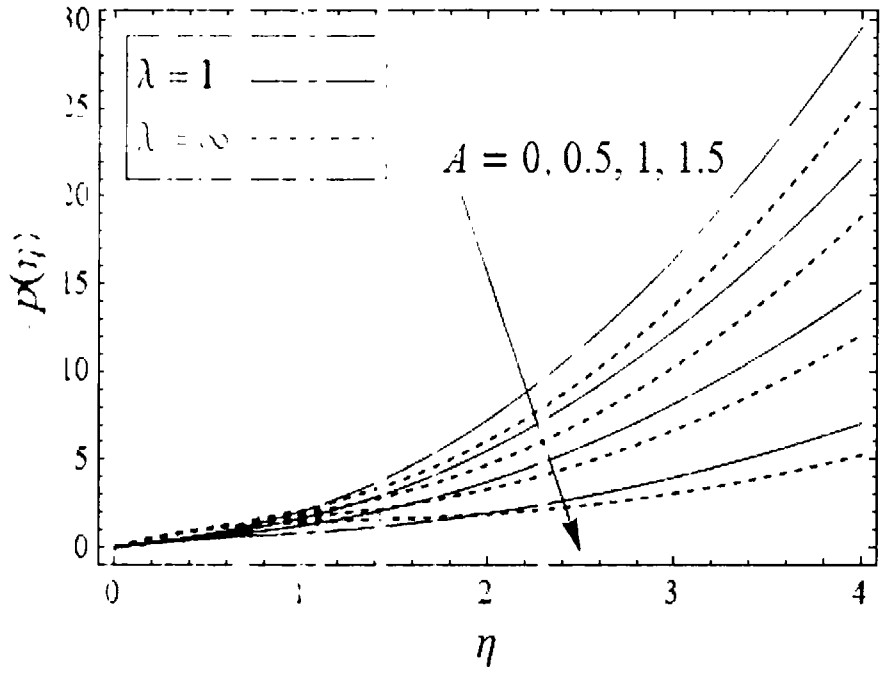

Fig. 7.7. Variation of $-p(\eta)$ for different values of A when $\lambda = 1$ and $\lambda = \infty$.

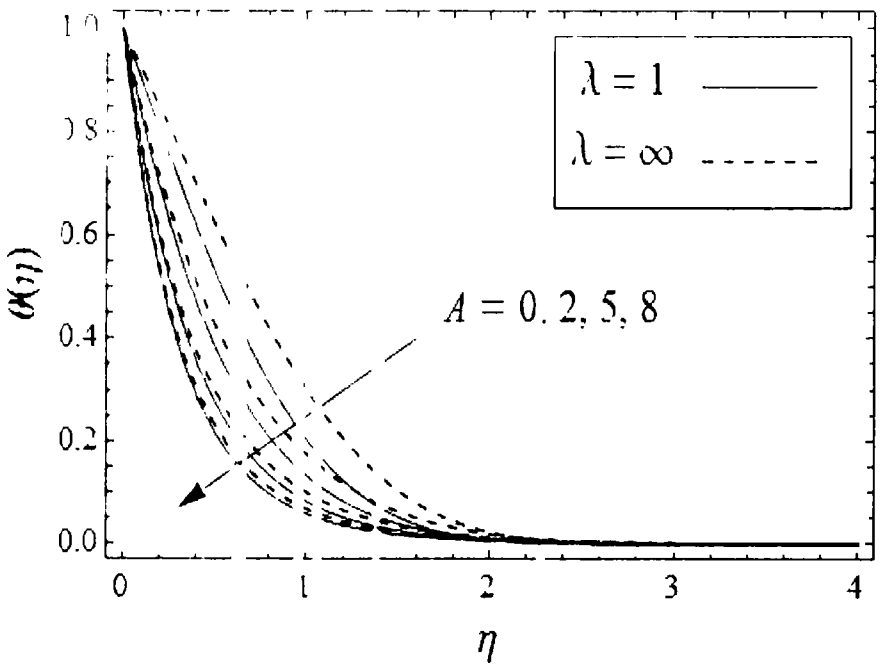

Fig. 7.8. Variation in $\theta(\eta)$ for different values of A and λ when $Pr = 1$.

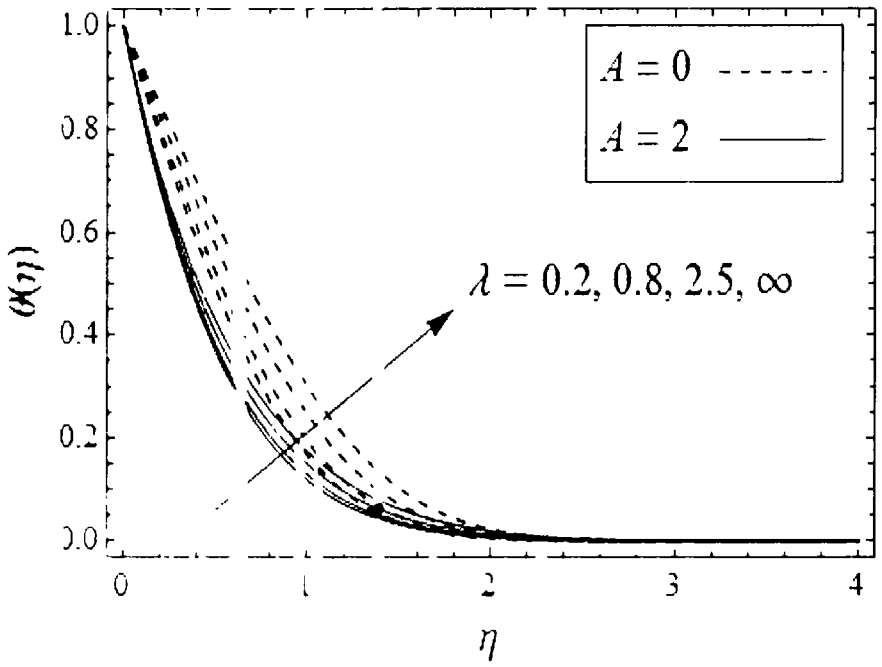

Fig. 7.9. Variation in $\theta(\eta)$ for different values of λ and A when $Pr = 1$.

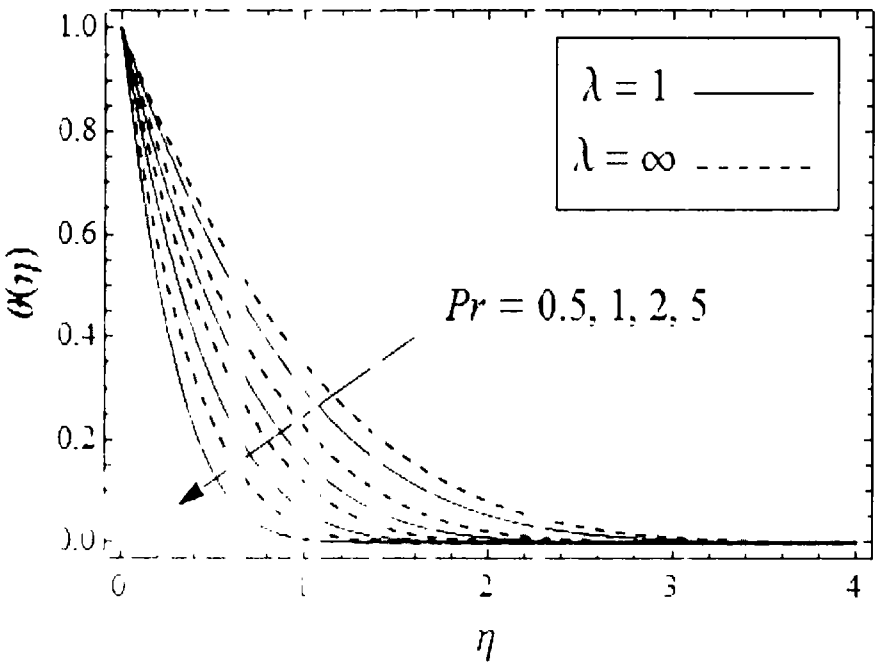

Fig. 7.10. Variation in $\theta(\eta)$ for different values of Pr and λ when $A = 1$.

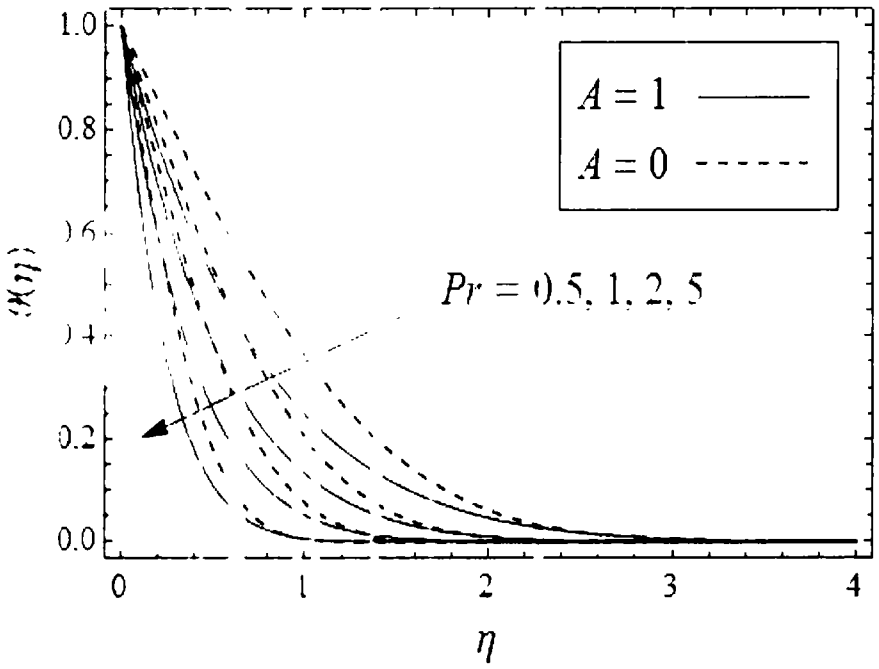

Fig 7.11. Variation in $\theta(\eta)$ for different values of Pr and A when $\lambda = 1$.

Table 7.1: Numerical values for the skin friction coefficient $f''(0)$ for various values of λ and A. The values in the parenthesis are given by Santra et al. [148].

λ	$A = 0$	$A = 1$	$A = 5$	$A = 50$	$A = 100$
0.01	0.009994 (0.00999.0)	0.009995	0.009996	0.009998	0.009999
0.05	0.049245 (0.04924.)	0.049254	0.049364	0.049744	0.049815
0.1	0.096639 (0.09663.)	0.096645	0.097474	0.098978	0.099264
0.5	0.414733 (0.41473.)	0.421773	0.440708	0.475200	0.481994
1	0.687618 (0.68761.)	0.714975	0.780883	0.904371	0.929885
2	0.979046 (0.97904.)	1.058510	1.249381	1.643876	1.733929
5	1.211821 (1.21182.)	1.384896	1.854787	3.175248	3.567803
10	1.275873 (1.27587.)	1.491554	2.129354	4.484463	5.404635
50	1.308716 (1.30871.)	1.550981	2.313818	6.112016	8.336686
100	1.310810 (1.31081.)	1.554897	2.327023	6.281861	8.712896
500	1.311853 (1.31185.)	1.556854	2.333675	6.371818	8.920022
∞	1.311956 (1.31195.)	1.557046	2.334332	6.380862	8.941168

Table 7.2: Numerical values for the $-\theta'(0)$ for various values of Pr.

Pr	$\lambda = 0.1$	$\lambda = 1$	$\lambda = \infty$	$A = 0$	$A = 10$	$A = 100$
	$A = 1$	$A = 1$	$A = 1$	$\lambda = 1$	$\lambda = 1$	$\lambda = 1$
0.1	0.500049	0.487277	0.461699	0.366244	1.161069	3.578919
0.5	0.078508	1.028799	0.933355	0.714680	2.591787	8.001272
1	0.523383	1.040575	1.284502	0.985666	3.663082	11.31356
2	1.152020	2.018342	1.770419	1.359311	5.177554	15.99468
5	1.398468	3.057204	2.717160	2.083981	8.181352	25.26648
10	4.802738	4.035593	3.772494	2.888600	11.56521	35.67804
50	10.73049	9.016135	8.193578	6.244961	25.82568	78.82254
100	15.17721	13.84586	11.49833	8.749920	36.47870	109.8120

7.3 Conclusions

In this chapter, we have investigated heat transfer analysis in the time-dependent axisymmetric stagnation-point flow over a disc lubricated with power-law fluid. We have taken $n = 1/3$ so that results can be compared in the special case. The numerical solutions of the governing equations are developed using Keller-box method. The motivation is to determine the effect of the slip parameter λ and unsteadiness parameter A on the flow characteristics. Main findings of the present study are

(i) Numerical values of f and f' increase by increasing the unsteadiness parameter A and by decreasing slip parameter λ.

(ii) Temperature θ increases with an increase in λ and decreases for large values of A and Pr.

(iii) $f'(\eta)$ increases by increasing both λ and A. Thus slip on the surface causes a reduction in the value of $f'(0)$

(iv) $-\theta'(0)$ decreases by increasing λ. However, it increases by increasing A and Pr.

Chapter 8

MHD mixed convection stagnation-point flow of a viscous fluid over a lubricated vertical surface

In this chapter we have discussed the MHD mixed convection flow impinging orthogonally on a vertical lubricated surface. A power-law fluid is utilized for the lubrication purpose. Mathematical model for the considered flow problem is illustrated by a set of partial differential equations. To obtain the interfacial conditions, it is assumed that the velocity and shear stress of both the fluids are continuous at the interface layer. Dimensionless variables are invoked to transform the original system in the form of ordinary differential equations. The Keller-box method is implemented to obtain numerical solutions. The impact of physical parameters on the flow characteristics is given in the shape of graphs and tables. A comparison of present and available results in the special case validates the obtained numerical solutions [77-81, 159]

8.1 Mathematical formulation

Consider mixed convection, steady, two-dimensional flow towards a stagnation-point over a vertical plate. A power law lubricant spreads over the surface forming a thin layer. We assume $T_w(x)$ and T_∞ as the surface and ambient temperatures respectively such that $T_w < T_\infty$ is for the cooled and $T_w > T_\infty$ is for the heated plate. A magnetic field having uniform strength B is imposed normal to the flat plate. The plate is resting in xz-plane and the fluid flows above the plate having free stream velocity $u_e(x)$, as shown in Fig. 8.1 below.

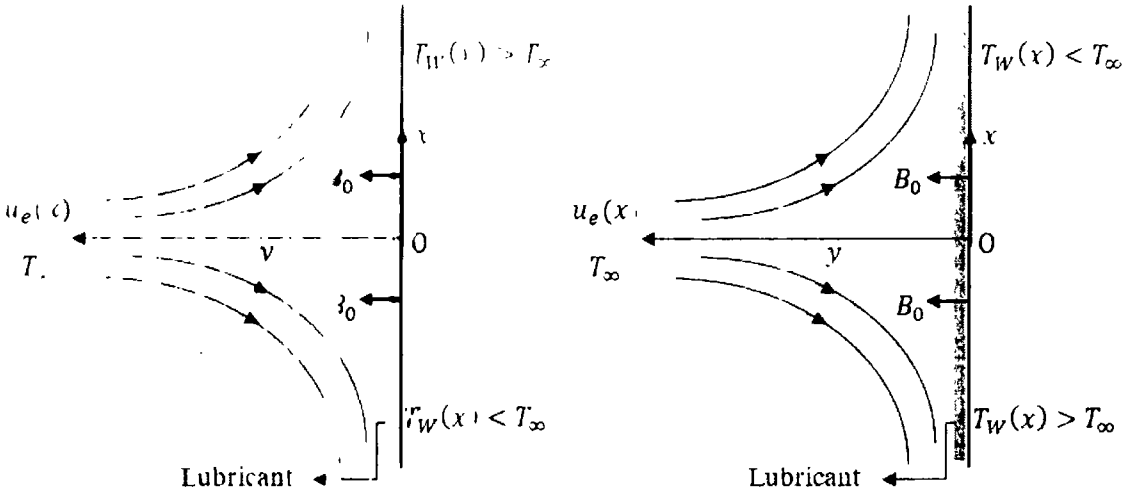

(i) assisting flow (ii) opposing flow

Figure 8.1 Flowing phenomenon showing assisting and opposing flow.

Hemenz [1] proved that the stagnation-point flow has the same attributes regardless the shape of the figure. The power-law fluid comes out from the centre of the plate with the flow rate Q given by Eq. (2.1).

Assuming T_w and u_e as the linear functions of x we have

$$T_w(x) = T_\infty + T_0\left(\frac{x}{L}\right), \quad u_e = U_e\left(\frac{x}{L}\right), \tag{8.1}$$

where L, T_0 and U_e are characteristic length, reference temperature and reference velocity respectively. The equations representing the boundary layer flow and heat transfer are (2.2) and

$$u\frac{\partial u}{\partial x} + v\frac{\partial u}{\partial y} = u_e\frac{du_e}{dx} + \nu\frac{\partial^2 u}{\partial y^2} \pm g\gamma_1(T - T_\infty) + \sigma\frac{B^2}{\rho}(u_e - u), \tag{8.2}$$

$$u\frac{\partial T}{\partial x} + v\frac{\partial T}{\partial y} = \alpha^*\frac{\partial^2 T}{\partial y^2}, \tag{8.3}$$

in which g, γ_1, σ and B represent respectively the gravitational acceleration, thermal expansion coefficient, electrical conductivity and magnetic field. The positive sign mentioned in Eq. (8.2) is for the assisting and negative sigh for the opposing flow.

To discuss present flow situation, the boundary conditions are applied at the surface, interface of both the fluids and at infinity The no-slip boundary condition at the surface are represented by Eqs. (2.7) and (2.8) and

$$T(x,0) = T_\infty + T_0\left(\frac{x}{L}\right) \tag{8.4}$$

Similarly, the interfacial conditions are given by (2.15) and (2.17). The conditions at the free stream imply

$$u(x,\infty) = U_e\left(\frac{x}{L}\right), \qquad T(x,\infty) = T_\infty. \tag{8.5}$$

Defining the dimensionless variables

$$= y\sqrt{\frac{U_e}{L}}, \quad u = U_e\left(\frac{x}{L}\right) f'(\eta), \quad v = -\sqrt{\frac{U_e}{L}\nu}\, f(\eta), \qquad T = T_\infty + T_0\left(\frac{x}{L}\right)\theta(\eta). \tag{8.6}$$

The governing equations yield

$$''' - f' + ff'' + 1 + d\theta + M(1 - f') = 0, \tag{8.7}$$

$$\theta'' + Pr(f\theta' - f'\theta) = 0, \tag{8.8}$$

$$f(0) = 0 \quad f''(0) = \lambda\, f''(0)^{2-n}, \quad f'(\infty) = 1, \tag{8.9}$$

$$\theta(0) = 1 \quad \theta(\infty) = 0, \tag{8.10}$$

where $M = \sigma\frac{B^2L}{\rho}U_e$ is the Hartmann number and $d = Gr/Re^2$ represents mixed convection parameter, in which $Gr = g\gamma_1 T_0 L^3/\nu^2$ is Grashof and $Re = U_eL/\nu$ is Reynolds number. It is important to mention that $a > 0$ and $d < 0$ respectively correspond to assisting and opposing flows. The slip parameter λ in Eq. (8.9) is defined as

$$\lambda = \frac{k\sqrt{\nu}}{\mu}\frac{e^{2n}x^{2n-1}}{\rho^{3/2}(2Q)^n}, \tag{8.11}$$

where $e = U_e/L$.

8.2 Results and discussion

The values of f', f'', θ and θ' are obtained by solving Eqs. (8.7) and (8.10) using Keller-box method for certain values of pertinent parameters.

To find the influence of Hartmann number M, slip parameter λ, mixed convection parameter d, Prandtl number Pr and flow behavior index n on $f'$and θ, Figs. 8.2-8.10 have been plotted. The response of pertinent parameters on $f''(0)$ and $-\theta'(0)$ have been given

in Tables 8.1-8.3.

Figs. 8.2 and 8.3 are displayed to analyze the behavior of wall slip due to lubricant on the velocity and temperature distributions. Fig. 8.2 depicts the dependence of f' (velocity component along x axis) on slip parameter λ. According to this figure f' increases with decreasing the magnitude of λ. It means the lubricant increases the fluid velocity. For the case when λ approaches to zero, i.e. in the case of full-slip, the effects of viscosity are suppressed by the lubricant. Fig. 8.3 demonstrates how the slip parameter λ effects the temperature profile θ. We observe that the numerical value of temperature profile θ is increased by increasing slip parameter λ showing that temperature of the fluid is reduced by augmenting lubrication on the plate.

The impact of Hartmann number M on f' and θ when $\lambda = 3, Pr = 1, d = 0.1$ is depicted in Figs. 8.4 and 8.5. Fig. 8.4 illustrates that applied magnetic field excites the bulk motion and supports the lubrication effects. According to Fig. 8.5, the temperature profile θ decreases by increasing the numerical value of M. Moreover, an increase in the numerical value of M reduces the thermal boundary layer thickness.

To observe the effects of d on f and θ for fixed λ, M, and Pr both for assisting as well as opposing flows, Figs. 8.6 and 8.7 are plotted. Fig. 8.6 depicts that velocity profile f' and mixed convection parameter d are directly proportional to each other for the assisting flow and are inversely proportional for the opposing flow. Influence of d on temperature θ is presented in Fig. 8.7. This figure shows that by increasing d the temperature of fluid decreases for the case of assisting flow and it increases when there is opposing flow. Fig. 8.8 elucidates how Prandtl number Pr effects the temperature θ in the existence of lubrication when $M = 1$ and $d = 0.1$. From this figure, it is clear that as we increase the numerical value of Pr for some fixed value of λ, the temperature profile decreases. As we move from no-slip to full-slip (i.e. λ decreases), this decrease is more rapid. The impact of flow behavior index n on f' and θ is illustrated in Figs. 8.9 and 8.10. Fig. 8.9 shows that the horizontal velocity component f' is increased by increasing n. According to Fig. 8.10 the temperature θ decreases by increasing flow behaviour index n.

Influence of slip parameter λ on $f''(0)$ and $-\theta'(0)$ when $M = 1$ and $Pr = 1$ are presented in Table 8.4. The cases for the assisting flow and opposing flow are considered. We observe that by increasing λ, $f''(0)$ is increased and $-\theta'(0)$ is decreased. However, the rate of

in rease o. dec rease is sl wer when there is opposing flow. The numerical computations fo $\lambda = \infty$ are carried out a $\lambda = .1000$ The impact of M on $f''(0)$ and $-\theta'(0)$ is elucidated in Table 8. ! when λ, Pr a d d are con tant. It has b en observed that by increasing M, both $f'(0)$ and $-\theta'(0)$ incre a e. The effe :ts of Pr on $f''(0)$ and $-\theta'(0)$ for assisting as well as opposing flows, are sh wn in Table 8.3. A close ook at this table clarifies that as the Pr is increase l, $f''(0)$ is d crea ed and $-\theta'(0)$ is increased in the assisting flow case. H wever, oth quantities re increase l in the oppos ing flow case.

Numeric al values of $f''(0)$ and $-\theta'(0)$ for the no-slip case agree well with the values already described in the li erature [77 81, 159] and are presented in Tables 8.4-8.6.

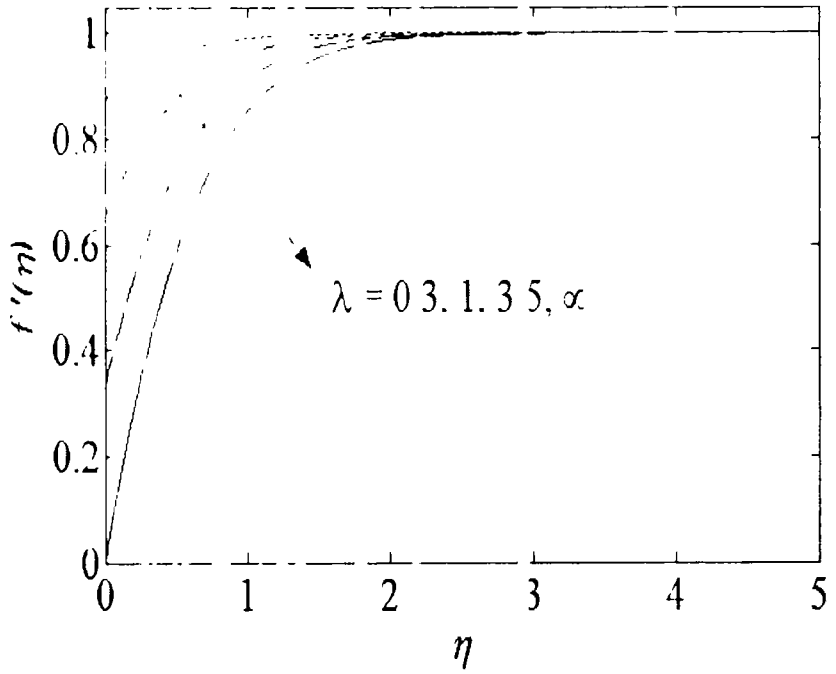

Fig. 4.2. Response of $f'(\eta)$ aga nst λ when $M = 1, Pr = 1, d = 0.1, n = 1/2$.

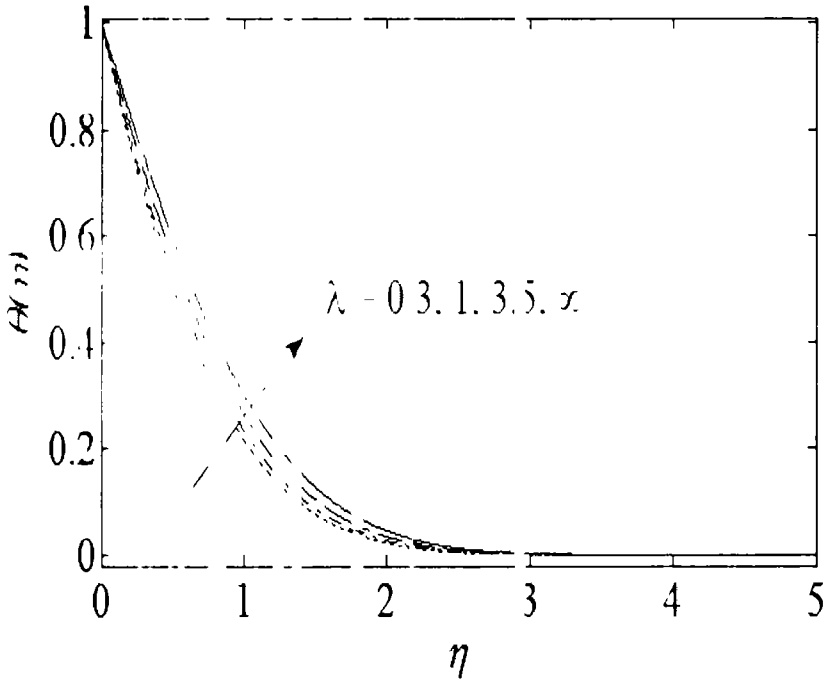

Fig. 3.3. Response of $\theta(\eta)$ against λ when $M = 1, Pr = 1, d = 0.1, n = 1/2$.

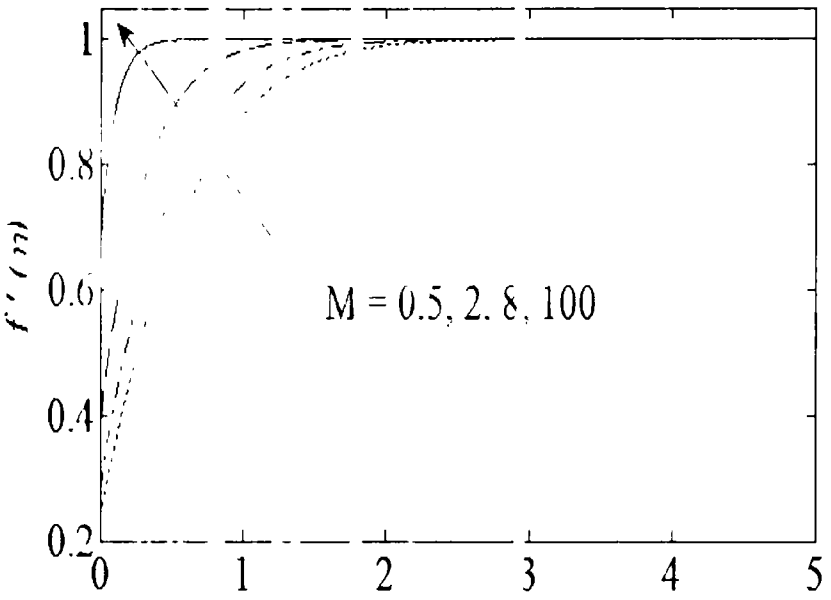

Fig. 3.4. Response of $f'(\eta)$ against M when $\lambda = 5, Pr = 1, d = 0.1, n = 1/2$.

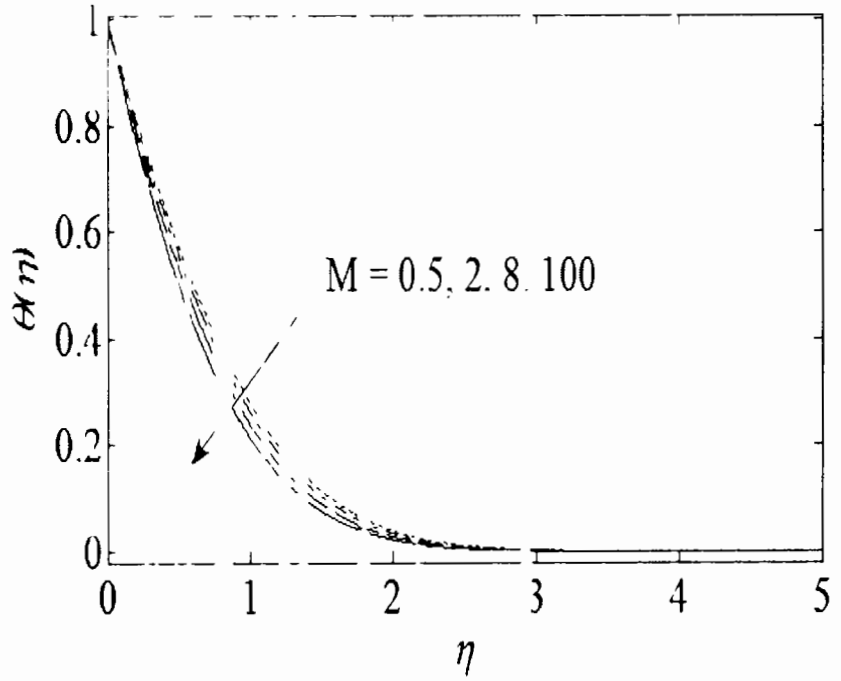

Fig. 8.5. Response of $\theta(\eta)$ against M when $\lambda = 5, Pr = 1, d = 0.1, n = 1/2$.

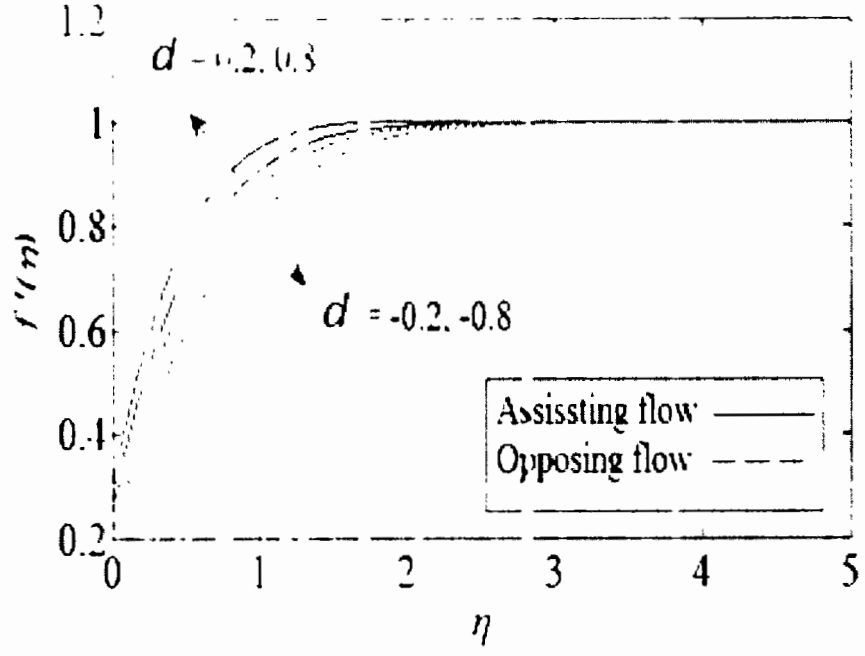

Fig. 8.6. Response of $f'(\eta)$ against d when $\lambda = 5, Pr = 1, M = 1, n = 1/2$.

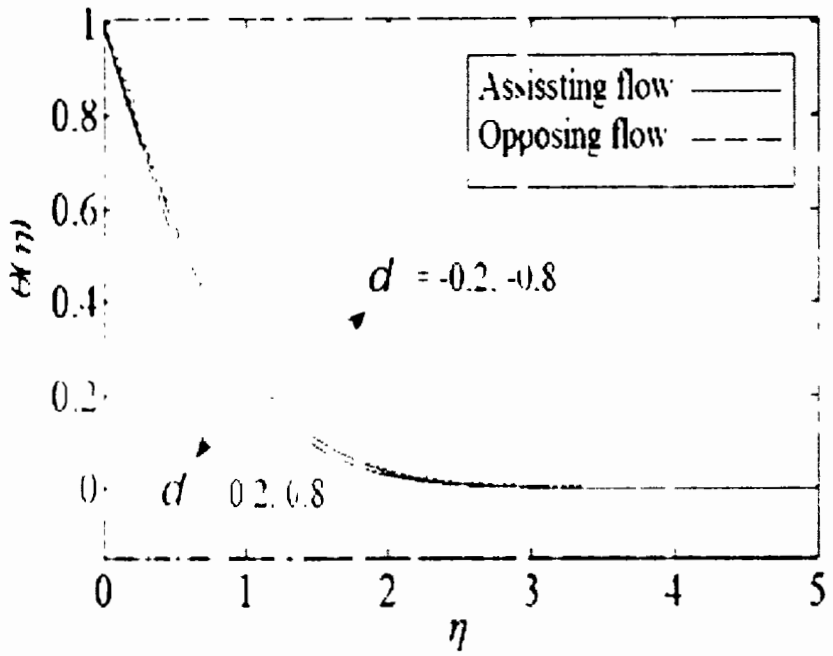

Fig 8.7 Response of $\theta(\eta)$ against d when $\lambda = 5, Pr = 1, M = 1, n = 1/2$.

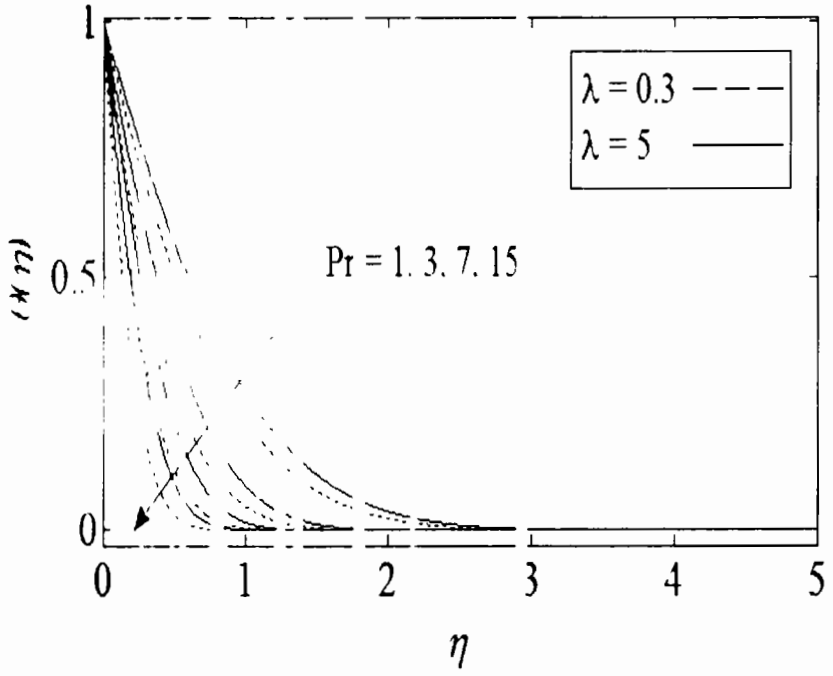

Fig. 8.8 Response of $\theta(\eta)$ against Pr in the presence of slip when $M = 1$, $d = 0.1$ and $n = 1/2$.

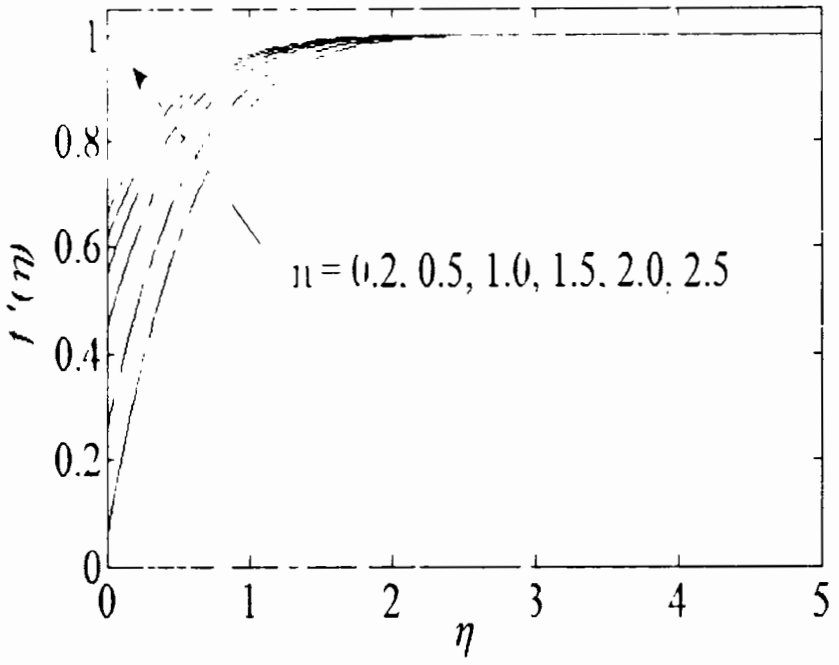

Fig. 8.9. Response of $f'(\eta)$ against n when $\lambda = 5, Pr = 1, M = 1$ and $d = 0.1$.

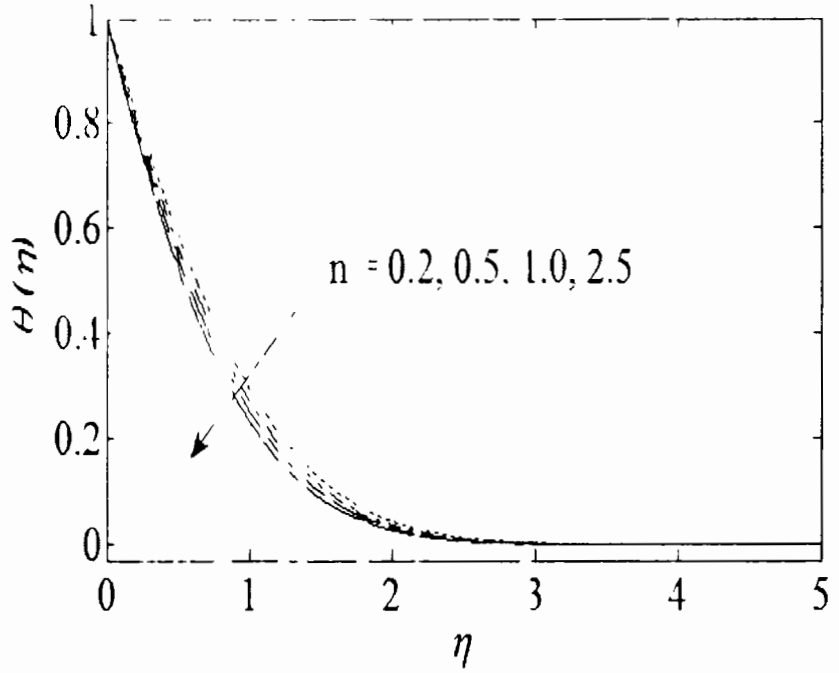

Fig. 8.10. Response of $\theta(\eta)$ against n when $\lambda = 5, Pr = 1, M = 1$ and $d = 0.1$.

Table 8.1: Influence of slip parameter λ on $f''(0)$ and $-\theta'(0)$ when $M = 1$ and $Pr = 1$ when $d = 0.1$ (assisting flow) and $d = -0.1$ (opposing flow).

λ	$f''(0)$ (assisting flow)	$-\theta'(0)$ (assisting flow)	$f''(0)$ (opposing flow)	$-\theta'(0)$ (opposing flow)
0.01	0.0101122	1.2599325	0.0097796	1.2427839
0.05	0.0495158	1.2525857	0.0478723	1.2354619
0.1	0.0965228	1.2437203	0.0932823	1.2266314
0.5	0.3994496	1.1837080	0.3850065	1.1667000
1.0	0.6527857	1.1290828	0.6276409	1.1129564
2.0	0.9466651	1.0593235	0.9075208	1.0442861
5.0	1.2769618	0.9700909	1.2198865	0.9570234
10	1.4346705	0.9220959	1.3682181	0.9103471
50	1.5837308	0.8725170	1.5079733	0.8623061
100	1.6038870	0.8654437	1.5268410	0.8554656
500	1.6202576	0.8596270	1.5421597	0.8498433
∞	1.6243922	0.8581573	1.5460290	0.8484232

Table 8.2: Influence of M on $f''(0)$ and $-\theta'(0)$ when $\lambda = 1$ and $Pr = 1$ when $d = 0.1$ (assisting flow) and $d = -0.1$ (opposing flow)

M	$f''(0)$ (assisting flow)	$-\theta'(0)$ (assisting flow)	$f''(0)$ (opposing flow)	$-\theta'(0)$ (opposing flow)
0.1	0.6149555	1.1057394	0.5831787	1.0845621
0.5	0.6335879	1.1174154	0.6052519	1.0988763

1.0	0.652757	1 1290828	0.6276409	1.1129564
2.0	0.682219	1 1463037	0.6615126	1.1333866
5 0	0 7360881	1 1753963	0.7220656	1.1671049
10	0 7821 44	1 1978075	0.7733190	1.1924990
50	0.880034	1 2343744	0.8771720	1.2329398
100	0.910861	1 2424560	0.9092798	1.2416976
500	0.9574734	1 2506954	0.9571130	1.2505353
1000	0.969476	1 2519452	0.9692902	1.2518645
2000	0.978189	1 2526083	0.9780941	1.2525678
50000	0.9955494	1 2532860	0.9955459	1.2532844
∞	0.9999994	1 2533220	0.9999987	1.2533211

Table 8 3: Influence of Prandtl number Pr on $f''(0)$ and $-\theta'(0)$ when $\lambda = 1$ and $M = 1$ when $d = 0.1$ (assisting flow) and $d = -0.1$ (opposing flow).

Pr	$f''(0)$ (assisting flow)	$-\theta'(0)$ (assisting flow)	$f''(0)$ (opposing flow)	$-\theta'(0)$ (opposing flow)
0.05	0.6593814	0 3047311	0.6208986	0.3009513
0 1	0 6584386	0 3913332	0.6218514	0.3852558
0 5	0.6547115	0 8142949	0.6256484	0.8015589
1.0	0.6527577	1 1290828	0.6276409	1.1129564
2 0	0 6507812	1 5655846	0.6296540	1.5457547
5.0	0.6483054	2 4160414	0.6321715	2.3911373
10	0.6466401	3 3625665	0.6338614	3.3339433

50	0.6436939	7.3144593	0.6368419	7.2785393
100	0.6428188	10.2620591	0.6377242	10.2237614

Table 8.4: Comparison showing the influence of Pr on $f''(0)$ when $\lambda = \infty$, $M = 0$ and $d = 0$.

Pr	Ramachandran et al. [77]	Devi et al. [78]	Lok et al. [80]	Hassanien & Gorla [79]	Fazlina et al. [81]	Present
0.7	1.7063	1.7064	1.7064	1.70632	1.7063	1.706333
1	-	-	-	-	1.6754	1.675450
3	1.5179	1.5180	1.5180	-	1.5179	1.517922
10	-	-	-	1.49284	1.4928	1.492848
20	1.4485	1.4485	1.4486	-	1.4485	1.448492
40	1.4101	-	1.4102	-	1.4101	1.410067
60	1.3903	1.3903	1.30903	-	1.3903	1.390283
80	1.3774	-	1.3773	-	1.3774	1.377401
100	1.3680	1.3680	1.3677	1.38471	1.3680	1.368043

Table 8.5: Comparison showing influence of Pr on $-\theta'(0)$ when $\lambda = \infty$, $M = 0$ and $d = 0$.

Pr	Ramachandran et al. [77]	Devi et al. [78]	Lok et al. [80]	Hassanien & Gorla [79]	Fazlina et al. [81]	Present
0.7	0.7641	0.7642	0.7641	0.76406	0.7641	0.764073
1	-	-	-	-	0.8708	0.870788

7	1. '224	1 7223	1.7226	-	1.7224	1.722480
10	-	-	-	1.94461	1.9446	1.944644
20	2. 4576	2 4574	2.4577	-	2.4576	2.457652
40	3. 011	-	3.1023	-	3.1011	3.101146
60	3. 5514	3 551'	3.5560	-	3.5514	3.551412
80	3. 9095	-	3.9195	-	3.9095	3.910952
100	4. 2116	4 2113	4.2289	4.23372	4.2116	4.213370

Table 6 Comparison showing influence of d on $f'(0)$ and $-\theta'(0)$ when $\lambda = \infty$, $M = 0$ and $Pr = 0.7$.

a	$f''(0)$ Ahmed & Nazar [159]	$f''(0)$ Present work	$-\theta'(0)$ Ahmed & Nazar [159]	$-\theta'(0)$ Present
−0.6	0 9194	0.9193778	0.6673	0.6672568
−0 8	0 8079	0.8078804	0.6510	0.6510393
−1 0	0 6917	0.6916868	0.6332	0.6332424
−1 2	0 5696	0 5696416	0.6134	0.6134485
−1 4	0 4401	0.4401302	0.5909	0.5908937
−1 6	0 3003	0.3003289	0.5574	0.5574276
0.1	1 2823	1.2823140	0.7157	0.7157189
0.5	1 4755	1.4755318	0.7383	0.7382642
0)	1 6610	1.6610101	0.7591	0.7591422
1.6	1 9707	1.9707155	0.7916	0.7916414

8.3 Conclusions

In this chapter, MHD mixed convection flow stagnated over a vertical wall lubricated with power-law fluid is investigated. Numerical solutions are attained to analyze the influence of slip parameter λ, Hartmann number M, mixed convection parameter d, power- law index n and Prandtl number Pr on the flow characteristics. Results are presented in the form of tables and figures for certain values of parameters by considering assisting as well as opposing flow situations. Some findings of this study are

(i) The lubricant excites the base fluid velocity inside the boundary layer. Moreover, the effects of viscosity are supressed by the lubricant in the case of full-slip.

(ii) The temperature of the base fluid decreases by increasing lubrication on the surface.

(iii) By increasing the slip on the surface, the wall shear stress, i.e. $f''(0)$ decreases and heat transfer coefficient, i.e. $-\theta'(0)$ increases but the rate of increase or decrease is less in magnitude for the opposing flow.

(iv) The similarity solutions only exist for $n = 1/2$. A non-similar solution is obtained when $n \neq 1/2$

Chapter 9

Effects of lubrication in MHD mixed convection stagnation-point flow of a second grade fluid adjacent to a vertical plate

The present chapter describes effects of mixed convection on MHD flow of a second grade fluid above a vertical plate. The fluid impinges orthogonally on the plate which has a slim coating of power-law lubricant. A system of ordinary differential equations is obtained by employing the similarity transformations to the original partial differential equations. To handle the present flow situation it is assumed that velocity and shear stress of the second grade fluid and the lubricant are continuous at the interface. A well reputed numerical technique called Keller-box method is utilized to solve coupled nonlinear equations. Influence of slip, magnetic and mixed convection parameters, Weissenberg and Prandtl numbers on the velocity, skin friction coefficient, temperature and heat transfer rate at the surface is presented in the form of graphs and tabular data for both assisting and opposing flows. The results in the case of reduced no-slip condition are compared with the available numerical data [159]. A good agreement of these results certifies our effort.

9.1 Problem description

Consider steady, mixed convection, two-dimensional flow of a second grade fluid due to stagnation point adjacent to a vertical lubricated plate. A power-law fluid has been utilized for the lubrication purpose. The plate temperature T_w is linearly dependent to the distance x from the origin. It is assumed that the plate is resting in xz-plane and a transverse magnetic field B is applied on the plate as shown in Fig. 8.1.

Equations representing the boundary layer flow are (2.2), (8.3) and the following equation

$$\rho\left(\frac{\partial u}{\partial t}+u\frac{\partial u}{\partial x}+v\frac{\partial u}{\partial y}\right)=\rho u_e\frac{du_e}{dx}+\mu\frac{\partial^2 u}{\partial y^2}+k_1\left(u\frac{\partial^3 u}{\partial x\,\partial y^2}+\frac{\partial u}{\partial x}\frac{\partial^2 u}{\partial y^2}+\frac{\partial u}{\partial y}\frac{\partial^2 v}{\partial y^2}+v\frac{\partial^3 u}{\partial y^3}\right)$$
$$\pm g\gamma\,(T-T_\infty)+\sigma\frac{B^2}{\rho}\,(u_e-u). \tag{9.1}$$

To discuss present flow situation, the boundary conditions are applied at the surface, interface of both fluids and free stream Eqs. (2.7) and (8.4) represent the boundary conditions at fluid-solid interface while the boundary conditions at fluid-fluid interface are represented by Eqs (2.17 and (8.5). The conditions at the free stream imply

$$u(x,0) = U_w\left(\frac{x}{L}\right), \qquad \frac{\partial u(x,y)}{\partial y} = 0, \qquad T(x,0) = T_\infty. \tag{9.2}$$

Introducing Eq (8.6), one gets the following system of equations.

$$f''' - f'' + ff'' + 1 + We\left(2f'f'' - f''^2 - ff^{iv}\right) + d\theta + M(1-f') = 0, \tag{9.3}$$

$$f(0) = 0, \quad f''(0) + \beta W\, f'(0) f''(0) = \lambda f'(0)^{2n}, \quad f'(\infty) = 1, \quad f''(\infty) = 0. \tag{9.4}$$

The heat equation and relative boundary conditions are mentioned in Eqs. (8.8) and (8.10). The parameter λ is defined in Eq. (8.11).

9.2 Numerical results and discussion

The values of f', f'', θ and θ' are obtained by solving Eqs. (9.3), (9.4), (8.8) and (8.10) using Keller-box method for certain values of pertinent parameters.

To illustrate the influence of magnetic parameter M, slip parameter λ, mixed convection parameter l, Weissenberg number We and Prandtl number Pr on f' and θ, Figs. 9.1-9.9 have been plotted. Numerical values of wall shear stress $Re_x^{1/2}C_f$ and and local Nusselt number $Re_x^{-1/2}Nu_x$ are given in Tables 9.1-9.4. This numerical data is utilized to discuss the influence of involved parameters on $Re_x^{1/2}C_f$ and $Re_x^{-1/2}Nu_x$.

Figures 9.1 and 9.2 are displayed to analyze the behavior of slip parameter on the velocity and temperature profiles. Fig 9.1 depicts the dependence of f' (velocity component along x axis) on slip parameter λ. According to this figure f' increases when slip is increased at the surface. It means that lubricant excites the velocity of the fluid. The case when λ approaches to zero, i.e. full- slip regime, the effects of viscosity are suppressed by the lubricant. Fig. 9.2 demonstrates how the slip parameter λ effects the temperature θ. It is observed from this figure that the fluid temperature is suppressed by increasing slip. This is because velocity is enhanced by increasing slip and as a result the impact of wall

temperature on the flowing fluid is reduced.

Figs. 9.3 and 9.4 display the variation in f' and θ for various values of magnetic parameter M when P, d and We are fixed. Magnetic parameter can affect the fluid velocity in three ways either it excites the fluid velocity or it suppresses the fluid velocity or alters the boundary layer thickness. In the present case Fig. 9.3 illustrates that with increasing M velocity is increased and momentum boundary layer thickness is decreased. Following the same argument for the previous set of figures the temperature θ decreases by increasing M (Fig.9.4). Furthermore, the thermal boundary layer thickness is reduced by increasing M. Variation in f' and θ for the influence of viscoelastic parameter We for fixed λ, M, d and Pr has been reported in Figs. 9.5 and 9.6. Fig. 9.5 shows that f' decreases by increasing We. The reason is that by increasing We, the viscous effects for the viscoelastic fluid are more prominent and as a result velocity of the fluid is decreased. A reverse phenomenon has been observed near the surface as slip is increased. It means slip dominates the viscous effects inside the boundary layer. Temperature in this case is a decreasing function of We and results are shown in Fig. 9.6. To analyze the effects of d on f' and θ both for assisting and opposing flows, Figs. 9.7 and 9.8 are plotted. Fig. 9.7 depicts that velocity f' is an increasing function of the mixed convection parameter d for the assisting flow and is decreasing function for the opposing flow. The reason is that when the fluid is in contact with the heated plate, the molecules of the fluid are excited and as a result the velocity of the fluid enhances. On the other hand, velocity of the fluid decreases near the cooled plate. Fig. 9.8 shows the influence of d on the temperature θ. We observe that by increasing d the temperature of fluid reduces for assisting flow situation and it increases for the opposing flow. Impact of Pr on the numerical values of θ is displayed in Fig. 9.9. As expected temperature θ reduces for large values of Pr. From the explicit definition of Pr, we observe that it is inversely related to thermal diffusivity α^*. Therefore, increasing Pr, results in the decrement of α^* causing a decrease in heat transfer. This reduction becomes more prominent for the increased slip case.

Numerical values of $Re_x^{1/2}C_f$ and $Re_x^{-1/2}Nu_x$ for the influence of λ when M=1, K= 0.5 and Pr = 1 are presented in Table 9.1. The cases for assisting and opposing flows has been discussed. It is observed that $Re_x^{1/2}C_f$ is an increasing and $Re_x^{-1/2}Nu_x$ is a decreasing

function o λ for both the cases But magnitude of increase or decrease is smaller when there is an opposing flow. Table 9.2 is devoted for the analysis of $Re_x^{1/2}C_f$ and $Re_x^{-1/2}Nu_x$ for the influence of magnetic parameter M. We see that by increasing M, both $Re_x^{1/2}C_f$ and $Re_x^{-1/2}Nu_x$ gain the magnitude. The rate of increase of both quantities is larger in full-slip regime and is smaller in no-slip regime for both the cases. Effects of Pr on $Re_x^{1/2}C_f$ and $Re_x^{-1/2}Nu_x$ on the lubricated surface has been depicted in Table 9.3. The results show that by increasing Pr, $Re_x^{1/2}C_f$ decreases and $Re_x^{-1/2}Nu_x$ increases in the case of assisting flow and both quantities accelerate in opposing flow situation. Table 9.4 incorporates the effects of We on $Re_x^{1/2}C_f$ and $Re_x^{-1/2}Nu_x$ during assisting and opposing flows for $\lambda = 3$, $M = 1$ and $Pr = 1$. We see that $Re_x^{1/2}C_f$ and $Re_x^{-1/2}Nu_x$ are reduced by enhancing We in each case. Tables 9.5 and 9.6 are developed to examine the variation in $Re_x^{1/2}C_f$ and $Re_x^{-1/2}Nu_x$ for the influence of We, M and Pr. A comparison of obtained results with those of Ahmed and Nazar [159] validates the accuracy of the provided solutions.

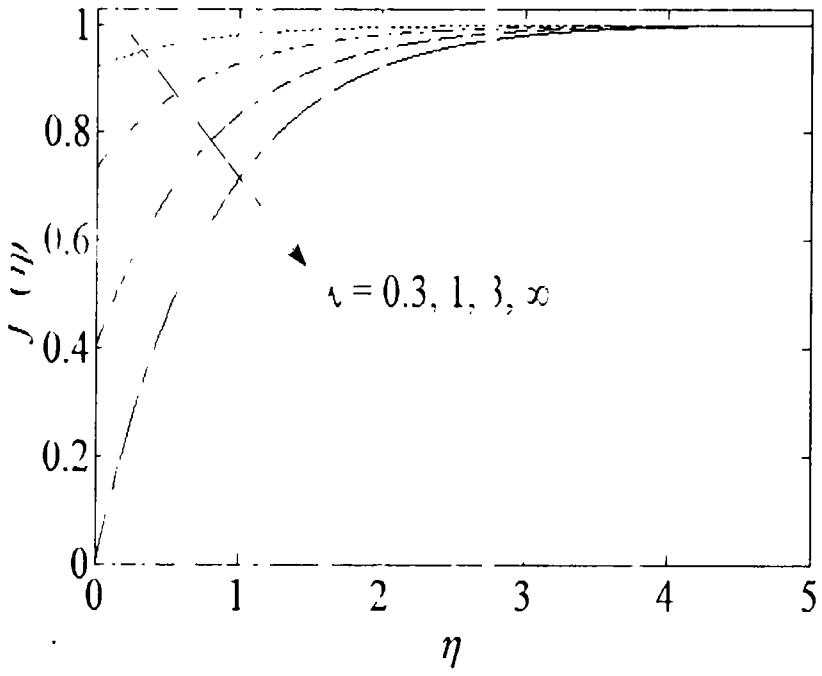

Fig. 9.1: Impact of λ on $f'(\eta)$ when $M = 1, We = 0.5, d = 0.1, Pr = 1$.

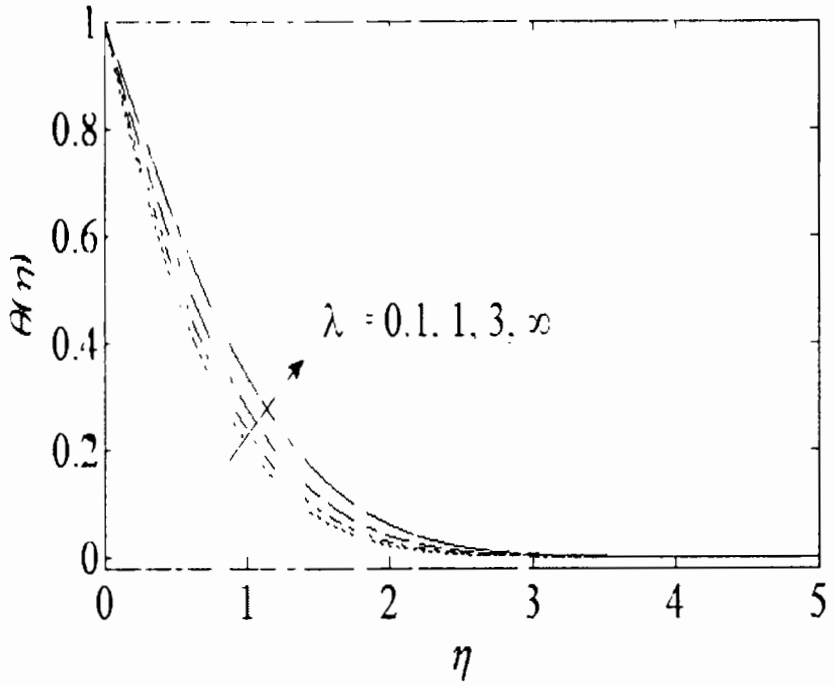

Fig. 9.2: Impact of λ on $\theta(\eta)$ when $M = 1, We = 0.5, d = 0.1, Pr = 1$.

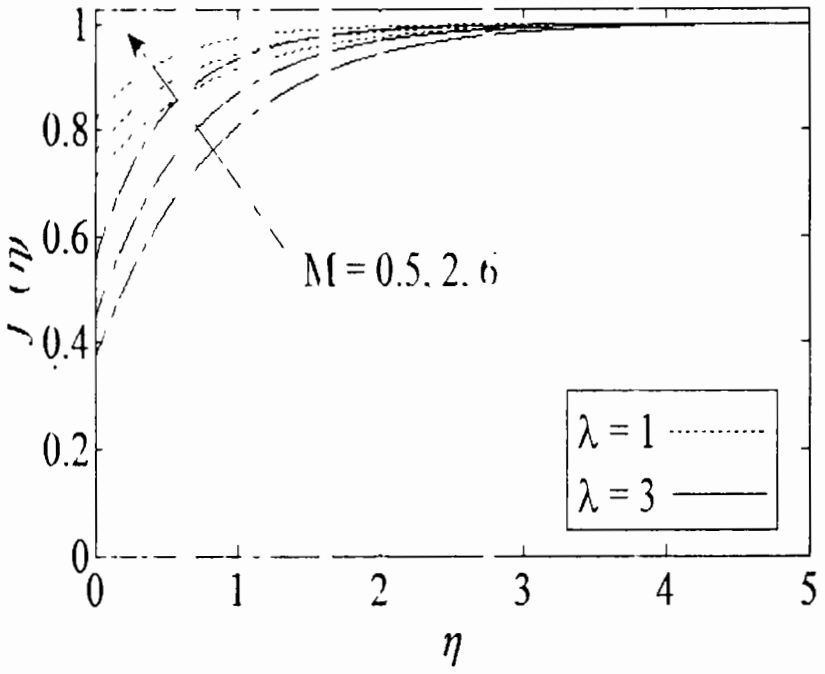

Fig. 9.3: Impact of λ on $f'(\eta)$ by altering slip when $We = 0.5, d = 0.1, Pr = 1$.

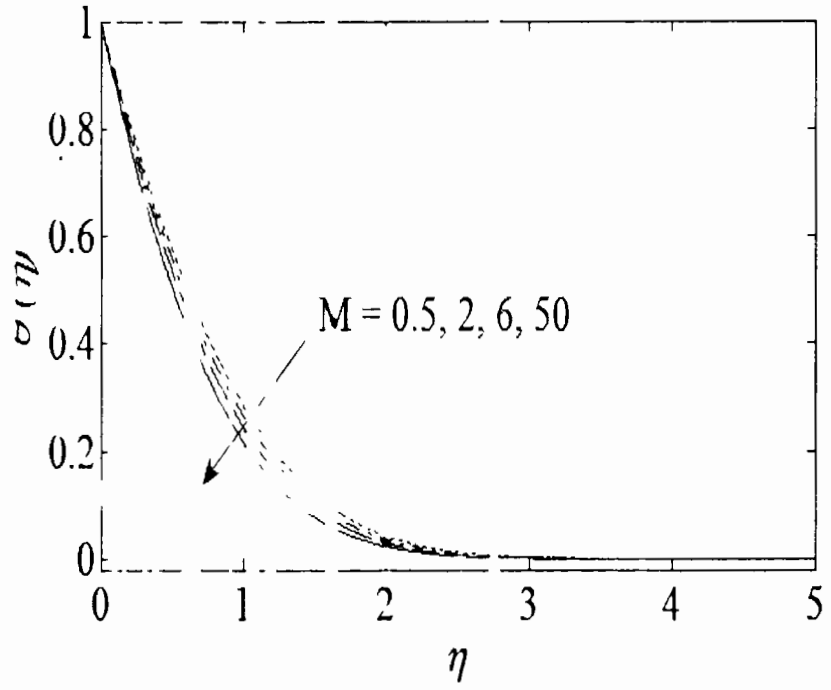

Fig. 9.4: Impact of M on $\theta(\eta)$ when $\lambda = 3, We = 0.5, d = 0.1, Pr = 1$.

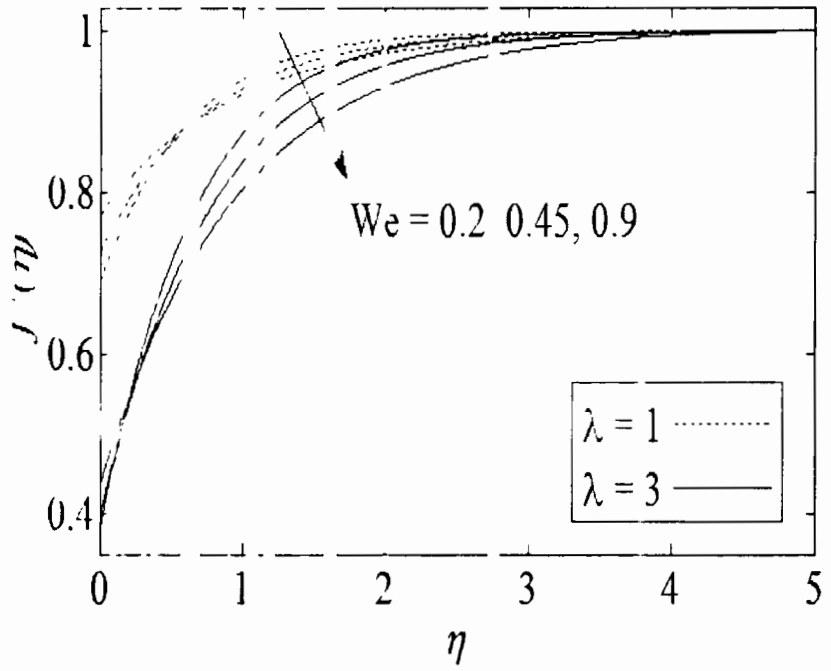

Fig. 9.5: Impact of We on $f'(\eta)$ by altering slip when $M = 1, d = 0.1, Pr = 1$.

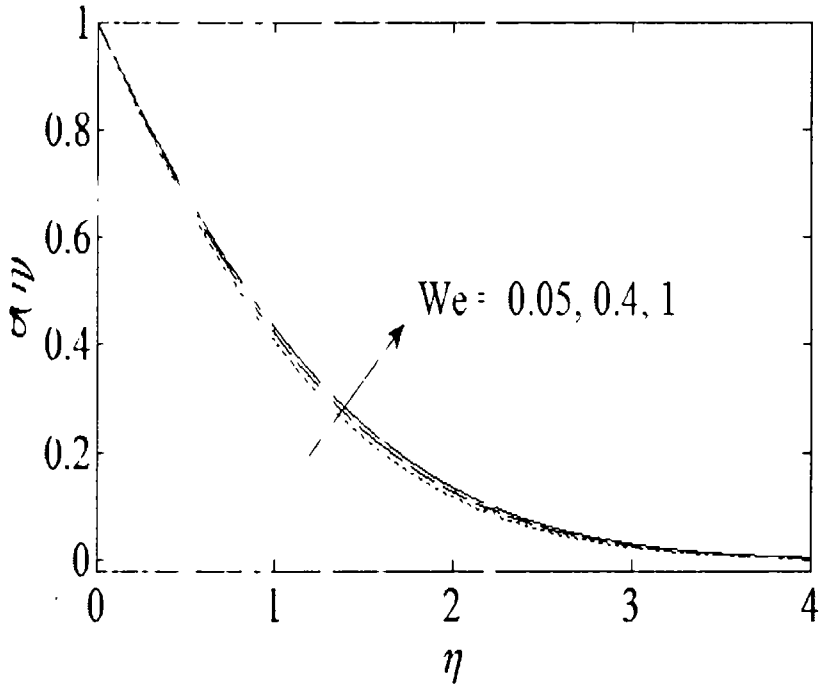

Fig. 9.6: Impact of We on $f'(\eta)$ when $\lambda = 4, M = 1, d = 0.1, Pr = 0.5$.

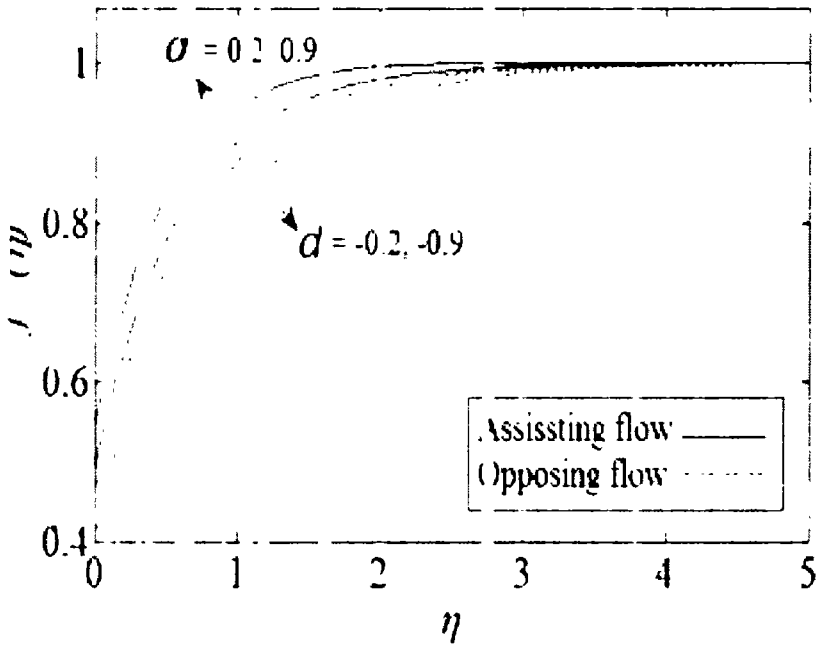

Fig. 9.7: Impact of d on $f'(\eta)$ when $\lambda = 3, Pr = 0.5, M = 3, We = 0.5$

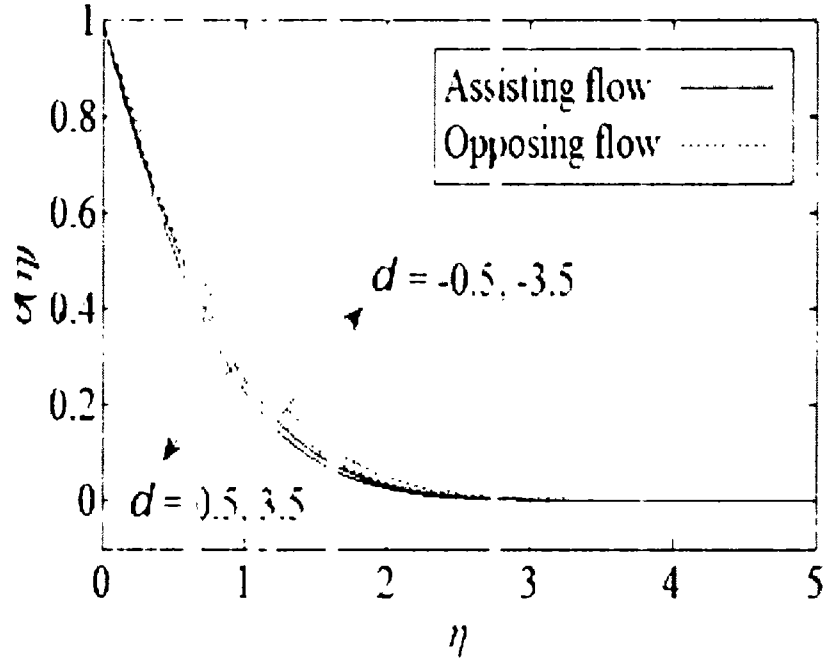

Fig. 9.8: Impact of a on $f'(\eta)$ when $\lambda = 3, Pr = 1, M = 3, We = 0.5$

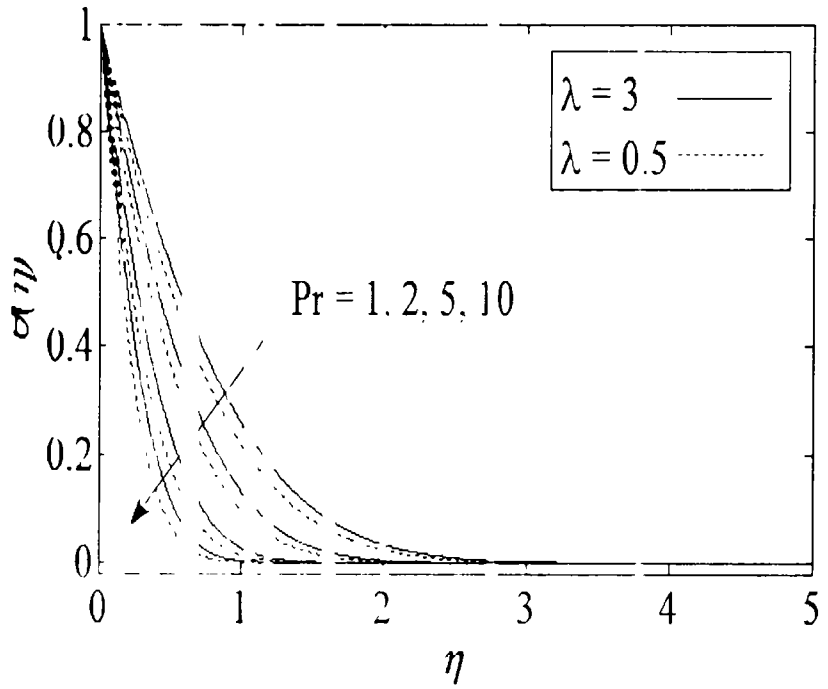

Fig. 9.9: Impact of Pr on $\theta(\eta)$ in the presence of slip when $M = 3, d = 0.1,$ and $We = 0.5$.

Table 4.1: Influence of λ on $Re_x^{1/2}C_f$ and $Re_x^{-1/2}Nu_x$ when $We = 0.5, M = Pr = 1$ both for assisting flow ($d = 0.1$) and opposing flow ($d = -0.1$).

λ	$Re_x^{1/2}C_f$ (assisting flow)	$Re_x^{-1/2}Nu_x$ (assisting flow)	$Re_x^{1/2}C_f$ (opposing flow)	$Re_x^{-1/2}Nu_x$ (opposing flow)
0.1	0.0396940	1.2468289	0.0392670	1.2329180
0.5	0.1880087	1.1962867	0.1855159	1.1817533
1.0	0.3490132	1.1396209	0.3431851	1.1246462
2.0	0.5924081	1.0498891	0.5784548	1.0350918
5.0	0.9224531	0.9185478	0.8898624	0.9065654
10	1.0695407	0.8554430	1.0263591	0.8456094
50	1.1853942	0.8032163	1.1337357	0.7951291
100	1.1991614	0.7968415	1.1465225	0.7889483
500	1.2100200	0.7917863	1.1566146	0.7840427
∞	1.2127123	0.7905292	1.1591178	0.7828222

Table 4.2: Influence of M on $Re_x^{1/2}C_f$ and $Re_x^{-1/2}Nu_x$ when $\lambda = Pr = 1$ and $We = 0.5$ both for assisting flow ($d = 0.1$) and opposing flow ($d = -0.1$).

M	$Re_x^{1/2}C_f$ (assisting flow)	$Re_x^{-1/2}Nu_x$ (assisting flow)	$Re_x^{1/2}C_f$ (opposing flow)	$Re_x^{-1/2}Nu_x$ (opposing flow)
0.1	0.3401739	1.1164548	0.3322275	1.0965899
0.5	0.3446500	1.1281423	0.3378313	1.1108543
1.0	0.3490132	1.1396209	0.3431851	1.1246462
2.0	0.3552778	1.1562173	0.3507113	1.1442641
5.0	0.3655151	1.1833976	0.3626590	1.1757119

10	0.3732894	1.2037015	0.3714764	1.1987397
50	0.3868833	1.2361132	0.3863826	1.2347291
100	0.3905841	1.2433106	0.3903140	1.2425701
500	0.3957243	1.2508222	0.3956649	1.2506633
1000	0.3969675	1.2519991	0.3969371	1.2519187
10000	0.3990310	1.2531760	0.3990285	1.2531679
50000	0.3995571	1.2532920	0.3995564	1.2532904
∞	0.3999820	1.2533220	0.3999820	1.2533220

Table 9.3: Influence of Pr on $Re_x^{1/2}C_f$ and $Re_x^{-1/2}Nu_x$ when $\lambda = M = 1$ and $We = 0.1$ both for assisting flow ($d = 0.1$) and opposing flow ($d = -0.1$).

Pr	$Re_x^{1/2}C_f$ (assisting flow)	$Re_x^{-1/2}Nu_x$ (assisting flow)	$Re_x^{1/2}C_f$ (opposing flow)	$Re_x^{-1/2}Nu_x$ (opposing flow)
0.05	0.3509393	0.3039639	0.3411310	0.3003373
0.1	0.3506510	0.3403749	0.3414380	0.3845350
0.5	0.3495519	0.8074892	0.3426122	0.8054638
1.0	0.3490132	1.1496209	0.3431851	1.1246462
5.0	0.3478845	2.4762945	0.3443735	2.4541926
10	0.3474944	3.4690130	0.3447793	3.4441100
50	0.3468439	7.6403326	0.3454490	7.6103073
100	0.3466601	10.762119	0.3456363	10.730519

Table 9.4: Influence of We on $Re_x^{1/2}C_f$ and $Re_x^{-1/2}Nu_x$ when $Pr = M = 1$ and $\lambda = 3$ both for assisting flow ($d = 0.1$) and opposing flow ($d = -0.1$).

We	$Re_x^{1/2}C_f$ (assisting flow)	$Re_x^{-1/2}Nu_x$ (assisting flow)	$Re_x^{1/2}C_f$ (opposing flow)	$Re_x^{-1/2}Nu_x$ (opposing flow)
0.05	1.07475540	1.01137079	1.0298616	0.9996494
0.08	1.0540099	1.01114689	1.0107714	0.9974826
0.1	1.0063865	1.0065586	0.9668427	0.9927064
0.3	0.8581134	0.9939460	0.8292726	0.9802323
0.6	0.7069658	0.9872453	0.6878929	0.9732819
0.9	0.6005525	0.9880183	0.5875407	0.9737522
1.2	0.5204170	0.9925383	0.5113612	0.9780998

Table 9.5: Comparison showing the influence various parameters on $Re_x^{1/2}C_f$ when $\lambda = \infty$ for assisting as well as opposing flow situations. The numerical values written in the brackets are calculated by [159].

M	We	$Pr = 0.2$		$Pr = 10$	
		$d = 0.2$	$d = -0.2$	$d = 0.2$	$d = -0.2$
1	0.2	1.5591[illegible]	1.09561434	1.1058027	1.0096210
		(1.5591)	(0.9561)	(1.1058)	(1.0096)
	1	0.8174[illegible]	0.68443491	0.7905304	0.7141263
		(0.8174)	(0.6844)	(0.7905)	(0.7141)
	2	0.6472373	0.5432061	0.6291413	0.5636410
		(0.6472)	(0.5432)	(0.6291)	(0.5636)
2	0.2	1.4554268	1.2948136	1.4171454	1.3346086
		(1.4554)	(1.2948)	(1.4171)	(1.3346)

	1	1.0 513271	0.9470308	1.0312133	0.9682148
		(1 051)	(0.9470)	(1.0312)	(0.9682)
	2	0.8 119355	0.7617252	0.8286659	0.7758104
		((841)	(0.7617)	(0.8287)	(0.7758)
1)	0 2	3.0 220059	2.9400916	3.0066963	2.9555134
		(: 022)	(2.9401)	(3.0067)	(2.9555)
1)	1	2.2 116015	2.1901398	2.2338363	2.1979406
		(: 241)	(2.1901)	(2.2338)	(2.1979)
1)	2	1.8 193215	1.7805365	1.8143020	1.7856210
		(1 819)	(1.7805)	(1.8143)	(1.7856)

Table 9 6: Comparison showing the influence various parameters on $Re_x^{-1/2} Nu_x$ when $\lambda = \infty$, for assisting as well as opposing flow situations. The numerical values written in the brackets are calculated by [159]

		$Pr = 0.2$		$Pr = 10$	
M	We	$d = 0.2$	$d = -0.2$	$d = 0.2$	$d = -0.2$
	0 2	0.4 261279	0.4096336	1.7909049	1.7564229
		((426)	(0.4096)	(1.7909)	(1.7564)
	1	0.3 919391	0.3784332	1.6090485	1.5763975
		((391)	(0.3784)	(1.6090)	(1.5764)
	0.2	0.4 403162	0.4288206	1.9159220	1.8907467
		((440)	(0.4288)	(1.9159)	(1.8907)
	1	0.4 085240	0.3993254	1 7320370	1.7096146
		((408)	(0.3993)	(1.7320)	(1.7096)
1)	0 2	0.4 832037	0.4795827	2.3335900	2.3242681
		((483)	(0.4795)	(2.3336)	(2.3243)
1)	1	0.4 585322	0.4555471	2.1333937	2.1258812
		((458)	(0.4555)	(2.1334)	(2.1259)

9.3 Conclusions

In this paper, effects of lubrication in MHD mixed convection stagnation point flow of a second grade fluid adjacent to a vertical plate has been investigated. A thin coating of a power-law fluid is used for the lubrication purpose. Numerical solutions are found to analyze the influence of slip parameter λ (ranging from no-slip to full-slip), magnetic parameter M, mixed convection parameter d and Prandtl number Pr on the flow characteristics. Results are presented in the form of tables and figures for certain values of parameters by considering assisting as well as opposing flow situations. Some findings of this study are

(i) The lubricant excites the velocity f' of the fluid and the effects of viscosity are suppressed by the lubricant in the case of full-slip.

(ii) The fluid temperature θ is suppressed by increasing slip on the surface.

(iii) f' is increased and momentum boundary layer thickness is decreased by augmenting the magnetic parameter M.

(iv) θ decreases by increasing M and the thermal boundary layer thickness is reduced.

(v) f' decreases and θ increases by increasing We.

(vi) f' is an increasing function of the mixed convection parameter d for the assisting flow and decreasing function for the opposing flow.

(vii) The temperature of fluid reduces for assisting flow situation and it increases for the opposing flow.

(viii) θ reduces by increasing the values of Prandtl number Pr.

(ix) Skin friction coefficient $Re_x^{1/2}C_f$ decreases and local Nusselt number $Re_x^{-1/2}Nu_x$ increases by increasing slip on the surface.

(x) $Re_x^{1/2}C_f$ and $Re_x^{-1/2}Nu_x$ gain the magnitude by increasing magnetic parameter M.

(xi) $Re_x^{1/2}C_f$ decreases and $Re_x^{-1/2}Nu_x$ increases during assisting flow and both quantities increase during opposing flow by increasing Pr.

(xii) Both $Re_x^{1/2}C_f$ and $Re_x^{-1/2}Nu_x$ are reduced with an increase in We.

Bibliography

[1] L. Prandtl, In Verhandlungen des dritten internationalen Mathematiker-Kongresses in Heidelberg 1904, A. Krazer, ed., Teubner, Leipzig, Germany, p. 484, 1905.

[2] H. Schlichting, Boundary Layer Theory, McGraw-Hill, New York, 1964.

[3] K. Hiemenz, Die Grenzschicht an einem in den gleichformingen Flussigkeitsstrom eingetauchten graden Kreiszylinder, Dingler's Polytech. J. 326, 321-324, 1911.

[4] T. Y. Chiam, Stagnation-point flow towards a stretching plate, J. Phys. Soc. Jpn., 63, 2443-2444, 1994.

[5] C. Y. Wang, Stagnation flow towards a shrinking sheet, Int. J. Nonlinear Mech., 43, 377-382, 2008

[6] F. Homann, Der Einfluss grosser Zahigkeit bei der Stromung um den Zylinder und um die Kugel, Z. angew. Math. Mech. (ZAMM), 16, 153–164, 1936.

[7] N. Frossling, Verdunstung, Warmeubertragung und Geschwindigkeitsverteilung bei zweidimensionaler und rotationssymmetrischer laminarer Grenzschicht-stromung, Lunds Univ. Arsskr. N.F. Avd. 2 35, No. 4, 1940.

[8] L. Howarth, The boundary layer in three-dimensional flow. Part II: The flow near a stagnation-point Phil Mag. VII, 42,1433 1440, 1951

[9] A. Davey, Boundary layer flow at a saddle point of attachment, J. Fluid Mech., 10, 593-610, 1961.

[10] D. F. Yang Unsteady laminar boundary layers in an incompressible stagnation flow, ASME J. Appl. Mech., 25, 421–427, 1958.

[11] J. C. Williams, Non-steady stagnation-point flow, AIAA J., 6, 2417–2419, 1968.

[12] E. I. W. Cheng, H. N. Ozisik and J. C. Williams, Non-steady three-dimensional stagnation-point flow, ASME J. App. Mech , 38, 282--287, 1971.

[13] K. Nazar, N. Amin, D. Filip and I. Pop, Unsteady boundary layer flow in the region of the stagnation-point on a stretching sheet Int. J. Eng. Sci., 42, 1241–1253, 2004.

[14] T. Fang and C. F. Lee, Three-dimensional wall-bounded laminar boundary layer with span-wise cross free stream and moving boundary, Acta Mech., 204, 235–248, 2009.

[1] . berg and S. Q.) u, A uniformly valid series solution to the unsteady stagnation-point flow towards an impulsively stretching surface, Sci. in China Series G: Phys., Mech. & Astro., 53, 521-526, 2010.

[16] Y. Zhong and T. Wang, Unsteady stagnation-point flow over a plate moving along the direction of flow impingement, Int. J. Heat Mass Trans., 54, 3103–3108, 2011.

[17] I. Pop and T. Y. Na, Unsteady flow past a stretching sheet, Mech. Res. Comm., 23, 413-422, 1996.

[18] J. T. Stuart, The viscous flow near a stagnation-point when the external flow has uniform vorticity, J. Aero. Sci., 26, 124–128, 1959.

[19] K. Tamada, Two-dimensional stagnation-point flow impinging obliquely on a plane wall, J. Phys. Soc. Jpn., 46, 310-311, 1979.

[20] J. M. Dorrepaal, An exact solution of the Navier-Stokes equation which describes non-orthogonal stagnation-point flow in two dimensions, J. Fluid Mech., 163, 141-147, 1986.

[21] J. M. Dorrepaal, Is two-dimensional oblique stagnation-point flow unique? Can. Appl. Math. Quart., 8, 61-66, 2000.

[22] P. Drazin and N. Riley, The Navier-Stokes equations: a classification of flows and exact solutions, London Mathematical Society Lecture Note Series, Cambridge Univ. Press, Cambridge, 334, 1-196, 2006.

[23] R. M. Tooke and M. G. Blyth, A note on oblique stagnation-point flow, Phys. Fluids, 20, 033101, 2008.

[24] A. Bonelli, G. Giantesio and M. C. Patria, MHD oblique stagnation-point flow of a Newtonian fluid, ZAMP, 63, 271-294, 2012.

[25] Y. Y. Lok, J. H. Merkin and I. Pop, MHD oblique stagnation-point flow towards a stretching/shrinking surface, Meccan., 50, 2949-2961, 2015.

[26] Y. Y. Lok, N. Amin and I. Pop, Non-orthogonal stagnation-point flow towards a stretching sheet, Int. J. Nonlinear Mech., 41, 622-627, 2006.

[27] B. S. Tilley and I. D. Weidman, Oblique two-fluid stagnation-point flow, Eur. J. Mech. B, 17, 205-217, 1998.

[28] I. Labropulu and A. Ghaffar, Oblique Newtonian fluid flow with heat transfer towards a stretching sheet, Comp. Prob. Eng., 307, 93-103, 2014.

[29] P. O. Weidman and V. Putkaradze, Axisymmetric stagnation flow obliquely impinging on a circular cylinder, Eur. J. Mech. B 22, 123–131, 2003.

[30] A. Ghaffari, T. Javed and F. Labropulu, Oblique stagnation-point flow of a non-Newtonian nanofluid over stretching surface with radiation: A numerical study, Thermal Sc , doi: 0.2298/TSCI150411163G, 2015.

[31] T. Javed, A. Ghaffari and H. Ahmad, Numerical study of unsteady MHD oblique stagnation-point flow with heat transfer over an oscillating flat plate, Can. J. Phys. 93, 1138-1143, 2015.

[32] A. Ghaffari, T. Javed and A. Majeed, Influence of radiation on non-Newtonian fluid in the region of oblique stagnation-point flow in a porous medium: A numerical study, Tran. Porous Med., 113, 245-266, 2016.

[33] J. T. Stuart, A solution of the Navier-Stokes and energy equations illustrating the response of skin friction and temperature of an infinite plate thermometer to fluctuations in the stream velocity, Proc. Royal Soc. Lon., Series A, 231,116–130, 1955.

[34] K. A. R. Gorla, Heat transfer in an axisymmetric stagnation flow on a cylinder, App. Sci Res., 32, 541-553, 1976.

[35] K. Saleh and A. B. Rahimi, Axisymmetric stagnation-point flow and heat transfer of a viscous fluid on a moving cylinder with time-dependent axial velocity and uniform transpiration, J. Fluids Eng., 126, 997-1005, 2004.

[36] A. S. Abbasi and A. B. Rahimi, Three-dimensional stagnation-point flow and heat transfer on a flat plate with transpiration, J. Thermophys. Heat Trans., 23, 513–521, 2009.

[37] A. S. Abbasi and A. B. Rahimi, Investigation of two-dimensional stagnation-point flow and heat transfer impinging on a flat plate, J. Heat Trans., 134, 024501-1–024501-6, 2012.

[38] M. Massoudi and M. Razeman, Heat transfer analysis of a viscoelastic fluid at a stagnation-point, Mech. Res. Comm., 19, 129-134, 1992.

[39] E. M. A. Elbashbeshy and M. A. A. Bazid, Heat Transfer over an Unsteady Stretching Surface, J. Heat Mass Trans., 41, 1-4, 2004.

[40] K. R. Rajagopal, On the boundary conditions for fluids of the differential type, in:

A. Sequeira (Ed. Navier-Stokes Equations and Related Nonlinear Problems, Plenum Press, New York, 273-278, 1995.

[43] B. W. Beard and K. Walters, Elastico-viscous boundary layer flows. I. Two-dimensional flow near a stagnation-point. Proc Cambridge Phil. Soc., 60, 667-674, 1964a.

[44] K. R. Rajagopal, and P. N. Kaloni, Some remarks on boundary conditions for flows of fluids of the differential type, Control Mechanics and its Applications, Hemi. Press, New York, 989

[45] K. R. Rajagopal, T. Y Na and A S. Gupta, Flow of a viscoelastic fluid over a stretching sheet, Rheol. Acta, 23, 213-215, 1984.

[46] K. R. Rajagopal and A. S Gupta, An exact solution for the flow of a non-Newtonian fluid past an infinite plate, Mecca., 19, 158, 1984.

[47] A. C. Srivatsava, The flow of a non-Newtonian liquid near a stagnation-point, Z. Angew Math. Phys., 9 80-84 1958.

[48] G. Rajeswari and S. L. Rathna, Flow of a particular class of non-Newtonian visco elastic and visco-inelastic fluids near a stagnation-point, Z. Angew. Math. Phys., 13, 43-57, 962.

[49] D. W Beard and K. Walters. Elastco-viscous boundary layer flows. Part I: two-dimension flow near a stagnation-point, Proc. Camb. Phil. Soc., 60, 667-674, 1964b.

[50] V. K. Garg and K R. Rajagopal, Stagnation-point flow of a non-Newtonian fluid, Mech. Res. Comm., 17. 415-421, 1990.

[51] P. D. Ariel, On extra boundary condition in the stagnation-point flow of a second grade fluid, Int. J. Eng. Sci., 40, 145-162, 2002.

[52] M. Ayub, H Zaman, M Sajid and T. Hayat, Analytical solution of stagnation-point flow of a viscoelastic fluid towards a stretching surface, Comm. Nonlinear Sci. Num. Simul., 13: 822-1835, 2008.

[53] T. Labropulu, J. M Dorrepaal and O. P. Chandna, Viscoelastic fluid flow impinging on a wall with suction or blowing, Mech. Res. Comm., 20, 143, 1993.

[54] T. K. Mahapatra, . Dholey and A. S. Gupta, Oblique stagnation-point flow of an incompressible viscoelastic fluid towards a stretching surface, Int. J. Nonlinear

Me h., 42, 484-49 , 20 .

[5] F. Labropulu, X. u and M. Chinichian, Unsteady stagnation-point flow of a non-Ne tonina second grade fluid Int. J. Math. Math. Sci., 60, 3797-3807, 2003.

[5] D. i, F. Labropu u and I. Pop, Oblique stagnation-point flow of a visco-elastic lu d with heat tra sfer, I t. J. Nonlinear M ch , 44, 1024-1030, 2009.

[5] V. K. Stokes, Cou le str sses in fluids, Phys. Fluids, 9, 1709–1715, 1966.

[5] M. Dev akar and T K. V. Iye gar, Run up flow of a couple stress fluid between par llel plates, No linea Ana .: Mod. Cont , 15, 29–37, 2010.

[5] M. Devakar and T K. V Iyer gar, Stokes' problems for an incompressible couple str ss fluid, Nonli ear Anal.: Mod. Cont., 1 181–190, 2008.

[5] T. Hayat, M. Mus afa, Z. Iqbal and A. Alsaedi, Stagnation-point flow of couple str ss fluid with n lting heat transfer, App. Math. Mech., 34, 167–176, 2013.

[5] K. Muthuraj, S Sr iva and L. Lourdu Immaculate, Heat and mass transfer effects on MHD fully de elop d flow of a couple stress fluid in a vertical channel with vis ous dissipatio and o scill ting wall tem perature, Int. J. App. Math. Mech., 9, 95- 117, 2013.

[6] D. Srinivasachary , N. Srinivasacharyulu, and O. Odelu, Flow and heat transfer of co ple stress fluid in a p rous channel with expanding and contracting walls, Int. Co m. Heat Mass Tra s , 36. 180 -185, 2009.

[6] P. . Hiremath and P. M Patil Free convection effects on the oscillating flow of a co ple stress fluid hrough a p rous mediu , Acta Mech., 98, 143-158, 1993.

[6] J. C. Umavathi, A J. Chamka , M. H. Manjula and A. Al-Mudhaf, Flow and heat tra sfer for a coup e str ss fluid sandwiched between viscous fluid layers, Can. J. Phy s., 83, 705-72 2005

[6] K. Ramesh and M Devakar, Effects of Heat and Mass Transfer on the Peristaltic Tra sport of MH Couple Stress Fluid through Porous Medium in a Vertical As mmetric Chan el, J Fluid , 163832 (19 pages), 2015.

[6] A. J. Chamkha, Hydr magn tic mixed convection stagnation-point flow with suc ion and blowi g, In . Comm. Heat Mass Trans., 25, 417-426, 1998.

[6] A. . Chamkha and C. Issa, Mixed convection effects on unsteady flow and heat tra sfer over a str ched surfa e, Int. Comm Heat Mass Trans., 26, 717-727, 1999.

[66] M. Kumari, Variable viscosity effects on free and mixed convection boundary layer flow from a horizontal surface on in a saturated porous medium-variable heat flux, Mech. Res. Comm., 28, 339-348, 2001.

[67] K. V. Prasad, K. Vajravelu and P. S. Datti, Mixed convection heat transfer over a non linear stretching surface with variable fluid properties, Int. J. Nonlinear Mech., 45, 320-330, 2010.

[68] H. A. Attia, Hydro magnetic stagnation-point flow with heat transfer over a permeable surface Arab. J. Sci. Eng., 28, 107-112, 2003.

[69] M. Kumari and G. Nath, Steady mixed convection stagnation-point flow of upper convected Maxwell fluids with magnetic field, Int. J. Nonlinear Mech., 44, 1048-1057, 2009.

[70] P. Singh, N. S. Tomer and D. Sinha, Numerical study of heat transfer over stretching surface in porous media with transverse magnetic field, Proc. Int. Confer. Challenge Appl. Math. Sci. Tech., ISBN 023-032-875-X, 422-430, 2010.

[71] P. Singh, A. Jangid, N. S. Tomer and D. Sinha, Effects of thermal radiation and magnetic field on unsteady stretching permeable sheet in presence of free stream velocity, Int. J. Engg. Math. Sc., 6, 163-169, 2010.

[72] U. Ziya, M. Kumar and V. Bisht, Radiation heat transfer effect on a moving semi-infinite tilted porous heated plate with uniform suction in the presence of transverse magnetic field Gaurita, 60, 69-79, 2009.

[73] U. Ziya and M. Kumar, Transient MHD free convection flow of an incompressible viscous dissipative fluid through inclined porous plate, Int. J. Essential Sci., 2, 18-27, 2008.

[74] T. K. Mahapatra, S. K. Nandy and A. S. Gupta, MHD stagnation-point flow of a power-law fluid towards a stretching surface, Int. J. Nonlinear Mech., 44, 124-129, 2009.

[75] M. M. Abdelkhalek, The skin friction in the MHD mixed convection stagnation-point with mass transfer, Int. Comm. Heat Mass Tran., 33, 249-258, 2006.

[76] O. Aydin and A. Kaya Mixed convection of a viscous dissipating fluid about a vertical flat plate, Appl. Math. Modelling, 31, 843-853, 2007.

[77] N. Ramachandran T. S. Chen and B. F. Armaly, Mixed convection in stagnation

flows adjacent to vertical surfaces, ASME J Heat Tran., 110, 373-377, 1998.

[74] C. D. S. Devi C, I. S. Takhar and G. Nath, Unsteady mixed convection flow in stagnation region adjacent to a vertical surface, Heat Mass Tran., 26, 71-79, 1991.

[75] I. A. Hassanien and R. S. R. Gorla, Combined forced and free convection in stagnation flows of micropolar fluids over vertical non-isothermal surfaces, Int. J. Eng. Sci., 28, 783-792, 1990.

[80] Y. Y. Lok, N. Amin and I. Pop, Unsteady mixed convection flow of a micropolar fluid near the stagnation point on a vertical surface, Int J. Thermal Sci., 45, 1149-1157, 2006

[81] T. M. Ali, R Nazar, N M. Arifin and I. Pop, MHD mixed convection boundary layer flow toward a stagnation-point on a vertical surface with induced magnetic field, J. Heat Tran vol 133/022502-5, 2011.

[82] A. Ishak, R Nazar and I. Pop, Magneto hydrodynamic (MHD) flow of a micro polar fluid towards a stagnation-point on a vertical surface, Comp. & Math. with Appl., 56, 3188-3194, 2008.

[83] A. Ishak, R Nazar, N. Bachok and I. Pop, MHD mixed convection flow near the stagnation-point of a vertical permeable surface, Physica A: Stat. Mech. & Appl., 389, 40-46, 2010.

[84] T. Hayat, Z. Abbas and I. Pop, Mixed convection in the stagnation-point flow adjacent to a vertical surface in a viscoelastic fluid, Int. J. Heat Mass Tran., 51, 3200-3206, 2008.

[85] T. Hayat, Z Abbas, I Pop and S. Asghar, Effects of radiation and magnetic field on the mixed convection stagnation-point flow over a vertical stretching sheet in a porous medium, Int. J. Heat Mass Tran., 53 466-474, 2010.

[86] A. Malvandi, M. R Safaei, M. H. Kaffash and D. D. Ganji, MHD mixed convection in a vertical annulus filled with Al_2O_3 water nanofluid considering nanoparticle migration, J Mag & Mag. Mat., 382, 296–306, 2015.

[87] M. Mirzaei, N Sua, H Soleimani and D. Soghraie, Effects of magnetic field on free convection in inclined cylindrical annulus containing molten potassium, Int. J. Appl. Mech., 07, 1500[illegible], 2015.

[88] M. R. Safaei, H. Togun, K. Vafai, S. N. Kazi and A Badarudin, Investigation of heat transfer enhancement in a forward-facing contracting channel using FMWCNT nanofluids, Num. Heat Tran. Part A: Appl., 66, 1321–1340, 2014.

[89] M. Naveed, Z. Abbas and M. Sajid, Hydromagnetic flow over an unsteady curved stretching surface. Eng. Sci. Tech., an Int. J , 19, 841-845, 2016.

[90] A. Khalid, I Khan A. Khan and S. Shafie, Unsteady MHD free convection flow of Casson fluid past over an oscillating vertical plate embedded in a porous medium, Eng. Sci. Tech. an Int. J. 18, 309-317, 2015

[91] N. Sandeep, C. Sulochana and B. R. Kumar, Unsteady MHD radiative flow and heat transfer of a dusty nanofluid over an exponentially stretching surface, Eng. Sci. Tech., an Int. J., 19, 227-240, 2016.

[92] C. S. K. Raju, N. Sandeep, V. Sugunamma, M. Jayachandra Babu, and J. V. R. Reddy, Heat and mass transfer in MHD Casson fluid over an exponentially permeable stretching surface, Eng. Sci. Tech., an Int. J., 19, 45-52, 2016.

[93] T. V. Karman, Uber laminare und turbulente Reibung, ZAMM-J. App. Math. Mech., 1, 233-252 1921

[94] W. G. Cochran, The flow due to a rotating disc, Proc. Camb. Phil. Soc., 30, 365-375, 1934.

[95] E. R. Benton, On the flow due to a rotating disk, J. Fluid Mech., 24, 781-800, 1966.

[96] E. M. Sparrow and J. L Gregg, Mass transfer, flow, and heat transfer about a rotating disk, ASME J. Heat Tran., 82, 294-302, 1960.

[97] T. Kakutani, Hydromagnetic flow due to a rotating disk, J. Phys. Soc. Jpn., 17, 1496-1506, 1962.

[98] E. M. Sparrow and R. D. Cless, Magnetohydrodynamic flow and heat transfer about a rotating disk, ASME J App. Mech. 29, 181-187, 1962.

[99] G. S. Pande, On the effects of uniform high suction on the steady hydromagnetic flow due to a rotating disk, Appl. Sci. Res., 31, 205-212, 1971.

[100] L. T. Watson and C. Y Wang, Deceleration of a rotating disk in a viscous fluid, Phys. Fluids, 22, 2267-2269, 1979

[101] S. K. Kumar, W. J Thacker and L T. Watson, Magnetohydrodynamic flow past a porous rotating disk in a circular magnetic field, Int. J. Num. Methods in Fluids, 8, 659-669, 1988

[102] M. Miklavcic and C. Y Wang, The flow due to rough rotating disk, J. App. Math. Phys., 54, 1-12, 2004.

[103] S. Asghar, M. Jalil M. Hussain and M. Turkyilmazoglu, Lie group analysis of flow and heat transfer over a stretching rotating disk, Int. J. Heat Mass Tran., 69, 140-146, 2014.

[104] M. Turkyilmazoglu, MHD fluid flow and heat transfer due to a shrinking rotating disk, Comp. & Fluids, 90, 51-56, 2014.

[105] M. Turkyilmazoglu and P. Senel, Heat and mass transfer of the flow due to a rotating rough and porous disk, Int. J. Thermal Sci., 63, 146-158, 2013.

[106] M. Turkyilmazoglu, An implicit spectral method for the numerical solution of unsteady flows with an application to rotating disk flow and heat transfer, Isi Bilimi Ve Teknigi Dergisi / J. Thermal Sci. & Tech , 32 (2), 99-106, 2012.

[107] M. Turkyilmazoglu, Exact solutions for the incompressible viscous fluid of a porous rotating disk flow Int. J. Nonlinear Mech., 44 (4), 352-357, 2009.

[108] M. Turkyilmazoglu, Three dimensional MHD stagnation flow due to a stretchable rotating disk, Int. Heat Mass Tran., 55, 6959-6965, 2012.

[109] H. K. Kuiken, The effect of normal blowing on the flow near a rotating disk of infinite extent, J. Fluid Mech., 47, 789-798, 1971.

[110] T. Watanabe and I. Ohama, Magnetohydrodynamic boundary layer flow over a rotating disk. Z Angew Math. Phys. (ZAMP), 71, 522-524, 1991.

[111] C. Y. Wang, Off-centered stagnation flow towards a rotating disc, Int. J. Eng. Sci., 46, 391-396, 2008

[112] S. H. Nourbakhsh A. A. P. Zanoosi and A. R. Shateri, Analytical solution for off-centered stagnation flow towards a rotating disc problem by homotopy analysis method with two auxiliary parameters, Comm. in Nonlinear Sci. & Num. Simul., 16, 2772-2787, 2011.

[113] T. Kuriakose and G. Nath, Unsteady MHD film flow over a rotating infinite disk, Int. J. Eng. Sci., 42, 1099-1117, 2004.

[1.4] S. Munawar, A. Mehmood and A. Ali, Time-dependent stagnation-point flow over rotating disk impinging oncoming flow, Appl. Math. Mech. -Engl. Ed., 34, 85–96, 2013.

[1.5] W. I. Thacker, S. K. Kumar and L. T. Watson, Magnetohydrodynamic flow and heat transfer about a rotating disk with suction and injection at the disk surface, Comp. & Fluids, 16, 183–193, 1988.

[1.6] D. M. Hannah, Forced flow against a rotating disc, British Aeronaut. Research Council Rep. and Memo., No 2772, Uni. Michigan, 1947.

[1.7] A. S. Tifford and S. T. Chu, On the flow around a rotating disc in a uniform stream, Aeronaut Sci., 9, 259–281, 1952.

[1.8] S. Asghar, K. Hanif, T. Hayat and C. M. Khalique, MHD non Newtonian flow due to non-coaxial rotations of an accelerated disk and a fluid at infinity, Comm. in Nonlinear Sci. & Num. Simul., 12, 465-485, 2007.

[1.9] H. A. Attia, Steady flow over a rotating disk in a porous medium with heat transfer, Nonlinear Anal: Mod. & Cont., 14, 21-26, 2009.

[1.10] H. M. L. C. Navier, Memoire sur les lois du mouvment des fluids, Memoires del Academie Royale des Sci. de l'Inst. de France, 6, 389-440, 1823.

[1.11] J. C. Maxwell. On stresses in rarefied gases arising from inequalities of temperature, Phil. Tran R. Soc. London, 170, 231-56, 1879.

[1.12] G. S. Beavers and D. D Joseph. Boundary condition at a naturally permeable wall, J. Fluid Mech., 30 197 207, 1967.

[1.13] A. Zeckel, L. Strong and S. Middleman, Viscous film flow in the stagnation region of the jet impinging on planar surface, AIChE J., 40, 1611–1617, 1994.

[1.14] T. G. Blyth and P. Parkinson. Stagnation point flow against a liquid film on a plane wall, Acta Mech. 180, 203–219, 2005.

[1.15] W. A. Ebert and E. M. Sparrow, Slip flow and in rectangular and annular ducts, J. Basic Eng., 87, 1018-24, 1965

[1.16] E. M. Sparrow, G. S. Beavers and L. Y. Hung, Flow about a porous-surfaced rotating disc, Int. J. Heat Mass Tran., 14, 993-6, 1971.

[1.17] E. M. Sparrow, G. S. Beavers and L. Y. Hung. Channel and tube flows with surface mass transfer and velocity slip, Phys. Fluids, 14, 1312-9, 1971.

[128] C. Y. Wang, Stagnation flows with slip: Exact solutions of the Navier-Stokes equations, Z. Angew Math. Phys., 54, 184-189, 2003.

[129] C. Y. Wang, Flow due to a stretching boundary with partial slip: An exact solution of the Navier-Stokes equations, Chem. Eng Sci., 57, 3745-7, 2002.

[130] H. I. Anderson, Slip flow past a stretching surface, Acta Mech., 158, 121-5, 2002.

[131] P. D. Ariel, Axisymmetric flow due to a stretching sheet with partial slip. Comp. Math. Appl., 54, 1069-1083, 2007.

[132] T. Hayat, A. Shafiq and I. Pop, Slip effects on mixed convective stagnation-point flow and heat transfer over a vertical surface, SKASM, October 29-30, 2013.

[133] M. Sajid, I. Ahmad and T. Hayat, Unsteady boundary layer flow due to a stretching sheet in porous medium with partial slip, J. Porous Media, 12, 911-7, 2009.

[134] M. Sajid, N. Ali Z. Abbas and T. Javed. Stretching flows with general slip boundary conditions, Int. J. Mod. Phys. B., 30, 5939-47, 2010.

[135] P. D. Ariel, T. Hayat and S. Asghar. The flow of an elastico-viscous fluid past a stretching sheet with partial slip, Acta Mech., 187, 29-35, 2006.

[136] T. Hayat, T. Javed and Z. Abbas, Slip flow and heat transfer of a second grade fluid past a stretching sheet through a porous space, Int. J. Heat Mass Tran., 51, 4528-4 2008

[137] B. Sahoo, Effects of partial slip on axisymmetric flow of an electrically conducting viscoelastic fluid past a stretching sheet, Cent. Eur. J. Phys., 8, 498-508, 2010.

[138] B. Sahoo, Effects of slip viscous dissipation and Joule heating on the MHD flow and heat transfer of a second grade fluid past a radially stretching sheet, Appl. Math. Mech., 31, 159-73 2010

[139] L. Crusteri and E. Osalus , On MHD and slip flow over a rotating porous disk with variable properties Int. Comm. in Heat Mass Tran., 34, 492-501, 2007.

[140] S. Munawar, A. Mehmood and A. Ali, Effects of slip on flow between two stretchable disks using optimal homotopy analysis method, Can. J. App. Sci., 1, 50-68, 2011.

[141] T. Labropulu and D. Li, Stagnation-point flow of a second grade fluid with slip, Int. J. Nonlinear Mech , 43. 941-947, 2008.

[142] N. A. Abdul Latif, M J. Uddin, O. A. Beg, A. I. Ismail and O. Anwar Bég,

Un teady forced bioconvection slip flow of a micropolar nanofluid from a stretching/shrinking sheet Proceedings of the Institution of Mechanical Engineers, Par N: J. Nano-Eng. and Nano-Sys., doi:10 1177/1740349915613817, 2015.

[143] M. J. Uddin, M. N Kabir and O. Anwar Bég Computational investigation of Stefan blowing and multiple-slip effects on buoyancy-driven bioconvection nanofluid flow with microorganisms, Int J. Heat Mass Tran., 95, 116-130, 2016.

[144] D. D. Joseph, Boundary conditions for thin lubrication layer, Department of Aerospace Engineering and Mechanics, Uni. Minnesota, Minneapolis, Minnesota 55455, 1980.

[145] H. . Andersson, O . A. Valnes, Slip-flow boundary conditions for non-Newtonian lubrication layers, Fluid Dyna Res., 24, 213-217, 1999.

[146] S. Solbakken, H. . Anderson, Slip flow over lubricated surfaces, Flow Turbol. Combust., 73, 77-93, 2004.

[147] H. Andersson and M Kousselet, Slip flow over a lubricated rotating disc, Int. J. Heat Fluid Flow, 27, 329-335 2006.

[148] B. Santra, B S Dandapat and H. I. Andersson, Axisymmetric stagnation-point flow over a lubricated surface. Acta Mech., 194, 1-10, 2007.

[149] M. Sajid, K Mahmood and Z Abbas, Axisymmetric stagnation-point flow with a general slip boundary condition over a lubricated surface, Chin. Phys. Letters, 29, 024702, 2012.

[150] P. A. Thompson and S. M. Troian, A general boundary condition for liquid flow at solid surfaces, Nature, 389, 360-362, 1997.

[151] M. Sajid, T. Javed Z. Abbas and N. Ali, Stagnation-Point Flow of a Viscoelastic Fluid Over a Lubricated Surface, Int. J. Nonlinear Sci. & Num. Simul., 14, 285-290, 2013.

[152] M Sajid, M Ahmad, I Ahmad, M. Taj and A Abbasi, Axisymmetric stagnation-point flow of a third-grade fluid over a lubricated surface, Adv. Mech. Eng., 7, 1-8, 2015

[153] M. Ahmad, I. Ahmad and M Sajid, Heat Transfer Analysis in an Axisymmetric Stagnation-point Flow of Second Grade Fluid over a Lubricated Surface, Columbia Int Pub. American J. Heat Mass Tran., 3, 1 14, 2016.

[154] T. C. Na, Computational Methods in Engineering Boundary Value Problem, Acad. Press, New York, 979

[155] T. Cebeci and P. Bradshaw, Physical and Computational Aspects of Convective Heat Transfer, Springer-Verlag. New York, 1984.

[156] H. B. Keller and T. Cebeci, Accurate Numerical Methods for Boundary Layer Flows II: Two Dimentional Turbulent Flows, AIAA Journal, 10, 1193-1199, 1972.

[157] P. Bradshaw, T. Cebeci and J. H. Whitelaw Engineering Calculation Methods for Turbulent Flows, Acad London, 1981.

[158] H. B. Keller, A new difference scheme for parabolic problems, in Numerical Solution of Partial Differential Equations (J. Bramble, ed.), Vol. II. Acad., New York, 1970

[159] K. Ahmad and R. Nazar, Unsteady MHD mixed convection Stagnation-point flow of a viscoelastic fluid on a vertical surface, J Quart. Meas. Anal., 6, 105-117, 2010.

[160] W. Ibrahim and B Shanker, Unsteady MHD flow and heat transfer due to stretching sheet in the presence of heat source or sink, Comp. Fluids, 70, 21–28, 2012.

[161] N. M. Sarif, M. Z Salleh and R. Nazar, Numerical Solution of Flow and Heat Transfer over a Stretching Sheet with Newtonian Heating using the Keller Box Method, Proc. Eng , 53 542 554, 2013.

[162] R. B. Bird, R. C. Armstrong and O. Hassager, Dynamics of polymeric liquids, Fluid Mech , J. Wiley and Sons, vol 1. 1987.

[163] J. Harris, Rheology and non-Newtonian flow, Longman Group Ltd., 1977.

[164] R. P. Chhabra and J. F Richardson, Non-Newtonian flow and applied rheology: Engineering Applications, 2nd Edi. Elsevier. 2008.

[165] B. D. Coleman and W Noll, An approximation theorem for functional with applications in continuum mechanics, Arch. Ration. Mech. Anal., 6, 355-370, 1960.

[166] R. L. Fosdick and K. R. Rajagopal, Anomalous features in the model of second order fluids, Arch Rat. Mech. Anal., 70, 145-152, 1979